Cellular Obstruction Clearance Of Proximal Ventricular Catheters Using Low-Voltage Joule Heating

BY

ABHAY V. SANE
B.Tech, Institute of Chemical Technology
Matunga, Mumbai – 400019
Maharashtra, India 2011

THESIS

Submitted as partial fulfillment of the requirements
for the degree of Master of Science in Bioengineering
in the Graduate College of the
University of Illinois at Chicago, 2017

Chicago, Illinois

Defense Committee:

Dr. Andreas Linninger, Chair and Advisor, Professor, Department of Bioengineering
Dr. Vahe Caliskan, Clinical Associate Professor, Department of Electrical and Computer Engineering
Dr. Meenesh Singh, Assistant Professor, Department of Chemical Engineering

ACKNOWLEDGEMENTS

I would like to take this opportunity to express my immense gratitude to those who have supported me during my time at University of Illinois at Chicago working on my Master's dissertation.

I am thankful to the talented members of the Laboratory for Product and Process Design, all of whom were extremely helpful and supportive of my work. Their encouragement, guidance, advice and at times, thoroughly deserved criticism, were essential to accomplish my goals in this project.

I thank Dr. Meenesh for his support in the computational modeling that I used extensively for my work and his inputs on electrochemical phenomena that are a significant part of this project.

I am very grateful to Dr. Vahe Caliskan for his assistance in the design of electronic circuits that were the basis of developing my experimental setup, as well as acting as a mentor during my time at the University.

I am immensely grateful to Dr. Linninger, my thesis advisor. His vision, advice and guidance were absolutely critical in the progress of this project and my thesis. The lessons I learnt under his able coaching have provided me with technical and non-technical skills that will always stay with me. He was the driving force that pushed me to accomplish more things than I believed I was capable of and he will remain an inspiration to me.

Lastly, I would like to thank my friends and family members, without whom I would not have made it to this stage. I will always be grateful for their support and motivation.

Abhay V. Sane

TABLE OF CONTENTS

TABLE OF CONTENTS (continued)

CHAPTER **PAGE**

LIST OF FIGURES

LIST OF TABLES

SUMMARY

Hydrocephalus is the abnormal accumulation of cerebrospinal fluid (CSF) in the brain due to an imbalance in CSF production and absorption or due to impaired flow of CSF (Pople 2002). It is managed primarily by implanting a shunt system consisting of a catheter to drain excess CSF and a valve to regulate the flow of CSF. The shunt redirects CSF flow from the central nervous system, most commonly the lateral ventricle of the brain, to another region in the body for reabsorption. It helps in reestablishing a more balanced CSF flow and reduces the symptoms caused by hydrocephalus. The first such shunt to be used was reported by Nulsen and Spitz in 1952 (Nulsen and Spitz 1952). Since then, shunt systems have become the primary tool for the management of hydrocephalus. A significant proportion of the population is currently dependent on CSF shunts to maintain a functional life.

However, CSF shunts are severely prone to failure, with up to 40% of shunts failing within 1 year of implantation, and 50% within 2 years (Kestle et al. 2000). On an average, a patient with a shunt system will undergo multiple shunt revisions (Stone et al. 2013; Reddy, Bollam, and Caldito 2014; Iglesias et al. 2016) and hospital admissions for shunt complications are becoming more common than initial shunt placement (Simon et al. 2008). The annual cost of shunt revision procedures has been estimated to be $1 billion (Patwardhan and Nanda 2005). Malfunction of the proximal part of the shunt due to obstruction i.e. ventricular catheter obstruction has been found to be a significant contributor to shunt failure. An obstructed ventricular catheter fails to sufficiently redirect CSF flow and leads to reoccurrence of symptoms of impaired flow. This kind of shunt failure is corrected primarily by shunt revision, by replacement of the obstructed part or the entire shunt system. More recently, invasive surgical procedures such as endoscopic ablation or high intensity ultrasonic ablation of the obstructing material have been reported to recanalize

obstructed ventricular catheters. An in-situ obstruction clearance mechanism in a ventricular catheter that is able to maintain patency of the catheter, and at the same time, avoids the above invasive procedures will be of tremendous benefit in reducing the need for shunt revisions. In this thesis, local hyperthermia induced by low-voltage Joule heating is proposed as a method to clear cellular obstruction. By applying an alternating electric signal to electrodes inserted in the catheter lumen, it is possible to elevate the local temperature sufficiently to kill the tissue obstructing the catheter. It is shown that the applied signal induces conditions of hyperthermia inside the catheter lumen and causes cell death. It is also non-lethal to cells present outside the catheter, significantly reducing the risk of damage to nearby cerebral tissue. In this preliminary work, we establish a platform for designing a self-clearing ventricular catheter that can remove cellular obstruction in proximal ventricular catheters and maintain catheter patency.

I. HYDROCEPHALUS

A. Summary

An overview of hydrocephalus and its management is provided in this chapter. Various complications of shunting – the practice of implanting a catheter to drain accumulated CSF are described. One of the complications - ventricular catheter obstruction, is studied in detail, and current methods to overcome it are provided.

B. Cerebrospinal Fluid

Cerebrospinal fluid is a complex transparent fluid found in the mammalian central nervous system. It fills the various cavities in the brain (ventricles, arachnoid granules and sinuses, and aqueducts) and spinal cord and is also found in the sub-arachnoid space in both organs. The volume of CSF in an adult human is approximately 150 ml. Its functions include removal of metabolic waste as well as protection of the brain from mechanical trauma.

1. Classical hypothesis of CSF hydrodynamics

The classical hypothesis of CSF production is that the majority of CSF is produced in the ventricles of the brain by an active secretion process by cells in the choroid plexus (Orešković and Klarica 2011). The choroid plexus is a leaf-like structure that is found floating in the CSF in ventricles. The ventricular epithelial lining is made of ependymal cells and extends into the lining of the choroid plexus. It is found in both lateral ventricles, as well as the third and the fourth ventricle in humans. It is a highly vascularized structure consisting of multiple lobes of central capillary bundles and connective tissue surrounded by the modified ependymal cells. The capillaries in the choroid plexus are fenestrated and permit the movement of small molecules and fluid into the interstitial fluid surrounding the ependymal cells (Spector et al. 2015).

The ependymal cells lining the choroid plexus are highly polarized with a number of different transporters in the apical and basal membranes. The apical membrane contains numerous villi and cells are linked apically by tight junctions. The villi greatly increase the surface area of the choroid plexus, similar to the villi in the intestinal tract. The tight junctions at the apical end inhibit paracellular diffusion of molecules across the epithelium (Redzic and Segal 2004). These structural characteristics lend support to the prevailing theory that CSF is produced by active secretion of molecules in the choroid plexus via the transcellular pathway, with water being co-transported down the osmotic gradient through aquaporin channels. In all, around 450 ml – 600 ml of CSF is produced every day. Apart from the ventricles, secretion across the blood brain barrier by endothelial capillaries forms the interstitial fluid in the nervous system which is thought to drain into the CSF, acting as an extrachoroidal source. It is found to be low in volume as compared to CSF production by the choroid plexus with a proportion of 10% (Segal 1993) and 20-30% (Orešković and Klarica 2011) of total CSF produced attributed to extrachoroidal sources.

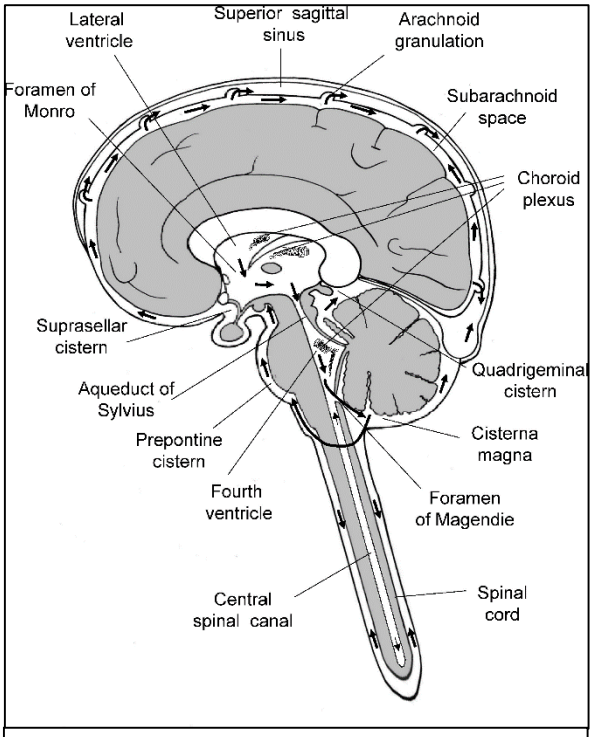

Fig.1. Natural flow path of cerebrospinal fluid in the brain. Reprinted from Progress in Neurobiology, 94 (3), Orešković D. and Klarica M., "*Development of hydrocephalus and classical hypothesis of cerebrospinal fluid hydrodynamics: facts and illusions*" (2011), with permission from Elsevier.

CSF circulation: According to the classical hypothesis, the CSF produced in the ventricles is not stationary, but flows along a natural path (Orešković and Klarica 2011;

Sakka, Coll, and Chazal 2011) as shown in Fig.1. The CSF formed in the lateral ventricles drains into the third ventricles via the intraventricular foramina and then into the fourth ventricle through the aqueduct of Sylvius. The CSF then drains through the apertures of Magendie and Lushcka, and circulates in the cisterns of the subarachnoid space before splitting into two streams; a smaller stream that goes into the spinal cord and a larger one that circulates in the subarachnoid space surrounding the brain and mixing with the interstitial fluid. It is eventually reabsorbed into the venous blood circulation in the venous sinuses. Although CSF flow has been proposed (A. A. Linninger et al. 2005) and observed (Yamada and Kelly 2016) to be of a pulsatile nature in response to blood flow in the brain, it is essentially unidirectional along the path described above.

2. Bulat-Orešković-Klarica hypothesis of CSF hydrodynamics

Several experimental observations (Bulat and Klarica 2011; Orešković and Klarica 2011) do not fit the classical hypothesis of CSF being primarily secreted by the choroid plexus in the ventricles, flowing via CSF pathways and reabsorbed in venous sinuses. A new hypothesis, proposed by Bulat, Orešković and Klarica proposes that CSF is primarily produced as a result of filtration from cerebral capillaries and micro-vessels into the interstitial fluid at all sites in the brain. The interstitial fluid and CSF form a functional unit and are in continuity, and is reabsorbed into venous capillaries and micro-vessels. The hydrostatic and osmotic pressure differences play an important role in the process of filtration and reabsorption. This hypothesis formulates that CSF production is distributed all over the cerebral tissue, and the not limited to the ventricles.

C. Hydrocephalus

When the flow of CSF is disturbed because of excess production, obstruction in the circulation path or a decrease in reabsorption, it leads to the abnormal accumulation of CSF in the ventricles or the subarachnoid spaces of the CNS. This condition is called Hydrocephalus. It is characterized by the expansion of the CSF space in the CNS and generally an elevated intracranial pressure (ICP). The excess fluid presses onto the brain parenchyma and, if untreated, hydrocephalus leads to tissue damage and in extreme cases, even death.

1. Symptoms

   The clinical symptoms that are presented in hydrocephalus patients vary with age. In infants, a patient usually has an increased head circumference and a bulging fontanel. Both symptoms can be traced to an elevated intracranial pressure pushing against the cranial tissue and skull. The cranial sutures of the skull in infants are not fully strengthened and they may appear to be strained. Patients have also been observed to suffer from nausea, vomiting or lethargy. Visual or cognitive defects and impaired motor function may also manifest over time (Nielsen and Breedt 2017). In adults, the intracranial pressure is not as high as that in infants, as the adult brain is more capable of adjusting the ICP. However, it manifests in symptoms like nausea, vomiting, gait disturbances, urinary incontinence, and dementia (Thompson 2009).

2. Epidemiology

   Hydrocephalus predominantly affects the pediatric population. It is estimated to that it occurs in 0.5 – 1.1 per 1000 infants (Tully and Dobyns 2014). In the 1960s, a different form of hydrocephalus was identified that affected the elderly called Normal pressure hydrocephalus (NPH). It was found to be treatable like pediatric hydrocephalus

by the use of shunts. The prevalence of NPH is estimated to be between 0.1 – 2.9%, but the number is probably higher as it is underdiagnosed. CSF shunting became a standard practice to manage hydrocephalus after its success in reducing hydrocephalus-related mortality (Chi, Fullerton, and Gupta 2005; Stein and Guo 2009). These studies highlight the prevalence of shunt dependence amongst the population.

3. Causes of Hydrocephalus

Although initially classified as an idiopathic disease, causes of hydrocephalus are now generally well known. It is now accepted to be "*a pathophysiological condition of disturbed dynamics of the CSF* " (Oi 2005). In infants, hydrocephalus may be congenital, i.e. present from birth, because of genetic abnormalities that cause conditions such as aqueductal stenosis, Chiari malformations, Dandy-Walker malformation, spina bifida and encephalocele. It may also be acquired due to intraventricular hemorrhages, diseases such as meningitis, congenital tumors, traumatic head injuries and other complications of premature birth. Such conditions may obstruct the exit of CSF from the ventricles to the cerebral cisterns, or may interfere with CSF flow within the cisterns. It can also develop as a long-term complication of surgical procedures such as hemispherectomies (Lew et al. 2013).

4. Classification of Hydrocephalus

Hydrocephalus is difficult to classify in a single system, such is the variation in its clinical characteristics (Kousi and Katsanis 2016). Functionally, it may be divided on the basis of its pathology (Sivagnanam and Jha 2012; Rekate 2009) into the following classes: Non-communicating or Obstructive: This form of hydrocephalus consists of some form of

obstruction along the CSF pathway. Symptoms may be relieved using surgical procedures such as endoscopic ventriculostomy, and need not necessarily involve shunt implantation.

Communicating or Non-obstructive: This is characterized by an absence of any apparent block along the CSF flow path. This form of Hydrocephalus is treated using shunts.

Another classification scheme divides Hydrocephalus based on the source or origin of the disease into the following categories:

Congenital: Hydrocephalus is present since birth due to genetic defects and abnormalities in fetus development

Acquired: Hydrocephalus is a secondary result due to another cause, such as a tumor, hemorrhage, infection etc.

Normal Pressure Hydrocephalus is another form of this disease that is known to affect the elderly population. It is called "normal pressure" as the elevated ICP is not as severe as those in pediatrics. It is usually a complication of some other condition, such as a hemorrhage, tumors and infections and at times it is idiopathic i.e. the cause is unknown. It has been strongly correlated with incidences of cerebrovascular diseases and hypertension (Krauss et al. 1996).

5. Treatment

Hydrocephalus is not a curable condition and it is treated to manage symptoms. The most common mode of treatment is the surgical implantation of CSF Shunts or catheters. Shunts establish an alternate pathway for CSF flow and redirect the CSF elsewhere in the body for reabsorption, with a valve to regulate the flow. The use of such a device was first reported in 1952 (Nulsen and Spitz 1952) and shunting rapidly became the primary approach to hydrocephalus management. Endoscopic third ventriculostomy (ETV) is

another technique that is increasingly gaining acceptance as an alternative to shunting. It is a surgical procedure in which a perforation is created in the wall of the third ventricle, thus making an alternate pathway for CSF to flow into the basal cisterns and be reabsorbed in the normal way. It may also be combined with Choroid Plexus Cauterization (CPC) using electrical or laser power to suppress formation of CSF and maintain ICP within a manageable range.

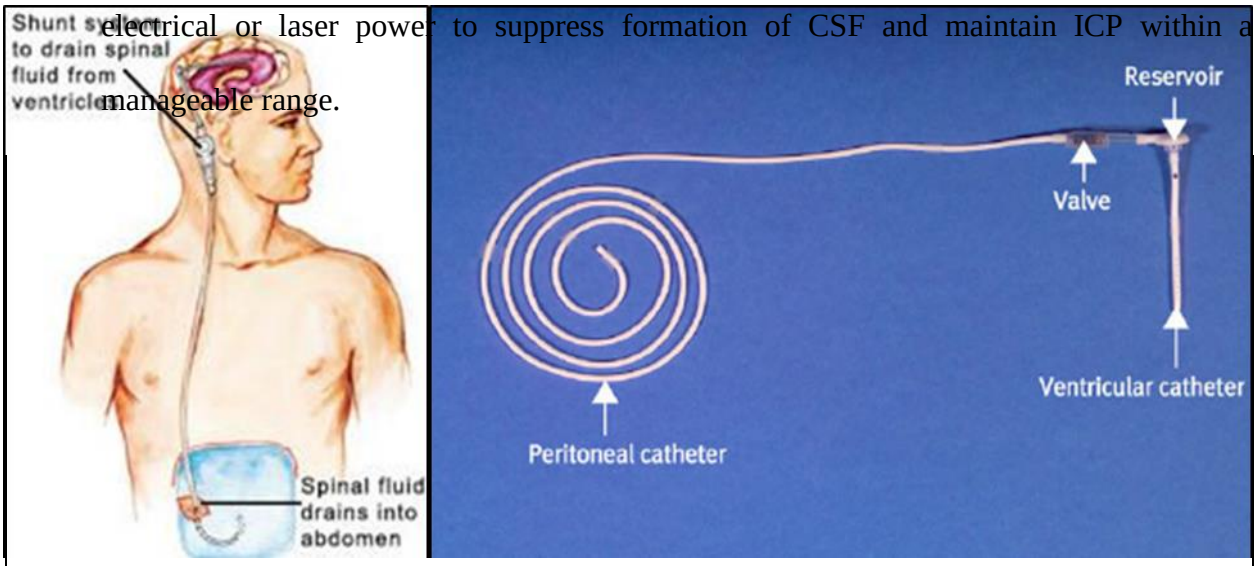

Fig. 2. Treatment of Hydrocephalus by CSF shunting. (A) Schematic of an implanted ventriculoperitoneal (VP shunt). The shunt allows CSF to be drained into the peritoneal cavity where it is reabsorbed. (B) Different components of a VP shunt. The ventricular catheter is typically inserted into a lateral ventricle. The valve is placed subcutaneously where it may be easily accessed for periodic checkups and flow rate adjustments. The distal or peritoneal catheter ends in the peritoneal cavity. Reprinted from Surgery - Oxford International Edition 27:(3), Thompson D., "*Hydrocephalus*", (2009) with permission from Elsevier.

D. <u>Shunting, Shunt malfunction and revisions</u>

A general CSF shunt consists of 3 parts (i) Ventricular catheter (ii) Valve (iii) Distal tubing. The ventricular catheter resides in the ventricles, and is a narrow, usually 12-Fr tube made of biocompatible silastic (silicone, PDMS). Rows of drain holes enable flow of CSF from the ventricles to the valve. The valve enables one-way flow towards the distal tube. Most modern shunts incorporate an anti-siphoning element that reduces over-drainage and its sequelae. The

distal tube is the run subcutaneously to the reabsorption site, which can be the peritoneum (VP shunts) and less commonly the atrium (VA shunts). In case the ventricular pathway is unobstructed, a lumbo-peritoneal shunt may be used to maintain CSF flow and relieve symptoms. VP shunts have been the preferred type of shunt system because VA shunts are prone to more severe complications (Symss and Oi 2015).

1. CSF Shunt revision

Epidemiological studies indicate that a large proportion of the population relies on life-long CSF shunts to manage hydrocephalus and maintain a functional life. Unfortunately, CSF shunts are prone to several malfunctions that may lead to shunt failure. A shunt failure is deemed to occur, when it can no longer serve the purpose of draining CSF appropriately, when hydrocephalus symptoms recur or when symptoms of other complications are observed. In these situations, a shunt revision becomes necessary to treat the patient.

2. Causes of shunt failures

Implanted CSF shunts can fail for a variety of reasons and lead to shunt dysfunction. Failure to adequately drain CSF results in the recurrence of hydrocephalus symptoms. Browd et. al. (Browd et al. 2006a, 2006b) describe in detail the various kinds of failures that are observed in CSF shunts.

(i) Mechanical failures – These are complications caused by mechanical malfunctions of the implanted shunts. They may come about because of obstruction of the shunt, displacement or disconnection of the parts of the shunt, fracture in the shunt wall, material degradation and calcification.

(ii) Shunt infections – Caused by introduction of pathogens, possibly commensals or foreign into the CNS during surgery. They can be reduced using proper clinical practices [Drake 2001] and are more common in developing countries lacking optimal standards in surgical or treatment environment.

(iii) Improper functioning – This shunt failure typically results in over or under drainage of CSF. Over-drainage leads to slit ventricle syndrome and a greater chance of proximal occlusion. Underdrainage fails to effectively relieve clinical symptoms.

The cause of CSF shunt failure has been found to be related to the duration of the implant before failure. Shunt infections are usually observed within a few weeks of the surgery. Obstruction of the proximal shunt develops over a period of a few months up to 2 years (Kast et al. 1994; Piatt 1995) , and distal shunt malfunctions become more common months 2 or more years after the initial insertion (Kast et al. 1994). Shunt revision may become necessary even 20 years after insertion (Vinchon, Baroncini, and Delestret 2012). A shunt inserted after a revision is more prone to shunt failure (Lazareff et al. 1998; Sagun Tuli et al. 2000) . Retrospective statistical analyses and long-term outcome analyses on CSF shunt failure highlight the severity of the problem of CSF shunt failure. 1st year failure rates have been reported to be as high as 50% (Sekhar, Moossy, and Guthkelch 1982), and long term survival shunt survival rates range from 34% to 42% (Kestle et al. 2000; Appelgren et al. 2010; Gebert et al. 2016), and can even be as alarmingly low as 22% for pediatrics (Reddy, Bollam, and Caldito 2014). These studies underline the persistent shortcomings of CSF shunts that are currently used in the treatment of hydrocephalus and underline the need for advanced shunts that can prevent or reduce the incidence of failure.

E. Proximal ventricular catheter obstruction

The majority of mechanical shunt failures are a result of proximal malfunction by obstruction. The sources of tissue obstructing the ventricular catheter are varied. Shunt explants have found to be obstructed with several cell types such as glial tissue (astrocytes, microglia and ependymal cells), connective tissue, and inflammatory reaction mediators like lymphocytes and macrophages (Kossovsky and Snow 1989; D. Singh et al. 2012; Harris and McAllister 2012). Occluded proximal catheters often show invagination of the ependymal cells lining the ventricular walls as well as an ingrowth of choroid plexus. The silicone surface is rough on a microscopic

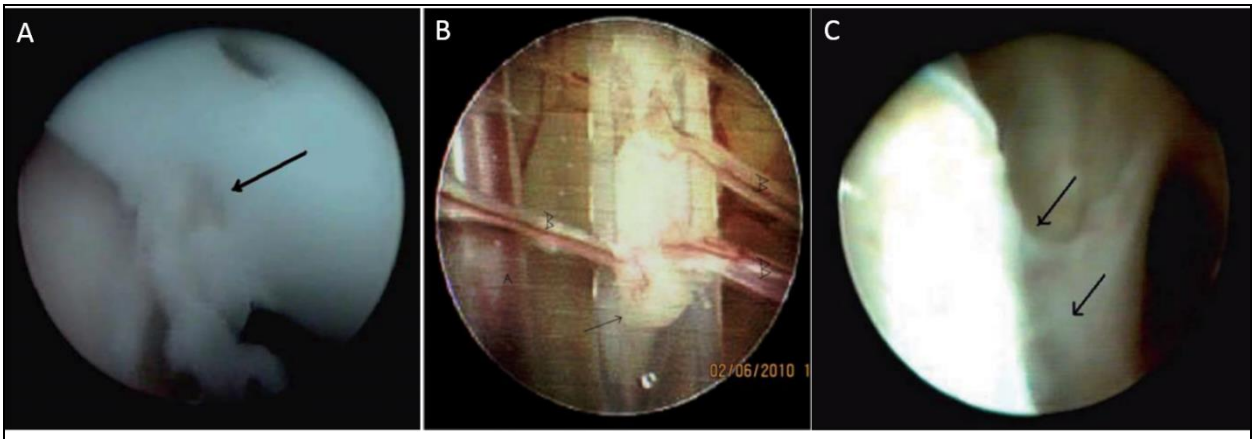

Fig. 3. Endoscopic images of blocked ventriculoperitoneal shunts. Arrows in the panels denote the obstruction (A) Shunt ports obstructed by ependymal growth permeation. (B) Coagulum like material in the shunt lumen (C) Biofilm surrounding and anchoring the shunt. Reprinted from British Journal of Neurosurgery 26 (5) Singh D. et. al. "*Endoscopic Observations of Blocked Ventriculoperitoneal (VP) Shunt: A Step toward Better Understanding of Shunt Obstruction and Its Removal*" (2012) with permission from Taylor and Francis.

scale, and can provide purchase for cells to adhere and multiply. Avoiding close proximity with both the ventricular wall and choroid plexus by careful positioning of the implanted catheter may decrease the incidence of obstruction. However, over-drainage of CSF leading to slit-ventricle syndrome is likely to increases the risk of contact between the catheter and surrounding tissue, and therefore, of obstruction. Similarly, the ventricular catheter may move during the course of a patient's life, and migration towards the ventricular wall is also possible (Blegvad et al. 2013).

The ventricular surface appear to undergo morphological changes in the event of hydrocephalus and shunt implantation. The ependymal cilia is found to have degenerated, and a higher number of reactive cells can be found on the choroid plexus surface (Go et al. 1976). These changes are likely to be the source of cell debris in the ventricles that also contribute to shunt obstruction. Another source of obstruction are the cells responsible for mediating inflammation. Although silicone is generally biocompatible, its close proximity to the ventricular wall has been known to induce foreign body reactions (Del Bigio 1998). Glial encapsulation of the ventricular shunt leading to obstruction can result due to this undesirable immune response. Proteins, especially albumin, have been found to be deposited on the catheter surface. Although the protein itself is insufficient to obstruct CSF flow (Brydon et al. 1996), they may stimulate an inflammatory response by acting as sites for antibody attachments (Del Bigio 1998; Harris and McAllister 2012). A less common specific hypersensitivity reaction to silicone or ethylene oxide (used to sterilize the shunt system before implantation) has also been reported to contribute towards obstruction (Blegvad et al. 2013). Hanak et. al. (Hanak et al. 2016) observed astrocytes and microglia to be the dominant cell type adhering to the silicone body. They propose that these cell types are likely to be in response to the shunt as a foreign body and act as a bridge for other tissues such as choroid plexus to adhere to the catheter body over time.

The risk of proximal obstruction is very high immediately after a new insertion of a shunt. The surgery inflicts a traumatic injury to the brain and is often accompanied by some bleeding. It can potentially initiate a cellular response leading to astrocyte proliferation and white blood cell aggregation, restricting CSF flow in the shunt lumen, like in Fig 3B, and ultimately blocking the flow. Replacing the obstructed proximal part can lead to a higher risk of complications, especially if tissues adhering to the shunt surface need to be torn away. The choroid plexus structure is highly

vascularized and a mechanical injury during shunt replacement can lead to intraventricular hemorrhage and bleeding into the ventricular space.

F. Technological modifications in CSF shunts to prevent proximal obstruction

An average pediatric patient will undergo multiple shunt revisions in their lifetime (Stone et al. 2013). It has also been observed that revised shunts are more prone to failure and proximal obstruction (Lazareff et al. 1998; Sagun Tuli et al. 2000; Iglesias et al. 2016). To overcome the problems of frequent shunt failure, many technological modifications have been put forward to improve shunt design and performance. However, the failure rate amongst the various types of shunts available today has not changed significantly from that 50 years ago (Stein and Guo 2008). Table VII, Appendix A lists some prominent modifications that have been implemented to reduce shunt failure and improve the functional life of these implants. We will discuss in detail some of the modifications that focus on preventing or reducing proximal obstruction.

Material modifications: Polydimethylsiloxane (PDMS) or silicone rubber has been the material of construction for catheters since its introduction in the 1950s (Weisenberg et al. 2016). Surface functionalization such as by using PVP to increase hydrophilicity was found to increase slipperiness to an extent where the proximal catheter was found to detach from the connectors to the rest of the shunt system (Weisenberg et al. 2016). Other suggested improvements that have shown promise are coatings of PEG, pHEMA, surface functionalization by anticoagulants, and anti-inflammatory agents to reduce obstruction (Harris and McAllister 2012). However, it must be noted that using different materials to reduce cell adhesion and cellular response may not work as desired because a foreign body reaction may still occur, especially due to the physical proximity of the implanted shunt to the ventricular wall or in cases of physical contact with the parenchyma.

This may lead to encapsulation of the catheter by glial cells and/or invasion of choroid tissue into the lumen (Del Bigio 1998; Blegvad et al. 2013).

Peel away sheath: The peel away sheath technique for implanting catheters was introduced to prevent debris from occluding catheter ports during insertion. The catheter is surrounded by a layer that can be removed after placement, avoiding contact between the catheter and brain tissue during insertion (Kehler et al. 2003). However, this technique has not significantly affected the incidence of proximal obstruction, possibly due to other sources such as the choroid plexus and glial tissue that develop into complete obstruction over a period of 1 year (Kehler et al. 2012).

Changes in Proximal shunt design: Various mechanical design changes were proposed to prevent catheter obstruction. However, they were not found to be very effective. Some of them are described below

(i) Flanged catheters: A flanged ventricular catheter with umbrella like projections positioned between catheter holes was designed and tested to prevent failure due to proximal obstruction. The protrusions were thought to help keep the catheter at a distance from the ventricular tissue, thereby preventing in-growth and development of occlusions. However, it was later observed that the flanges increased the long-term risk of occlusion, and revisions of this shunt increased the chances of hemorrhage and injury to the surrounding tissue (Weisenberg et al. 2016).

(ii) J-shaped catheters: Introduced by Hakim, the drain holes were found on the inner curvature, with the idea that it would increase the distance between the choroid plexus and the drain holes. They were not found to be very effective (Weisenberg et al. 2016).

Stereotactic guidance for optimal catheter placement: The ventricular catheter should ideally be placed in such a way that it is surrounded by CSF and is away from ventricular walls to avoid

tissue invasion and foreign body reactions leading to obstruction. Malpositioning of the ventricular catheter has been a primary factor that enhances risk of proximal shunt obstruction. Freehand catheter positioning typically involves multiple passes during placement and carries greater of hemorrhage creating conditions favorable for obstruction (Huyette et al. 2008). Stereotactic, image-guided and endoscopic catheter placement methods have been developed to ensure the ventricular catheter is surrounded by CSF alone and avoid proximity to the ventricular walls (Kaufman and Park 1999). An image-based neuronavigational system can be of immense help in accurate positioning of ventricular catheters (Kim et al. 2006). In a randomized shunt valve design trial, Tuli et. al. observed that a ventricular shunt completely surrounded by CSF has a lesser chance of failure compared to one embedded inside brain parenchyma (S. Tuli et al. 1999). Endoscopic ventricular catheter placement was reported to decrease the chances of proximal obstruction in a clinical study (Villavicencio et al. 2003). Jung et. al. reported a marked decrease in shunt revision because of proximal occlusion in optimally implanted shunts using an electromagnetic guidance system (Jung and Kim 2013).

Anti-siphon devices: CSF flow rates in a shunt are based on the pressure difference between the ventricular space and the distal end of the shunt. The ventricular pressure, however, is not constant but depends on a patient's posture and physical activity. Siphoning of excess CSF from the ventricle was observed when a patient moves to an upright position because of the sudden change in hydrostatic levels of the CSF. The over-drainage of CSF because of this "siphoning effect" can be severe enough to collapse the ventricles which greatly increases the risk of proximal obstruction. Anti-siphoning devices, that are now a standard part of a shunt system, have shown marked improvements in proximal shunt malfunction rates (Gruber and Roehrig 2010).

G. Methods to remove or clear proximal obstruction

An obstructed proximal shunt fails to adequately drain CSF and induces a recurrence of hydrocephalus symptoms. It is necessary to replace a completely obstructed proximal shunt to manage the symptoms. In recent years, techniques have been developed to remove the obstructing tissue and reinitiate CSF flow without replacing the obstructed ventricular catheter. This is typically achieved by coagulating the occluding tissue by focal ablation, either electrically (Hudgins and Boydston 1998; Pattisapu et al. 1999; Gnanalingham et al. 2005) or using ultrasound (Ginsberg et al. 2006). In the former case, a monopolar wire electrode or a stylus with an electrode at the tip is endoscopically introduced into the ventricular catheter till it reaches the obstruction. The obstructing material is then coagulated by passing a strong alternating electrical current (generally 0.1 – 5A) generated by an apparatus like a Bovie electrosurgical unit, through the material. The electrical current heats the material to temperatures above 60°C, at times even reaching 100°C and coagulates obstructing tissue. The process is similar to Radiofrequency (RF) ablation and is near instantaneous. In the case of ultrasound, the delivered waves mechanically dislodge occluding material to recanalize the ventricular catheter and breaks it into smaller particles. Cavitation i.e. production of bubbles in the medium due to ultrasound, and heating was also observed by Ginsberg et. al. during their tests. Both methods, however, have certain limitations. They require the threading of a stylus-like electrode or an ultrasound probe up to the obstruction site through the ventricular catheter lumen. A method to do so without the need for invasive surgery would be beneficial to the patient. The ablation methods are relatively severe and have the potential to cause unwanted damage to neighboring tissue, particularly if the catheter is non-optimally located close to the ventricular walls.

There has also been progress to design a self-cleaning ventricular catheter that does not need invasive surgery. Lee et. al. have developed a catheter integrated with MEMS based magnetic

microactuators that clears accumulated biological debris and maintains shunt patency. The magnetic actuators can be accessed non-invasively using external magnets (S. A. Lee et al. 2011; H. Lee et al. 2014). A self-cleaning shunt (SCS^{TM}) that consists of a mechanical actuator-based rod which can be made to move back and forth and rotate has also been developed. The rod mechanically shears the occluding material and can unblock the obstruction in the proximal shunt. This novel shunt clearing mechanism can also be non-invasively activated using an external magnets ("Microbot Medical Inc." 2017). These novel catheters are still being tested and it is possible that the minute size of the clearing assembly may not generate sufficient mechanical force to unblock the catheter.

H. Conclusion

Proximal shunt obstruction remains a major cause of shunt failure, and a method to clear the obstruction without affecting neighboring ventricular tissue will go a long way towards relieving incidences of shunt failure. Explant studies suggest that the obstruction is primarily caused by cellular attachment and proliferation. We propose to use a mild thermal method that is lethal to living cells, but is not as severe as endoscopic ablation methods currently in practice. In the next chapter, we will discuss the principles and effects of hyperthermia on biological tissue and later utilize this milder method to clear obstruction in proximal ventricular catheters.

II. HYPERTHERMIA

A. Summary

In this chapter, the practice of hyperthermia is introduced and reviewed. The thermal and non-thermal effects of electrical signal on biological tissue are described. We show how hyperthermia can act as a mild treatment to cause cell death and how this methodology can be adopted to solve proximal obstruction of ventricular catheters, and restore catheter patency.

B. Introduction

Hyperthermia is a therapeutic process of artificially elevating temperature of a tissue or the entire body above its regulated temperature range. The elevated temperature disrupts normal cellular processes, and on exposure to a sufficient thermal dose, induces irreversible cell injury and initiates cell death in the tissue. The effect on cells varies with the temperature attained. Classical hyperthermia is usually the term used for the process when the a moderate temperature elevation is attained, in the range 40°C – 48°C (Chicheł et al. 2007). Above 50°C, the technique is referred to coagulation, because of the observed effect of heat on cellular proteins. When the heating process increases temperatures from 60°C - 90°C, it is referred to as thermal ablation.

Several groups have reported the clinical benefits in using hyperthermia as an adjunct therapy along with the traditional chemotherapy and radiotherapy to treat tumors (Wust et al. 2002; Mallory et al. 2016). Tumors are generally in a state of stress because of the characteristic uncontrolled cell division, deficient vasculature and the hypoxic and nutrient deficient tumor microenvironment. They are, therefore, more susceptible to thermal damage than normal tissues at the relatively milder temperature range used in hyperthermia and enhances the effect of other oncotherapies (Horsman and Overgaard 2007).

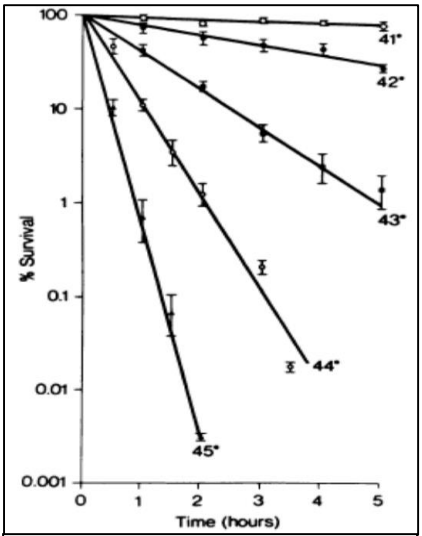

Fig. 4: Cell survival curves demonstrating the effect of hyperthermia on cancer cells lines. 43°C is accepted as a temperature threshold to induce cell death. Reprinted from Cancer Research 36 (3), Gerner E. et. al., "*A Transient Thermotolerant Survival Response Produced by Single Thermal Doses in HeLa Cells*" (1976) with permission from Elsevier.

Mechanism of action: Mammalian cells are suited to thrive at a homeostatic temperature of 37°C. Exposure to higher temperatures acts as a form of stress that may induce irreversible cellular damage. The extent of thermal injury depends on the intensity of energy delivered, duration of heating, tissue properties and the rate of heat removal. Classical hyperthermia induces a stress response in cells as evinced by the expression of the so called "heat shock proteins". In-vitro studies demonstrated that cell viability drastically falls when a temperature of 43°C or greater is attained (Dewhirst et al. 2003). Hyperthermia has been observed to adversely affect cellular cytoskeletal organization, membrane stability, nuclear protein structure and stability. Evidently, hyperthermia affects multiple cellular functions and disturbs multiple cellular pathways (Hildebrandt et al. 2002), and the total effect eventually leads to cell death. Both apoptotic and necrotic cell death may be induced occur, depending on the thermal dose (Harmon et al. 1990). At higher temperatures of thermal coagulation (>50°C) or radiofrequency ablation (>60°C), cellular proteins undergo denaturation and coagulate, decreasing the time necessary to induce cell death exponentially. Cells exposed to these treatments usually undergo coagulative necrosis.

C. Methods of inducing Hyperthermia

Hyperthermia treatments can be classified into two groups - whole body and local. In Whole body hyperthermia (WBH), the entire body is subjected to heating, using a heating jacket

or uniform radiation. The response to WBH is systemic in nature, and is used in very severe cases, for example heavily metastatic tumors. Local Hyperthermia is the more commonly adopted mode, in which a localized tissue region is heated by different means. A tissue can absorb incident electromagnetic (RF) or microwave radiation focused in a small volume by a receiver antenna. Similarly, incident energy from laser can induce hyperthermia locally. Nanoparticles of various materials have also been used to induce hyperthermia, as has been reported. Magnetic nanoparticles vibrate under the influence of a time-varying alternating magnetic field to generate heat by frictional losses (Bañobre-López, Teijeiro, and Rivas 2013). Gold nanoparticles absorb incident energy from infrared lasers and can locally heat the adjoining region. Their use allows for more efficient energy absorption and better control of thermal dose delivery for local hyperthermia (Cherukuri, Glazer, and Curley 2010).

D. A note on the Effect of electric fields on biological tissue

When an electric field is artificially induced in a biological tissue by using electrodes and an external power source, its effect on the tissue may be thermal as well as non-thermal. A direct current (DC), i.e. a non-alternating signal or a low frequency alternating signal applied to an electrode induces signal strength-dependent electrochemical reactions. Biological tissues are ionic conductors and the products of these reactions chemically attack the tissue. Applying an alternating signal to electrodes can generate heat by the motion of charged species within the tissue. At lower frequencies (in the kHz range), the heating is primarily resistive in nature. Ions and other polar species in the biological domain undergoes oscillatory motion trying to follow the rapidly changing direction of the electrical field. This motion generates heat by friction, and is termed resistive, impedance or Joule heating. At higher frequencies (>1MHz), the charged species do not undergo

displacement, but rather vibrate under the influence of the electric field. This is known as dielectric or capacitive heating.

Other non-thermal effects of applied electric fields on biological tissue have also been reported. Low amplitude (1-4 V/cm) alternating electric fields have been observed to disrupt cell division in tumors. The field is hypothesized to interfere with spindle formation in dividing cells and arrest tumor growth (Kirson et al. 2004, 2007; Davies, Weinberg, and Palti 2013). Irreversible electroporation is another non-thermal effect of pulsed electric fields on biological tissue. High-intensity pulsed electric fields (1000-3000 V/cm) disrupt the lipid bilayers in cell membranes to form pores in the membrane. This method has been applied to non-thermal ablation of tumors (Davalos, Mir, and Rubinsky 2005; Golberg and Yarmush 2013; Rossmeisl Jr et al. 2015). We will, however, be focusing on heating effects of an alternating electrical field in a biological medium by means of impedance or Joule heating.

Studies on the effect of hyperthermia on healthy tissue in the central nervous system, particularly the brain, reveal that even normal tissues are also susceptible to thermal damage in conditions of hyperthermia. Various animal studies that were undertaken to examine the effect of hyperthermia on the central nervous system have been summarized by Haveman (Haveman et al. 2005)and Sminia (Sminia et al. 1994). There is a large variation in the maximum tolerated thermal dose, ranging from 50 minutes at 41°C, to 60 minutes at 43°C. A moderate temperature elevation up to 44°C have generally been found to be lethal to healthy tissue of the CNS. Since proximal obstruction sources are predominantly cell types native to the CNS, these studies indicate the feasibility of adopting hyperthermia as a method to clear cellular obstruction and restore shunt patency.

We have seen that proximal shunts are prone to cellular obstruction, and modifications in material or design have unfortunately failed to prevent obstruction and the almost inevitable surgical revision. Interventions such as the tissue ablation probes are severe treatments and have the potential to cause damage to the tissues that form the ventricular wall. They also do not prevent the requirement of performing the treatment in a surgical room. To address the pressing need for a shunt system that can clear obstruction without resorting to surgical intervention, we propose to use locally induced hyperthermia by Joule heating to clear cellular obstruction in proximal ventricular catheters. An alternating electric signal applied to Pt-Ir electrodes in the lumen of the catheter will locally elevate temperatures along the path of the induced ionic current viz. in the shunt lumen and in close proximity to the catheter outer surface. Classical hyperthermia operates below a temperature of 48°C. We hypothesize, that the elevations in temperature because of the induced heat will be sufficiently localized to induce cell death in the occluded regions of the shunt alone. Therefore, we hope to avoid or minimize collateral damage to tissues that form the ventricular wall. Hyperthermia also provides an important advantage to deter recurrence of obstruction in the shunt because of its mechanism of action. Programmed cell death or apoptosis is a natural part of life process and does not activate inflammation cascades that is seen in physical injury or tissue ablation. This will reduce the risk of aggregation of microglia and other cells that respond to inflammatory cascades and signaling. Using a combination of in-vitro experiments and computational modeling, we will establish a preliminary design of a self-clearing proximal shunt that will eliminate proximal obstruction and reduce the incidence of shunt revision.

E. A note on Choroid Plexus Coagulation

Choroid plexus coagulation is a technique adopted by neurosurgeons in the management of pediatric hydrocephalus. In case of communicating hydrocephalus, with no apparent obstruction

to CSF absorption, a part of choroid plexus may be coagulated to reduce CSF production. Choroid plexus is also the most visible source of ventricular catheter obstruction. Tendrils of choroid tissue are seen growing inwards via drain holes and block CSF flow. Removal of such an avulsed catheter may lead to hemorrhage. In these cases, the obstructing tissue is removed using coagulation by electrocautery or monopolar radiofrequency ablation (Martínez-Lage et al. 1998). In a 10 year follow-up of pediatric patients that underwent CPC with/without ETV, it was observed that the choroid tissue did not regenerate after the coagulation procedure (Hideki Ogiwara, Kodai Uematsu, and Nobuhito Morota 2014). CP coagulation can be adopted for certain etiologies of hydrocephalus and may not be suitable for every case. This note demonstrates that there is a precedent to the use of thermal methods in lateral ventricles. Our proposed method aims to reduce the risk of injury to the tissues that form the ventricular wall and localize it to the catheter lumen and ports. This is achieved by adopting hyperthermia as the operative method as it is significantly milder in both the elevations in temperature and inflammatory response to injury compared to methods such as tissue coagulation, ablation or diathermy.

III. ELECTRODE – ELECTROLYTE INTERFACE

A. Summary

The proposed cellular obstruction clearance method in ventricular catheters consists of inducing hyperthermia by passing an AC current through ventricular lumen with the help of luminal electrodes. The environment at the surface of an electrode dipped in an electrolyte is sufficiently different than that in bulk electrolyte, and gives rise to unique properties at the electrode – electrolyte interface that influence the current density and hence the temperature distribution in the CSF space. Therefore, an overview of the processes that occur at the interface is provided. Electrical impedance spectroscopy measurements are performed to characterize the interface and interfacial phenomena. These measurements are used to construct an electrochemical model of our ventricular catheter design.

B. Formation of the electrical double layer

Free mobile charge carriers are necessary for an electric current to flow in a conductor. In a metallic conductor like a wire, the charge carriers are the free electrons that are not bound to an atom in the metallic lattice structure. In an electrolyte, the current consists of the motion of ions dissolved in solution and present along with solvent molecules. Because there are two different phases (electrode and electrolyte) with free charge carriers, a separation of charge occurs at the interfacial region until an equilibrium between the charged species is established. This rearrangement or charges may be a results of several activities – the dissolution of electrode material into the solution, the deposition of ions that have a chemical affinity to the electrode surface, or non-specific adsorption of ions onto the electrode surface. As a result, there exists some unbalanced charges on the electrode surface, and an equal but opposite unbalanced charges in the electrolyte near the electrode surface. This charge separation occurs spontaneously and gives rise

to a potential difference between the bulk metal electrode and the bulk electrolyte. It is known as the *half-cell potential* of the electrode-electrolyte. This potential difference is considered to exist across an interfacial structure known as the *electrical double layer*. In the absence of an externally applied potential, the potential difference arising from the spontaneous charge separation is also the *equilibrium potential* across the electrical double layer. The equilibrium established is such that there is no NET TRANSFER of electric charges across the double layer.

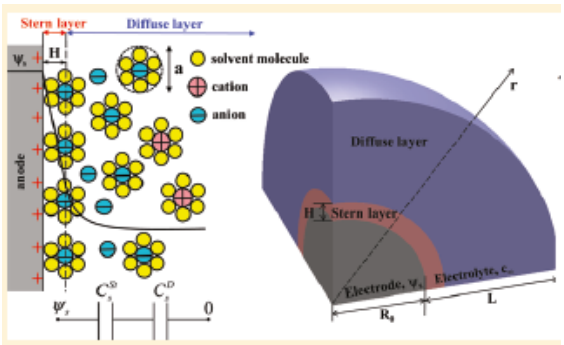

Fig. 5: Schematic of the electrical double layer at the electrode-electrolyte interface. The Stern layer and diffuse layer are marked, along with the standard model of a capacitor combination. Reprinted from J. Phys. Chem. C, 2011, 115 (33), Wang H. and Pilon L. "*Accurate Simulations of Electric Double Layer Capacitance of Ultramicroelectrodes*" with permission.

C. Structure of the electrical double layer

The electrical double layer at an electrode-electrolyte interface is in dynamic equilibrium in the absence of an external applied potential. The modern understanding of the structure of an electrical double layer is that it consists of 3 functionally distinct layers in the electrolyte. Closest to the electrode surface, is found a layer of solvated ions of the electrolyte known as the *Stern layer*. These ions are nonspecifically adsorbed, which means they are independent of the chemical properties of electrode material or ion species and depend on the charge carried by the ions. The steepest drop in potential at the interface is found across this region. As we move further away from the electrode surface, Brownian motion due to thermal agitation of the ionic and solvent species begins dominating their behavior. A region beyond the *Stern layer* consists of species in a

quasi-equilibrium state under the influence of the interfacial forces and random Brownian motion. This is known as the *diffuse layer*. The entire interfacial region is typically a few nanometers thick. In certain electrode-electrolyte pairs, another layer consisting of *specifically adsorbed ions* is also found closest to the metallic electrode surface. These ions are usually un-solvated and also contribute towards the potential drop at the interface.

D. Measuring Electrode potentials

As there always exists a potential difference between an electrode surface and the bulk electrolyte, it is impossible to study electrochemical processes at a single isolated interface. Therefore, it becomes necessary to introduce another electrode in the electrolyte to act as a reference potential. For this purpose, a standard Hydrogen electrode (SHE) or a saturated calomel electrode (SCE) are conventionally used as reference potentials. A standard hydrogen electrode is constructed with H_2 gas at 1 bar in contact with a 1 $mol \cdot lit^{-1}$ solution of $[H^+]$ ions on a passive interface such as Pt, and at a temperature of 298K. The potential of this electrode at equilibrium is assumed to be 0V and is used as a reference for the measurement of other electrode potentials. However, it is impractical to operate an SHE, and therefore, other electrodes such as a saturated calomel electrode or silver-silver chloride electrode are used as standard reference electrodes in regular laboratory practice. A saturated calomel electrode consists of a passive metal such as Pt in contact with a paste of calomel (Hg_2Cl_2) and saturated potassium chloride (KCl) in mercury. The paste is in contact with sat. KCl solution. The potential of this electrode is found to be +0.242V vs SHE. Another reference electrode, the silver-silver chloride system, is also popular as a reference. It consists of a silver in contact with silver chloride on its surface that in turn, is in contact with a saturated aqueous solution of KCl, and its potential is found to be 0.197V vs SHE. Reference

electrodes typically behave as ideal non-polarizable electrodes within moderate use, i.e. their potential remains steady despite a current passing through the electrochemical system.

To measure an electrode potential, the electrode-electrolyte system being studied, called a "working electrode" is connected to a reference electrode. A salt bridge may be used especially if the electrolytes are dissimilar to prevent solute polarization. The potential of the working electrode is changed until a current is detected in the completed circuit and this potential is taken to be the electrode potential for the system. As a means to compare different systems, all interfacial electrochemical reactions are written in a common formulation, as a *Reduction reaction*, with electrons on the left hand side of the equation.

$$A + ne^{-} \rightarrow A^{-n} \tag{3.1}$$

Factors such as temperature, pressure, and chemical composition affect the electrode potential. Hence, it has been customary to maintain standard conditions of temperature (298K), pressure (1atm) and when the concentrations of any ionic species is $1\text{mol}\cdot\text{lit}^{-1}$. In such conditions, the potentials are known as *standard electrode potentials*. The potentials are listed in Volts for various chemical systems w.r.t SHE in (Vanysek 2003).

E. Interfacial Processes

When an external potential is applied to an electrode, it moves the electrode potential away from its equilibrium potential, and may lead to non-equilibrium processes at the electrode-electrolyte interface. They may be divided into 2 categories – Faradaic and non-Faradaic processes. Typically, both processes occur to some extent at the interface, although one may dominate the other.

Faradaic processes: A faradaic process involves a chemical reaction or transformation of a molecule of the electrolyte. This is achieved by a transfer of one or more electrons across the interface. When the electron moves from the metallic electrode to a molecule *"A"* in the electrolyte, the process is called reduction, and is denoted by the following chemical reaction

$$A + ne^- \rightarrow A^{-n} \tag{3.2}$$

The electrode at which reduction occurs is by convention named the cathode. When the electron moves from the *"A"* to the electrode, the process is called oxidation.

$$A \rightarrow A^{+n} + ne^- \tag{3.3}$$

The electrode at which oxidation occurs is by convention named the anode. Faradaic processes are governed by Faraday's law of electrolysis, which states "The amount of substance liberated at an electrode is directly proportional to the quantity of electricity passed." In other words, the current measured in the external circuit is a measure of the total reaction occurring at the electrode surface. This may be written as

$$i = \frac{dQ}{dt} = nF\frac{dN}{dt} \tag{3.4}$$

where i = current in Amperes, Q = Coulombs of charge transferred across the interface, n is the stoichiometric number of electrons transferred in the reaction, F = Faraday's constant, N is the number of moles of chemical species oxidized/reduced at the electrode. Faraday's law is derived using a charge balance (of electrons in the metal electrode phase, and the reaction stoichiometry in the electrolyte phase).

Non-faradaic process: In non-faradaic processes, no electron is transferred across the interface. The composition of the electrical double layer at the electrode is altered in response to change in

electrode potential by adsorption or desorption of molecules from the electrode surface. This may referred to as the charging or discharging of the electrical double layer. This is typically seen as a transient current similar to those seen in the presence of a capacitor. For instance, when an external potential is applied to the electrode that was initially at equilibrium, an instantaneous and transient current may be detected in the external circuit, induced by a redistribution of charge in the electrolyte layer at the interface in response to applied electrode potential. The same may be observed when the applied potential is varied over time (such as in an AC signal), and an AC current can be detected in the external circuit.

F. Quantifying interfacial processes in electrochemical systems

Electrode potentials described above are quantities that are only defined under equilibrium condition, i.e. when no net current is flowing across the electrode-electrolyte interface. It is necessary to study the kinetics of interfacial processes in order to determine the total current that flows across an electrode-electrolyte interface. Processes that are involved in the charge transfer in Faradaic processes include mass transfer, diffusion of species, electron transfer and surface processes such as adsorption. A molecule in bulk diffuses to the electrode interfacial region, get adsorbed on to the electrode surface, undergo the reaction to form a product, and the product then desorps from the surface and diffuses away to the bulk. The slowest amongst all these steps controls the rate of reaction and the intensity of current flow. We shall look at a few principal equations that govern electrochemical interfacial processes.

1) Nernst Equation: The Nernst equation is a well-studied equation to calculate electrode potentials under conditions of zero net current at the interface. In these situations, the reaction at the surface is typically reversible and almost instantaneous. One such example is the reaction occurring at a silver-silver chloride electrode, which can be written as

$$AgCl_{(s)} + e^{-} \leftrightarrow Ag_{(s)} + Cl^{-}_{(aq)} \quad (3.5)$$

In such cases, when there is little or no electrical current flowing across the interface, the system can be assumed to be at equilibrium and the electrode potential is determined by the Nernst Equation:

$$E = E^{o} + \frac{RT}{nF} ln\left(\frac{[Cl^{-}_{(aq)}]}{[AgCl_{(s)}]}\right) \quad (3.6)$$

where E^o is the standard electrode potential, n is the stoichiometric number for electrons transferred when $AgCl_{(s)}$ is reduced to $Cl^{-}_{(aq)}$ and F is Faraday's constant. The potential is therefore a function of the ionic composition of the solution, the stoichiometry of reaction and the temperature. This equation is valid only for an electrode system involving a reversible reaction at equilibrium, i.e. when there is little or no net flow of current.

2) Butler-Volmer Equations: This set of equations relate the *Faradaic* current at an electrode to the applied potential, concentrations of the concerned species and properties of the electrochemical reaction. It is valid when the electrode reactions are not mass-transfer limited. The Faradaic current density, assuming both cathodic and anodic reactions occurring at the same electrode is given by:

$$i = i_0 \cdot \left(e^{-\alpha_c F\eta/RT} - e^{\alpha_a F\eta/RT}\right) \quad (3.7)$$

Here, i is the current density in Am^{-2}, η is the overpotential at the electrode, i_0 is the equilibrium current density for the electrochemical reaction occurring at the electrode, T is the temperature in Kelvins, α_a and α_c are the anodic and cathodic coefficients that quantify the symmetry of the equilibrium electrochemical reactions occurring at the electrode surface. The overpotential η at the interface is given by

$$\eta = V_{electrode} - V_{electrolyte} - E_{eq} \tag{3.8}$$

where $V_{electrode}$ is the externally applied potential, $V_{electrolyte}$ is the potential in the electrolyte next to the electrode and E_0 is the equilibrium potential for the species reaction. E_0 is typically computed using the Nernst Equation.

3) Tafel Equation: It is understood that both oxidation and reduction occur to some degree at an electrode surface, as given in the BV formulation, and the net current is composed of the sum of both reaction currents. At large overpotentials, the non-dominant reactions can be considered to be negligible, and the current-potential relationship is given by

$$\eta = a + b \cdot \log i \tag{3.9}$$

Eq. (4.5) is known as the Tafel equation, and it has been observed experimentally for large overpotentials and small currents. Here η is the overpotential, a and b are kinetic constants and i is the current at the interface. The Tafel equation is a simplified version of the Butler-Volmer formulation at large overpotentials, and the exponential relationship between the current and overpotential is maintained.

4) Capacitive current: The Butler-Volmer and Tafel equations deal only with the Faradaic component of the interfacial current that arises from electrochemical reactions. The non-faradaic component arises from the electrical double layer at the electrode-electrolyte interface that behaves as a *capacitor* in a circuit. When a DC potential is applied to an electrode, it causes a rearrangement of charges across the electrical double layer. This rearrangement can be detected as a momentary current in the system. In the electrolyte phase, the current is only observed in the region around the interface, and not in the bulk phase. However, when an alternating potential (AC signal) is applied to an electrode, a

capacitive current is observed as the oscillatory flux of ions in the bulk phase. This may enumerated as a *capacitive current* given by

$$i_{cap} = C_{dl} \cdot \frac{dV}{dt} \tag{3.10}$$

i_{cap} is the capacitive current density in Am^{-2}, C_{dl} is the specific capacitance in Fm^{-2}, V is the applied potential at the electrode.

The total interfacial current density is the sum of both reactive and capacitive components, as shown in Eqn. (3.11)

$$i_{total} = i_{rxn} + i_{cap} \tag{3.11}$$

The equations described above can be used to determine the electrical current in an electrochemical system in the presence of interfacial processes.

G. Electrochemical impedance spectroscopy

To accurately model the interfacial phenomena, it is necessary to obtain a representative model of the interface and interfacial processes to incorporate them into our computational model. Electrochemical Impedance spectroscopy was performed to characterize the electrode-electrolyte interface.

1. Working

A small perturbative AC signal is applied for a short duration between the working and counter electrode over a wide range of frequencies and the current drawn in the circuit is measured external to the cell. A plot of I vs V over the frequency range is generated and a best fit approximation is used to calculate interfacial properties based on a standard model. We chose the widely used Randles cell as it is known to be a good approximation at intermediate frequencies, and the impedance was used in our computational modeling. The Randles model

(Fig 3.2) of the electrode impedance consists of an electrochemical charge transfer resistance (R2) parallel to a double layer capacitance (C2), the combination being in series with a solution resistance (R1). A low charge transfer resistance indicates a high likelihood of an electrochemical reaction occurring at the interface.

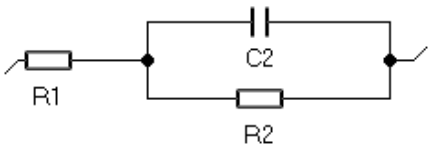

Fig 6: Randles model of electrochemical impedance at the electrode-electrolyte interface. R1 and R2 are resistances, while C2 is a capacitive element. R1 represents the resistance of the electrolyte layers in the vicinity of the electrode, R2 represents the charge transfer occurring because of the interfacial chemical reaction and C2 represents the capacitive behavior of the electrical double layer.

2. Methods

The EIS measurements were carried out at ambient temperature on the SP-300 potentiostat (BioLogic Science Instruments). A 3-electrode electrochemical cell is created using one Pt-Ir (90/10) ring electrode as the working electrode, a counter electrode (Pt) to complete the circuit and a reference electrode (Sat. Calomel) for potential measurements. 30 ml of electrolyte (aCSF made using the recipe in [Burrone 2002] is used as a substitute for CSF and all 3 electrodes are in contact with the electrolyte in a beaker . A sinusoidal signal over a frequency range of 5MHz to 5mHz is applied between the working and counter electrode and the current drawn at each frequency is measured. We chose a signal amplitude of 2000mV, to capture phenomena at large overpotentials. A Nyquist plot of the response of the cell is generated using the EC-Lab software (V11.01, Biologic Science Instruments), and a Z-fit test is performed on the measured impedance data to calculate interfacial properties based on the Randles model of

the interface. The signal is ON for a small duration such that we assume that the electrolyte composition remains unchanged during the measurement.

3. Results

The Z-fit obtained is shown in Fig 7. The parameters show the double layer capacitance to 8.9nF, which translates to an impedance of 35.76Ω and the charge transfer resistance to be 27.7Ω. Both values are significantly low and equivalent in order of magnitude to indicate that both processes are likely to occur in case of an overpotential condition. The χ^2 value of the goodness-of-fit is 69.52, which gives a value of $\alpha < 0.001$. Therefore, our calculated parameters match our measurements acceptably and can be used in our computational model.

Since the impedances are of the same order of magnitude, our EIS measurements indicate that electrochemical reactions and the double layer capacitance both influence the interfacial current. The total current at the electrode, and therefore, in the electrochemical system will be composed of both a capacitive and a reactive component.

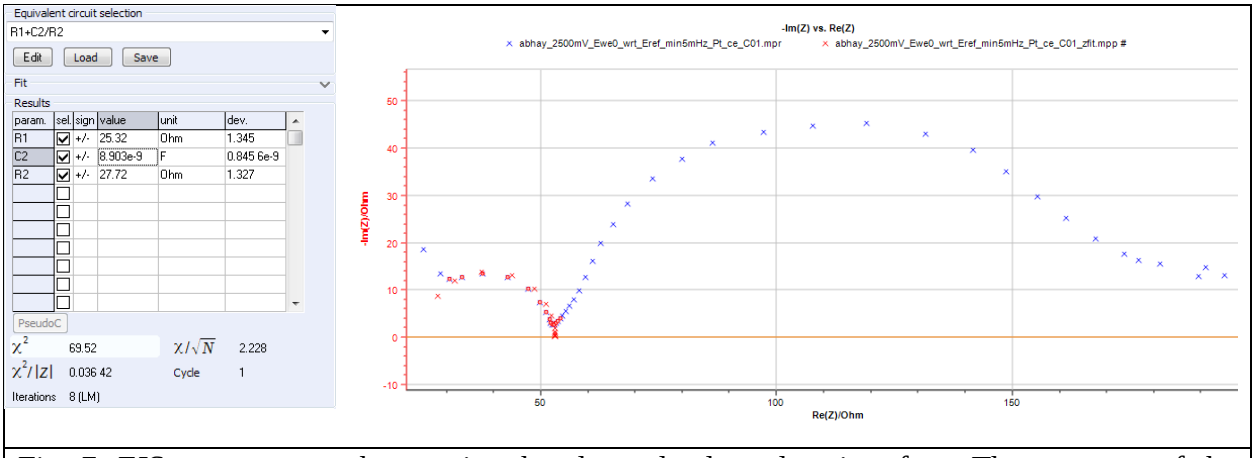

Fig. 7: EIS spectrum to characterize the electrode-electrolyte interface. The response of the interface to applied potential (blue trace) is represented as a Nyquist plot of the complex impedance over a frequency range of 5MHz to 5mHz. The amplitude of the applied sinusoidal signal was 2000mV. A Z-fit of the Randles model (red trace) is constructed over the intermediate frequency range of 2MHz to 5kHz to eliminate the effect of the electrode response at lower frequencies. This region shows a different behavior that is far from our signal frequency, and cannot be represented by the Randles model.

H. Novel design of a ventricular catheter

Having looked at the fundamentals of electrochemical processes that occur at the electrode-electrolyte interface, we shall look at how we can utilize them in our design of a ventricular catheter to clear cellular obstructions. We have seen in Chapter II how inducing hyperthermia can be an effective and low-intensity method to kill tissues. Exposure to temperatures from 43°C – 48°C have been known to induce cell death in a wide variety of tissues, including glial cells and connective tissues of the CNS that play an important role in obstructing ventricular catheters. We propose to induce hyperthermia in the ventricular catheter lumen and the region around the drain ports by applying an AC signal to strategically placed luminal electrodes. Taking advantage of a suitable electrode orientation, it could be feasible to generate ionic currents in the CSF in a way that cell death due to hyperthermia can be induced at the sites prone to obstruction and clear them without damaging the cerebral tissues surrounding the ventricular space. An AC signal is applied to electrodes positioned inside the lumen, to shield the ventricular lining from severe thermal damage. At the interface, as water is the predominantly available molecule and at significant overpotentials, hydrolysis is likely to occur. The reactions at the anode (+ve electrode) is

$$2H_2O \rightarrow 4e^- + O_{2_{(gas)}} + 4H^+ \tag{3.12}$$

As the reaction generates H^+, the equilibrium potential is pH dependent and is varies based on the H^+ concentration according to Eq. (3.13)

$$E_0 = E_0^{std} - 0.059pH \tag{3.13}$$

Here, E_0^{std} is 1.23V (Vanysek 2003). The reaction at the cathode at neutral or alkaline pH is the reduction of water to yield hydrogen gas and hydroxide ions, which has a standard equilibrium potential of -0.83V and is given below:

$$2H_2O + 2e^- \rightarrow H_{2_{(gas)}} + 2OH^- \quad (3.14)$$

E_0 varies according to OH^- concentration and is therefore, again pH dependent given by Eq. (3.15)

$$E_0 = E_0^{std} + 0.059 log_{10} pOH \quad (3.15)$$

Here, E_0^{std} is -0.83V (Vanysek 2003). The net reaction of hydrolysis in the system is obtained by adding the two equations.

$$2H_2O \rightarrow O_{2_{(gas)}} + 2H_{2_{(gas)}} \quad (3.16)$$

The applied signal will generate heat at the electrode surface and in bulk electrolyte and induce hyperthermia conditions at ventricular catheter sites prone to obstruction.

Heat generation in an electrochemical system: We consider three sources that contribute to heating in an electrochemical system. Heating occurs at the electrode-electrolyte interface due to irreversible activation losses caused by the overpotential, and the capacitive losses within the double layer. These losses are purely surface phenomena and the corresponding heat generation terms are modeled as surface heat sources (Cui and Cheng 2009). Surface heat generated due to the overpotential is given by

$$q_{rxn} = i_{rxn} \cdot (\eta + T \cdot \frac{\partial E_{eq}}{\partial T}) \quad (3.17)$$

q_{rxn} is the heat generated per unit area at the electrode surface, i_{rxn} is the current density at the electrode, η represents the irreversible losses while the $\frac{\partial E_{eq}}{\partial T}$ term represents reversible heat change due to the change in entropy of the system. The reversible term is neglected as we are applying an AC signal where the reversible changes cancel out over a single cycle. The heat dissipated in the double layer because of capacitive losses is given by

$$q_{S,cap} = V_{cap}^2 \cdot \omega \cdot C_{dl} \cdot DF \tag{3.18}$$

V_{cap} is the RMS potential (V) across the interfacial double layer which is found to be 0.23V using the Debye-Huckel formulation (Israelachvili 1992), ω is the frequency of the applied signal, C_{dl} is the specific capacitance (Fm^{-2}) of the double layer and DF is the *dissipation factor* signifying energy dissipated as heat in the dielectric. For the double layer interface, the dielectric is assumed to be water, which has a DF of 0.05 (Von Hippel 1954).

Another source of heat is the Ohmic or Joule heating due to ionic fluxes in the bulk electrolyte. This is given by

$$Q_{bulk} = \sum[J_i \cdot \vec{\nabla} V(\vec{x})] \tag{3.19}$$

Q_{bulk} is the heat generated per unit area and J_i is the flux of species *i* in the medium (in this case, the CSF). This term is applicable to the bulk electrolyte. We will be considering these heat sources in our electrochemical model. More details are discussed in Chapter VIII.

I. Conclusion

Biological media such as CSF are ionic conductors, and the introduction of a metallic electrode in such media always forms an electrode-electrolyte interface. The interfacial properties significantly influence the effects of an external electrical signal on such media. It is therefore important that interfacial phenomena are accounted for in our computational model. EIS measurements were carried out to study the interfacial impedance properties. Measurements indicate that the electrical double layer capacitance as well as charge transfer reactions both contribute to the total electrical current in the system. This must be reflected in the study of electrical heating in CSF by an external AC signal.

IV. EFFECT OF AC SIGNALS ON CELLS IN CULTURE

A. Summary

Cell death due to low-voltage Joule heating was verified on cells cultured in a plate. C6, a fast-growing and resilient Rat Glioma cell line available in our lab was used for these experiments. The alternating signal was applied to stainless steel electrodes in a circular configuration and cell viability was assessed by performing a tetrazolium MTT viability assay. The clearance zone was quantified by measuring the colorless area using a standard $1mm^2$ grid. The cause of cell death was verified to be thermal cell death by using a water bath restrict excess heating. The temperature elevation was measured by thermistors in the observed clear zone to verify the temperature elevation corresponds to classical hyperthermia.

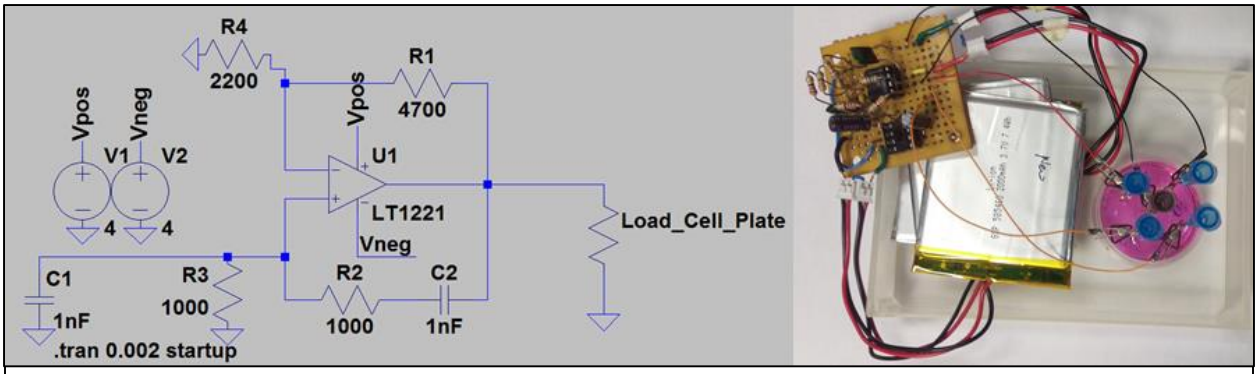

Fig. 8: Instrumentation for experiments on cells in culture. LTSpice circuit diagram of AC signal generator, using a Wein-Bridge oscillator (Left). A picture of the assembled circuit on a PCB is shown at the right. The AC signal is applied to stainless steel electrodes by alligator clips. The circuit is powered by Li-ion batteries (4.2V, 3000 mAh).

B. Instrumentation

A Wein-Bridge oscillator was assembled on a printed circuit board using discrete electronic components. The circuit was powered by a battery of 2 or 3 rechargeable Polymer Li-ion cells (Sparkfun) so as to enable keeping the entire assembly inside an incubator. The frequency of the signal generated could be modified by changing the value of resistors R1, R2 and C1, C2. The output of the signal generator was tested on an oscilloscope. A small series resistor (68Ω) was

placed in series with the output pin to measure the current drawn by the load, which varied based on the experiment.

C. In-vitro testing of cell death induced by applied electrical signal

The heating effect of alternating current was tested on a cell monolayer cultured in a plate. C6 glioma cells were plated in a 35 mm poly-d-lysine coated plate till it attains confluency. Stainless steel injection needles (25G and 18G) were fixed 1cm apart on a 35 mm culture dish cover using epoxy resin in a circular configuration as shown in Fig 4. The assembled circuit was connected to the electrodes by miniature alligator clips. After verifying the output signal and determining the current drawn by measuring the drop across the series resistor, the assembly was incubated at 37°C for 2 hours, 4 hours, 8 hours and 24 hours. The signal generation and electrode assembly was removed from the plate and the cells were allowed to re-equilibrate at 37°C for 1 hour, followed by an MTT assay. The cells unaffected by the treatment stained purple, while the clear zone indicated the zone of dead cells. To prove that the effect was due to heat, and not any other effect of electric fields, the cell plate was kept in a water bath, to act as a heat sink for the same duration as before.

A thermistor (NTC, 10kΩ) was suspended and the temperature measured in the plate at various locations until they remained steady. A multimeter (Elenco M-1750) in resistance measurement mode (source current approx. 17 μA at 10kΩ) was used to measure the thermistor's resistance periodically. The resistance was converted to the measured temperature using the Steinhart's equation (Eqn. 4.1), with the relevant coefficients obtained from the thermistor's specification sheet.

$$\frac{1}{T} = A + B \cdot ln\frac{R}{Rt} + C \cdot (ln\frac{R}{Rt})^2 + D \cdot (ln\frac{R}{Rt})^3 \quad (4.1)$$

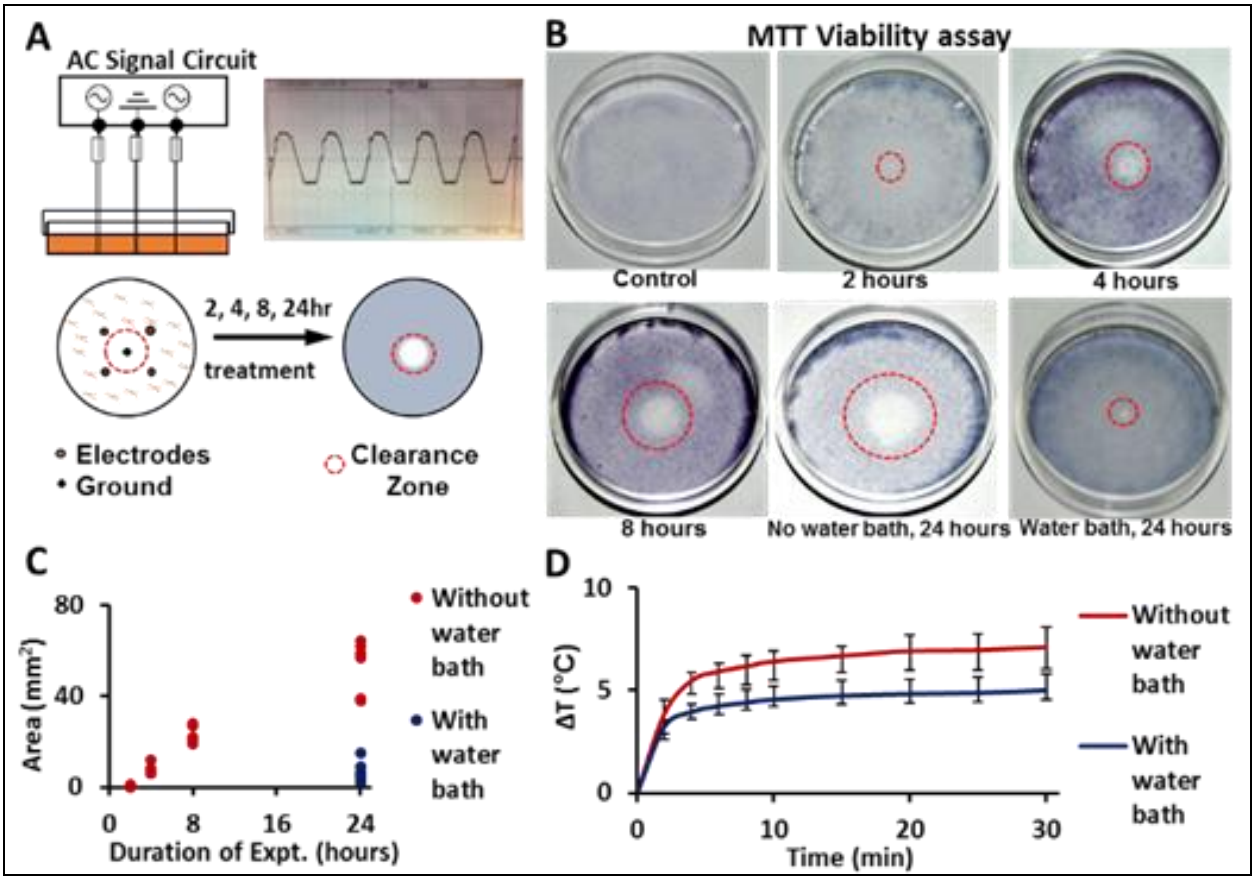

Fig 9: AC potential induces cell death in cells in culture by hyperthermia. (A) C6 Glioma monolayers cultured in 35 mm plates were exposed to a low-voltage AC signal to induce resistive heating in the medium. The generated waveform applied to the electrodes is shown in the inset. Experiments show that a circular configuration of electrodes successfully destroys cells to form a zone of cell death (red circles) around the central electrode. (B) Representative images of experimental cell plates shown using an MTT viability assay performed after exposure to 0 (control), 2, 4, 8 and 24 hours of Joule heating, as well as one with a water bath to decrease temperature elevation. Keeping a water bath outside the cell plate during electrical treatment decreases the cell death area measured by the MTT viability assay. (C) The effect of exposure durations on cell death area. Blue circles indicate the presence of a water bath to control temperature elevation (D) Temperature measurements verified heating as the cause of cell death. A smaller temperature rise was observed due to the presence of the water bath which acted as a heat sink. The measurements were performed under ambient conditions in DMEM medium using a thermistor placed close to the central ground electrode (coinciding with the observed region of cell death).

where T is the temperature in Kelvin, R is the measured resistance at temperature T, Rt is the nominal resistance at ambient temperature (10kΩ at 25°C), and coefficients A, B, C and D are obtained from the product specification sheet (A=3.354E-03, B=2.562E-04, C=2.082E-06,

D=7.300E-07). The resistance of the thermistor was calculated from the voltage measured across it and was compared with the resistance table in its specification sheet.

D. Results

Fig. 9 shows the action of Joule heating on a C6 glioma cell monolayer in a plate. The electrode configuration adopted leads to a higher current density and a corresponding higher temperature due to Joule heating at the central electrode. Cells that are alive take up the MTT dye and stain purple, enabling visual quantification of the area of zone of cell death. This region encircles the central electrode and depends on the duration of the applied signal, and representative experimental plates for each duration is shown for various experimental durations in Fig 9B. The region of cells affected significantly decreases by placing an external water bath around the cell culture plate that acts as a heat sink. The average area of the dead cell zone by the treatment while in a heat sink was found to be 7.04±4.51mm^2, with maximum area of 15 mm^2 after a 24 hour treatment (n=6). The external bath reduced the extent of temperature elevation to an average of 5°C, as compared to 7.1°C without the external water bath near the central electrode in the cell culture medium in the plate, as shown in Fig 9C. In a biological implant, this will be less than the damage threshold of 43°C. This observation verified our hypothesis that the cell clearance effect was because of the heat generated in the conductive culture medium by resistive or Joule heating. Fig 9D shows a plot of the area of dead cells measured using a standard grid of squares is observed to increase from an average of 8±2.45mm^2 after 4 hours treatment to 47.428±18.51mm^2 after 24 hours.

E. Conclusion

From our experiments as explained above, we showed that low-voltage Joule heating can induce cell death on cells in culture. The significantly smaller clearance zone in the presence of a

water bath establishes the cause of death to be thermal in nature. Temperature measurements verified that the induced heat causes cell death by classical hyperthermia. We then proceeded to test whether the heating effect can be localized to the lumen of a catheter.

V. LOCALIZATION OF HYPERTHERMIA IN A MOCK VENTRICULAR CATHETER

A. Summary

The localization of the thermal effects of our applied signal to the catheter lumen was tested. A cell suspension was gently introduced in the lumen of a mock ventricular catheter and allowed to proliferate for 3 days. The seeded catheter was suspended a separate external cell layer in a 35mm plate. The alternating signal was applied to luminal electrodes for a period of 24 hours and then the viability of the cells was determined by performing an MTT assay. Temperature measurements were carried out as before to determine the temperature elevation inside the catheter lumen and in the external medium 5 mm away from the catheter wall.

B. Methods

To prepare a mock ventricular shunt, medical grade silicone tube was cut in pieces of length 3cm, and rows of drain holes were punched using a needle. Pt ring electrodes (Johnson Matthey Inc., West Chester, PA) with insulation coated Pt lead wires spot (A-M Systems, Sequim, WA) welded to them were inserted into the lumen such that the leads were protruding outside from the drain holes and could be connected to the alternating signal generation PCB. C6 cells suspended in DMEM medium and injected gently inside the lumen and the mock shunt was submerged in fresh DMEM medium and incubated for 4-6 days. A separate plate of C6 cells was prepared till 75% confluency. The mock ventricular shunt was suspended in the C6 plate such that the exposed part of the leads are accessible through the lid of the plate and the shunt is not in contact with the cells adhered at the bottom, as shown in Fig 10A. The cells inside the lumen were treated for a duration of 4 hours and 24 hours, followed by incubation at 37°C for 1 hour and a viability assay.

The temperature of the cell culture medium inside and outside the lumen of the mock shunt was measured until it remained steady using a thermistor to verify that the temperature profile outside the catheter due to resistive heating would not be injurious to external tissue, such as the ventricle walls. A thermistor (NTC, 10kΩ) was used to measure the temperature inside and outside the lumen of the mock shunt as previously described.

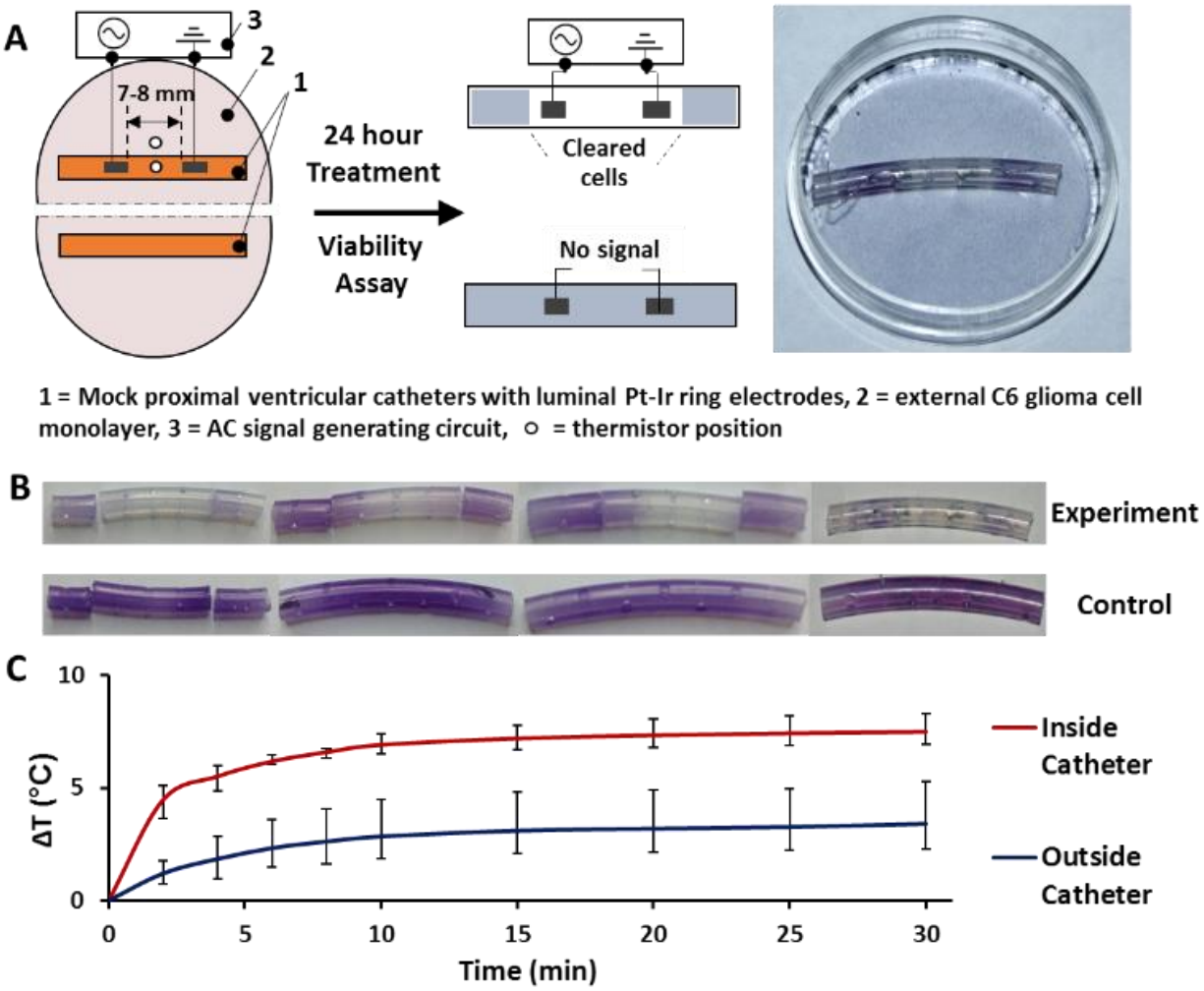

Fig 10: Localized effect of hyperthermia induced by AC potential on a C6 cell monolayer in a mock proximal ventricular catheter. The schematic of the experimental setup is shown in (A). Cells in the region between the luminal electrodes inside the proximal ventricular catheter are killed, while the cell monolayer in the external plate are unaffected after performing the MTT viability assay (right) (B) Representative images of experimental (top) and control catheters (bottom). A clear zone is seen in the middle of the experimental catheters which corresponds to the region between and around the luminal electrodes (n = 6). (C) Temperature measurements inside and outside the catheter (marked by black circles in panel A) show that heating is significantly greater inside the catheter lumen.

C. Results

Low-voltage Joule heating was successful in clearing cells seeded in the mock ventricular catheter lumen. Fig. 10B shows 4 samples of the mock ventricular shunts seeded with C6 glioma cells, with the shunts exposed to the electrical treatment induced hyperthermia at the top, and control shunts with no treatment at the bottom. A clear zone is seen in the middle of the catheter between the electrodes of the shunts exposed to hyperthermia. The cells outside the catheter in the external cell culture plate were not killed, as they stained purple after an MTT assay. One such external plate of cells is shown to the right in Fig 10A. Silicone is a poor conductor electricity and concentrates most of the applied alternating signal to the lumen of the silicone shunt. It helps in confining the heating effect to the lumen of the shunt and protects cells in the exterior. Temperature measurements carried out under ambient conditions in DMEM culture medium using thermistors indicated that temperature elevation rises up to 7°C in 10 minutes (Fig. 10C) and remains steady after that period inside the lumen. This will result in a temperature $\leq$ 44°C when the assembly is placed in a cell culture incubator (Set temperature 37°C) or in a biological tissue, which again falls in the range of hyperthermia.

D. Conclusion

The complete staining of the external cells after the viability assay demonstrate that the hyperthermia by Joule heating can be localized in the mock ventricular catheter lumen. We hypothesize that property of silicone being an electrical insulator aids in confining the current to the lumen of the catheter and around its ports. We believe that this method may be a possible candidate to further our aim to develop a self-clearing ventricular catheter.

VI. COMPUTATIONAL MODELING OF HYPERTHERMIA

A. Summary

A 3D model of a ventricular catheter implanted in a simplified lateral ventricular cavity surrounded by a layer of cerebral tissue was developed to validate our experimental observations based on a theoretical framework. Simulations were performed using the COMSOL MULTIPHYSICS v5.2 (Burlington, MA) to determine the current and temperature distribution in our model domain consisting of a ventricular catheter, the surrounding CSF-filled ventricular space and a layer of periventricular tissue. We considered 2 models that treated the medium conducting electrical signals in different ways – (i) a purely resistive model in which the medium was assumed to behave as a simple ohmic conductor and (ii) an electrochemical model in which we considered the medium to be an ionic conductor i.e. an electrolyte. In both models, we studied the predicted spatial distribution of the temperature and the current density to validate our experimental observations.

B. Model I – Resistive electrical model

In this model, we consider the CSF and the brain tissue domains to be ohmic conductors, each having an isotropic bulk conductivity. The different materials are assumed to exhibit no losses at contacting surfaces. An electric current flowing through a domain in this model generates heat purely by resistive or Joule heating in the bulk. The advantage of such a simplified model is that the resulting system of equation may be rapidly assembled and solved, even for a 3D geometry.

1. Model geometry

Our geometry consists of a ventricular catheter implanted in a lateral ventricle. The catheter was modeled on the basis of a commercially available ventricular

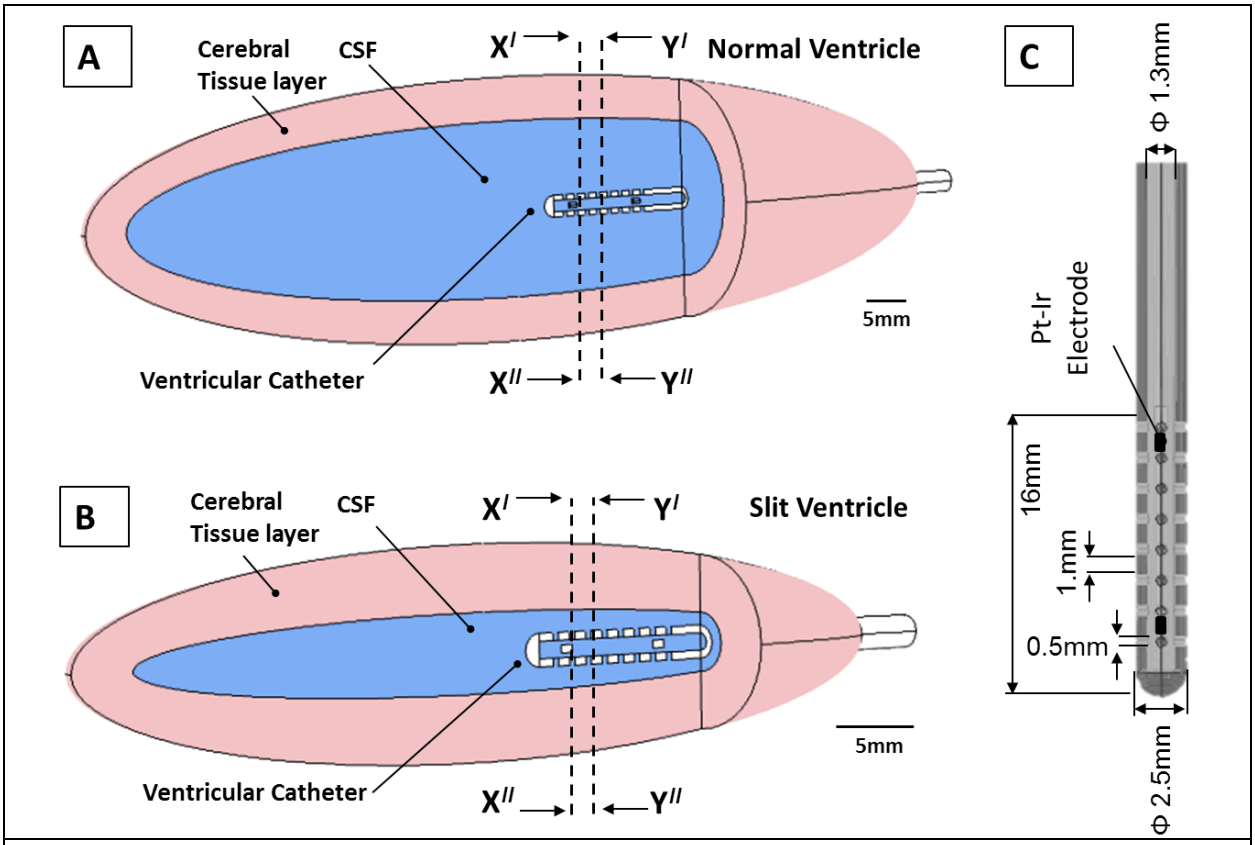

Fig. 11. Model of an implanted catheter in (A) a normal ventricle with a volume of 20.9ml. The ventricular cavity is simplified as an ellipsoid with a lateral semi-axis 10 mm. (B) A slit ventricle with a volume of 1.15ml. The ventricular cavity is simplified as an ellipsoid with lateral semi-axis 3mm. Lines X' – X" and Y' – Y" mark the planes at which a 2D heat map and line graphs of the temperature and current density are plotted. (C) The ventricular catheter modeled from specifications obtained from a commercially used catheter.

catheter (Standard Medtronic, I.D. 1.3mm, O.D. 2.5mm) shown in Fig. 11C (Medtronic, MN 2017b). Relevant material properties of CSF and silicone were taken from literature (Nelson and Nunneley 1998; Smith and Zhu 2010; A. Linninger et al. 2009) and COMSOL's material library, shown in Table I. Electrodes were positioned around the port area, to concentrate heating in that region. The lateral ventricle was approximated as an ellipsoid, surrounded by a brain tissue layer of thickness 5mm. The tissue layer allowed us to get a more accurate impact of the generated heat on the temperatures at the periventricular tissue forming the ventricular wall. We considered 2 cases: a normal sized ventricle (Fig. 11A) and a slit ventricle where the

catheter is in close proximity to the ventricular wall (Fig. 11B). In both cases, the catheter is assumed to be optimally placed in the center of the ventricle, equidistant from the ventricular walls.

2. Computational model

The electric field generated by the signal applied to the luminal electrodes is solved using Laplace's Equation (Eqn. 2).

$$\vec{\nabla} \cdot \left[\sigma \vec{\nabla} V(\vec{x})\right] = 0 \tag{6.1}$$

Here, $\vec{\nabla}$ is the gradient operator, σ is electrical conductivity, and $V(\vec{x})$ is the electric potential. Although we use an alternating current signal, we solve this equation at steady-state using RMS values as signal parameters. A spatial map of the potential and local current density is obtained after solving Eqn. (7.1). These are then used in the heat conductivity equation as factors in a heat source term. The temperature profile is obtained by solving a simplified version of Penne's Bioheat equation, which is a steady-state heat conductivity equation in a biological setting

$$\vec{\nabla} \cdot \left[k \vec{\nabla} T(\vec{x})\right] + \sigma \left\| \vec{\nabla} V(\vec{x}) \right\|^2 - Q_t = 0 \tag{6.2}$$

Here, k is the thermal conductivity of CSF, $\sigma \left\| \vec{\nabla} V(\vec{x}) \right\|^2$ is the heat source term, which in this case will be the heat generated by alternating electric current induced resistive heating. At relatively low frequencies (0.1 – 100 MHz), the electrical signal applied to electrodes will induce ionic currents that will generate heat by resistive or Joule heating. At higher frequencies that typically fall in the microwave range, (100 MHz to 100 GHz), dielectric heating where molecules vibrate without translational motion is the more significant contributor to heat generation. At our signal frequency (500 kHz), we assume Joule heating to be the primary

mode of heat generation. A 5mm thick layer of tissue is modeled around the ventricle. This region of the brain is heavily perfused by blood through a dense capillary network. This will act as a heat sink and is modeled by including a term Q_t given by Eqn. (6.3).

$$Q_t = \rho_b w_t C_{p_b}[T(\vec{x}) - T_b] \tag{6.3}$$

where ρ_b is the density of blood, w_t is the perfusion coefficient for brain, C_{p_b} is the specific heat capacity of blood, T_b is the temperature of blood that is assumed to be 310.15K. The tissue and blood are assumed to be in thermal equilibrium at steady state.

3. Initial and Boundary conditions for Field Potential $V(\vec{x})$

The initial field potential was assumed to be 0V at all points of the model. We use monopolar Joule heating for our method of inducing hyperthermia. Each luminal electrode was assigned to be a constant current source with an RMS value of 12.5 mA. The outer surface of the tissue layer surrounding the ventricular fluid space was set at zero potential as a Dirichlet condition.

$$V_\Omega(\vec{x}) = 0 \tag{6.4}$$

TABLE I
MATERIAL PROPERTIES FOR SIMULATIONS IN THE RESISTIVE ELECTRICAL MODEL

Parameter	CSF	Silicone	Brain Tissue	Blood
σ (S/m)	2	10^{-6}	0.2	-
k (W/mK)	0.61	0.25	0.52	-
ρ (kg/m^3)	1000	-	1079	1057
ε_r	80	20	150	-
C_p (J/kgK)	-	-	-	3600
w_t (ml/s/cm^3)	-	-	-	0.01

σ is the electrical conductivity, k is the thermal conductivity, ρ is the density, ε_r is the relative permittivity, C_p is the specific heat capacity, w_t is the blood perfusion in a tissue.

where Ω is the outer surface bounding the tissue layer. The catheter walls were included in electrical conduction step for greater accuracy, even though silicone is an electrically insulating material. [$\sigma_{silicone}$ (10^{-6} S/m) <<< σ_{CSF} (2 S/m)].

4. Initial and Boundary conditions for Heat Transfer

The initial temperature of the catheter, CSF, blood and the tissue layer was chosen as the core body temperature of 310.15K. The tissue that makes up the ventricular boundary is interspersed with extracellular fluid and a high rate of blood perfusion via capillaries that could act as an effective sink to extract any heat that exits the CSF. We use a thermally insulating condition using a Neumann boundary to predict the maximum temperature rise in the modeled ventricular space and surrounding cerebral tissue.

$$\overrightarrow{q_\Omega} = 0 \tag{6.5}$$

where $\overrightarrow{q_\Omega}$ is the heat flux normal to the bounding surface Ω of the tissue layer surrounding the lateral ventricle. We also neglect the effects of CSF pulsations and convective flow in the ventricular space that can also distribute the generated heat more evenly. Since we were expecting a moderate temperature elevation (<10°C), the material properties were assumed to be independent of temperature.

C. Results – Resistive electrical model

We carried out simulations to predict the temperature profile in an implanted ventricular catheter and we find that they support our experimental results. Fig 12A shows the temperature map in the center-plane of the model at steady state due to the application of 12.5mA alternating current to each of the 2 luminal electrodes for a normal ventricle. Figs 12B and 12C show the temperature and current density on a transverse line in the plane in two regions (1) lane X′ – X″ near a luminal electrode and a port, (2) plane Y′ – Y″ between the luminal electrodes. We see that

both the temperature elevation and current density is most prominent close to the electrodes, and falls sharply with distance from the modeled catheter. The current density was maximum at the electrodes, with a value of 630.65 $mAcm^{-2}$ inside the shunt lumen. This is also the site of

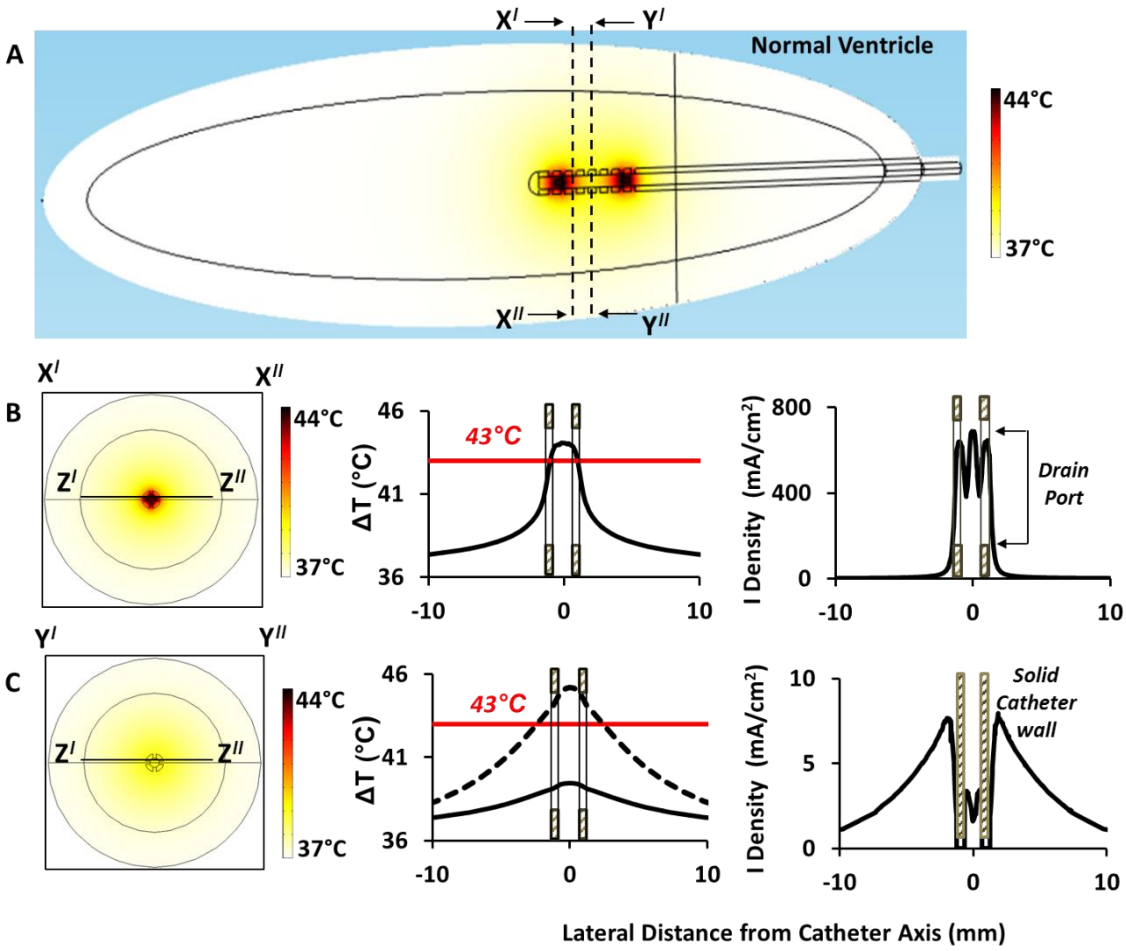

Fig. 12: Simulation results for a ventricular catheter implanted in a normal ventricle. Temperature and current density distributions are extracted from the model solutions. (A) Heat map in the central plane of the model. (B) Heat map in a cut section along plane X′ – X″ close to a luminal electrode. The temperature and current density are plotted versus distance from catheter central axis along the centerline Z′ – Z″. (C) Heat map in a cut section along plane Y′ – Y″ between the electrodes. The temperature and current density are plotted versus distance from catheter central axis along the centerline Z′ – Z″.

maximum temperature elevation, (6.84°C for a slit ventricle geometry and 7.05°C for a normal sized ventricle geometry). External to the catheter, current density was significantly lower at < $10mAcm^{-2}$ due to the insulating nature of the silicone catheter.

The slit ventricle is an extreme case in which the tissue layer at the ventricular will be exposed to maximum current flow and correspondingly the largest thermal dose because of the

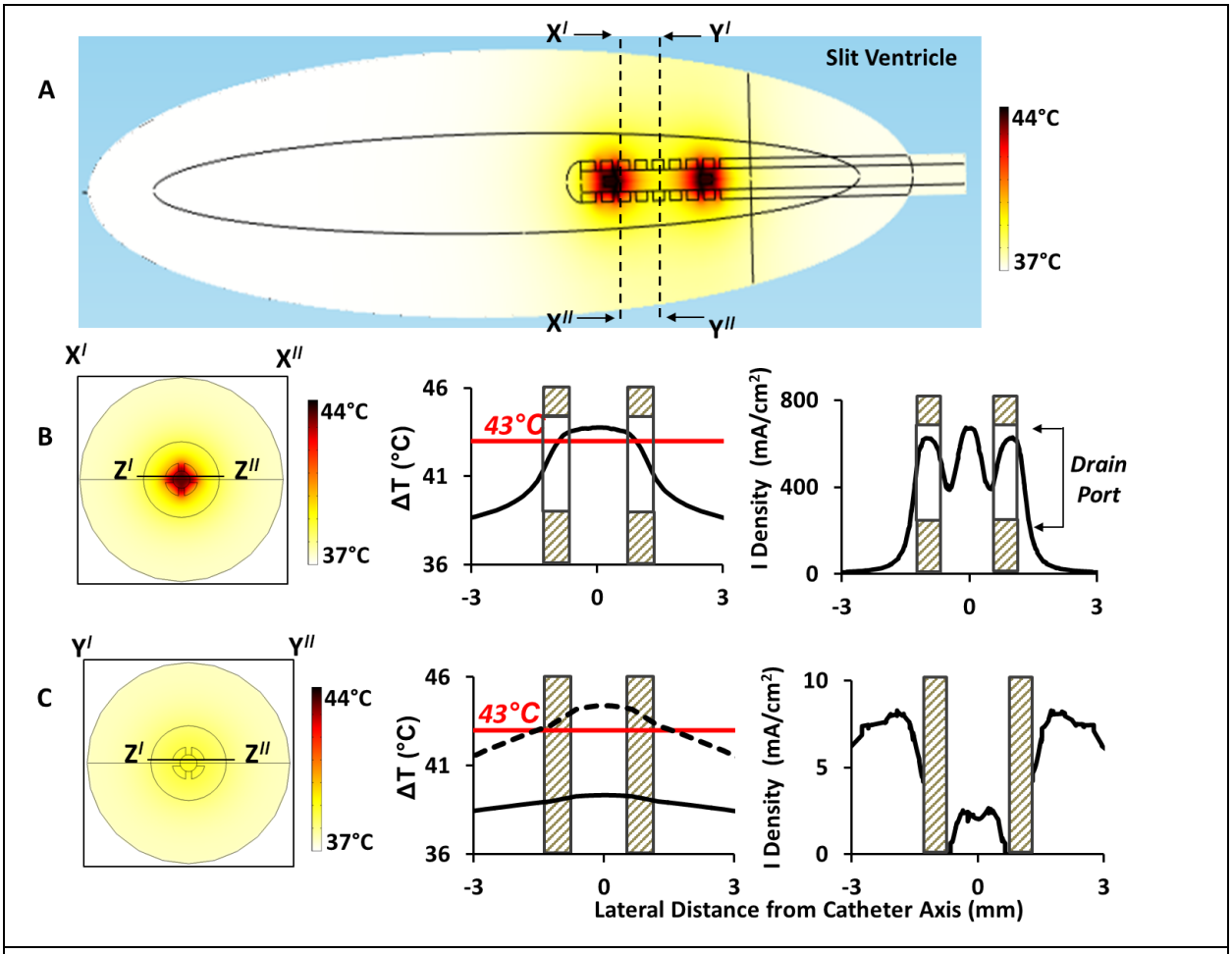

Fig. 13: Simulation results for a ventricular catheter implanted in a slit ventricle. Temperature and current density distributions after low-voltage Joule heating in a catheter implanted in a slit ventricle. (A) Heat map in the central plane of the model. (B) Heat map in a cut section along plane X′ – X″ close to a luminal electrode. The temperature and current density are plotted versus distance from catheter central axis along the centerline Z′ – Z″. (C) Heat map in a cut section along plane Y′ – Y″ between the electrodes. The temperature and current density are plotted vs versus the distance from the central axis of the catheter along the centerline Z′–Z″.

proximity of the catheter to the walls. The maximum temperature elevation at the boundary was found to be 38.8°C (Fig. 13). In case of a normal sized ventricle, the temperature at the boundary of the lateral ventricle increased by 0.46°C. In both cases, the ventricular wall remains < 40°C at steady state which is insufficient to severely harm neighboring brain tissue. The effect is thus

believed to be localized to the shunt lumen and the ports, which are the most commonly obstructed sites. In an implanted ventricular catheter, our objective is to disintegrate the cellular material obstructing the catheter without harming the tissue layer lining the lateral ventricle. This supports our hypothesis that hyperthermia can be locally induced using Joule heating in the CSF filled ventricle and can be utilized to clear cellular obstruction of the catheter.

The current design has obvious limitations, such as insufficient thermal dose delivered to the region between the electrodes (Figs. 12C and 13C). The electrode configuration and signal parameters we chose for the simulation were to mimic the experimental conditions we used previously. We increased the strength of our applied signal and determined that the threshold of cellular damage is only exceeded at the boundary of the lateral ventricle in the slit ventricle case with a 50mA RMS current applied to the luminal electrodes (shown in bold). The maximum predicted temperatures in different model domains after applying alternating currents of various intensities are listed in Table II.

TABLE II
PREDICTED MAXIMUM TEMPERATURES IN DIFFERENT DOMAINS AT VARIOUS CURRENT INTENSITIES

RMS Current (mA)	Maximum Temperature (°C) Normal ventricle			Maximum Temperature (°C) Slit Ventricle		
	Luminal CSF	Ventricular Wall	Tissue Outer Surface	Luminal CSF	Ventricular Wall	Tissue Outer Surface
10mA	38.27°C	37.07°C	37.03°C	38.20°C	37.34°C	37.13°C
20mA	42.07°C	37.28°C	37.13°C	41.82°C	38.36°C	37.52°C
30mA	48.41°C	37.64°C	37.28°C	47.84°C	40.06°C	38.17°C
40mA	57.28°C	38.13°C	37.50°C	56.27°C	42.43°C	39.08°C
50mA	68.69°C	38.77°C	37.78°C	67.12°C	**45.49°C**	40.25°C

D. Model II – Electrochemical model

This model accounts for electrochemical reactions and concentration polarization that occur in case of an externally applied potential to an electrochemical system, and that are often neglected in a simple resistive electrical model such as Model 1. Biological media such as tissues and fluids like CSF are electrolytes where the charge carriers are the ionic solutes present in the electrolyte. The conductivity of these media depend on the ionic composition and the ionic concentrations. The presence of an electrode-electrolyte interface also influences the effects of an external potential in the medium. The electrochemical model was created to account for these factors.

We performed a transient simulation over 1 cycle (2μs) of our alternating signal (with a frequency f = 500 kHz) to determine the ionic flux, current density and potential distribution in CSF in response to the changing potential at the electrodes. The time-averaged current density obtained from the electrochemical cell model was used in the bulk heat-source term (Q_{bulk}), whereas the time-averaged kinetic overpotential at the electrode surface and capacitive heat dissipation was used in the boundary heat-source terms ($q_{S,rxn}$ and $q_{S,cap}$) of the heat-transfer equation to predict temperature rise in the CSF and tissue regions of our model.

1. Electrochemical system

The electrochemical system in this model consists of CSF as the electrolyte and Pt-Ir electrodes as metallic electrodes. CSF composition is given in Table III. Since water is the most abundant molecule in our system and we assume reactions involving water to be the dominant reactions occurring in response to an external potential at the electrodes. One of the electrodes behaves as the anode, which is the site of oxidation of water to oxygen. The other

electrode behaves as a cathode and is the site of reduction of water to hydrogen. The reaction at the anode (+electrode) is known as the Oxygen Evolution Reaction (O.E.R) according to:

$$2H_2O \rightarrow 4e^- + O_{2_{(gas)}} + 4H^+ \tag{6.6}$$

with a standard equilibrium potential of 1.23V (Vanysek 2003). At the cathode, the reaction is termed the Hydrogen Evolution Reaction (H.E.R). If the medium is neutral or alkaline pH, water is reduced to yield hydrogen gas and hydroxide ions, which has a standard equilibrium potential of -0.83V and is given in Eqn. (7.7):

$$2H_2O + 2e^- \rightarrow H_{2_{(gas)}} + 2OH^- \tag{6.7}$$

The net reaction of hydrolysis in the system is obtained by adding equations (6.6) and (6.7).

$$2H_2O \rightarrow O_{2_{(gas)}} + 2H_{2_{(gas)}} \tag{6.8}$$

Additionally, the equilibrium between $H^+$and OH^- concentration is given by the dissociation of water as in (6.9)

$$H_2O \overset{K_w}{\leftrightarrow} H^+ + OH^- \tag{6.9}$$

Table III
CHEMICAL SPECIES PARAMETERS (Baştuğ and Kuyucak 2005; M. R. Singh et al. 2015)

Species	Initial Conc. (M)	Diffusion Coeff. (x $10^9\ m^2/s$)*	Mobility (x10^7 $m^2V^{-1}s^{-1}$)
H^+	4E-8	9.311	3.486
OH^-	2.5E-7	5.273	1.974
Cl^-	0.145	2.032	0.760
Na^+	0.145	2.032	0.760
H_2O	55.55(Excess)	-	-

* Diffusion coefficients at 298 K are used as the closest available in literature for our model temperature of 310K

where the ionic product K_w is 10^{-14}. These reactions at the electrode-electrolyte interface influence the potential map in the electrolyte and the resulting ionic fluxes in this model.

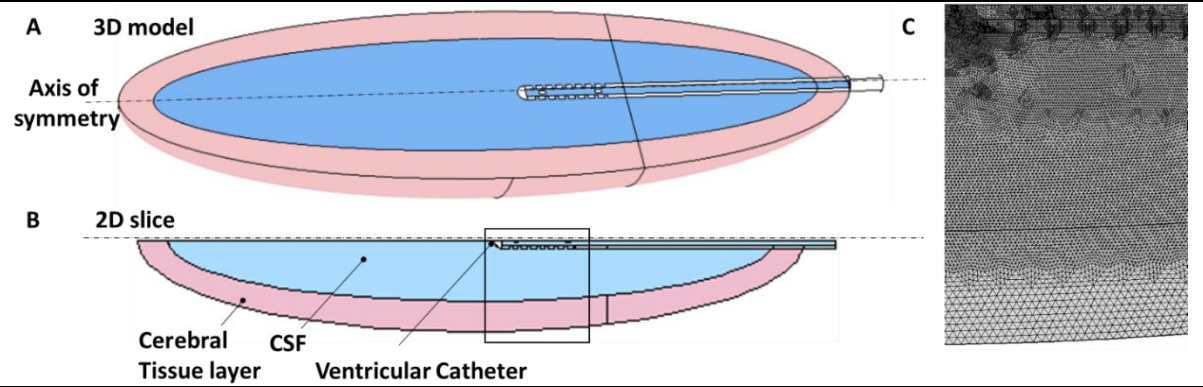

Fig 14: 2D electrochemical model domain for a normal ventricular geometry. Taking advantage of the rotational symmetry about the axis, shown in (A), a 2D slice of the 3D geometry is extracted and used to compute ionic fluxes and temperature elevation. Panel C is a part of the fine 2D unstructured triangular mesh (Panel B, black square) used for the analysis.

2. Model Geometry

We used the same geometry as that in Model 1, Fig. 11A and 11B. However, to reduce computational time, we took advantage of the axial symmetry of our model and performed simulations on a single 2D slice. The 2D slice, divided using an unstructured triangular mesh, was composed of 108,144 elements for the normal ventricle and 96,400 for the slit ventricle. A part of the mesh created for the slice of a normal ventricular geometry is shown in Fig 14, and mesh statistics obtained from COMSOL are tabulated in Table IV. An average element quality > 0.7 and minimum element quality > 0.1 can be considered to be acceptable.

Table IV
2D MESH STATISTICS

Description	Value
Minimum element quality	0.2142
Average element quality	0.9596
Triangular elements	95974
Edge elements	2408
Vertex elements	49

3. Computational model

A transient simulation was performed over 1 cycle (2μs) of the applied waveform (f = 500 kHz) to determine the ionic motion in CSF in response to the changing potential at the electrodes. The transient step solves the Nernst-Plank formulation (6.11-6.14), which is valid for dilute solutions and is performed on the fluid domain to predict the transport of ionic species under the influence of a time-varying alternating signal Eqn. (6.10).

$$V_{electrode} = V_0 \cdot \sin(\omega t) \tag{6.10}$$

where V_0 is the amplitude (10V) and ω is the angular frequency of the applied signal. The Nernst-Plank equations are given in equations (6.11-6.14):

$$\frac{\partial c_i}{\partial t} + \vec{\nabla} . \vec{\boldsymbol{J}}_{\boldsymbol{i}} = 0 \tag{6.11}$$

$$\vec{\boldsymbol{J}}_{\boldsymbol{i}} = -D_i \vec{\nabla} c_i - z_i \mu_i F c_i \vec{\nabla} V(\vec{\boldsymbol{x}}) + \vec{\boldsymbol{u}} . \vec{\nabla} c_i \tag{6.12}$$

$$\vec{\nabla} \cdot \sum_i z_i F \vec{\boldsymbol{J}}_{\boldsymbol{i}} = 0 \tag{6.13}$$

$$\sum_i z_i \cdot c_i = 0 \tag{6.14}$$

Here, for each ion *i*, c_i is the concentration, D_i is the Diffusion coefficient (m^2s^{-1}), z_i is the charge number, z_i is the charge number. μ_i is the ionic mobility ($m^2s^{-1}V^{-1}$), F is Faraday's constant ($96500 Cmol^{-1}$), and $\vec{J}_i$ is the ionic flux. $\sum_i z_i F \vec{\boldsymbol{J}}_i$ summed over all ions in CSF is equal to the electrolyte current density. $V(\vec{\boldsymbol{x}})$ is the potential at position vector $\vec{\boldsymbol{x}}$, and $\vec{\boldsymbol{u}}$ is the velocity vector of the bulk fluid. (6.11) indicates the conservation of mass in the system, (6.12) is the net sum of fluxes including diffusion and migration, (6.13) represents the conservation of charge and (6.14) denotes that electroneutrality is upheld in the system. Since the bulk fluid is assumed to be stationary ($\vec{\boldsymbol{u}} = 0$), fluid convection does not influence ionic transport and are therefore neglected. The mobility of a species *i* is given by the Nernst-Einstein relation

$$\mu_i = {}^{D_i \cdot F}/_{R \cdot T} \tag{6.15}$$

where R is the ideal gas constant (8.314 $Jmol^{-1}K^{-1}$) and T is the temperature in K. The electrical current generated at the electrode because of the overpotential η is given by the Butler-Volmer equation shown below

$$i_{rxn} = i_0 \cdot \left(e^{\alpha_a F\eta/RT} - e^{-\alpha_c F\eta/RT}\right) \quad (6.16)$$

Here, i_{rxn} is the current density in Am^{-2}, η is the overpotential at the electrode, i_0 is the equilibrium current density for the electrochemical reaction occurring at the electrode, *T* is the temperature in Kelvins, α_a and α_c are the anodic and cathodic coefficients that quantify the symmetry of the equilibrium electrochemical reactions occurring at the electrode surface. Electrochemical reaction parameters for both O.E.R and H.E.R are provided in Table V.

The overpotential η at the interface is defined in Eqn. (6.17)

$$\eta = V_{electrode} - V_{electrolyte} - E_0 \quad (6.17)$$

where $V_{electrode}$ is the externally applied potential, $V_{electrolyte}$ is the potential in the electrolyte next to the electrode and E_0 is the equilibrium potential for the species reaction. The equilibrium potentials, computed based on the Nernst Equation, are pH dependent and vary based on the instantaneous H^+ concentration at the electrodes. For the O.E.R, E_0 is given by Eqn. (6.18).

$$E_0 = E_0^{std} - \frac{2.303RT}{nF} pH \quad (6.18)$$

Here, E_0^{std} is 1.23V and n is the stoichiometric coefficient of the reaction. For the H.E.R, E_0 varies according to OH^- concentration and is therefore, again pH dependent given by (S10) with E_0^{std} is -0.83V (Vanysek 2003).

$$E_0 = E_0^{std} + \frac{2.303RT}{nF} pOH \quad (6.19)$$

Since we use an AC signal, the role of anode and cathode are switched in the second half of the cycle.

TABLE V.
ELECTROCHEMICAL REACTION PARAMETERS (M. R. Singh et al. 2015)

PARAMETER	O.E.R	H.E.R
α_A	1.0	2.57
α_C	0.1	2.57
i_0[Am^{-2}]	1.4E-3	10

In addition to the reactive current, a capacitive current is also induced in the electrolyte because of the interfacial double layer. This capacitive current density i_{cap} is given by Eqn. (6.20).

$$i_{cap} = C_{dl} \cdot \frac{dV_{electrode}}{dt} \quad (6.20)$$

C_{dl} is the double layer specific capacitance (Fm^{-2}). The electrochemical parameters for hydrolysis are obtained from literature Table VI,(M. R. Singh et al. 2015). The total capacitance of the electrodes was measured to be 8.9 nF using electrochemical impedance spectroscopy. The net interfacial current I_{total} is the sum of the reactive and capacitive currents.

$$I_{total} = A_{elec} \cdot (i_{rxn} + i_{cap}) \quad (6.21)$$

where A_{elec} is the surface area of the electrode and i_{rxn} and i_{cap} are as above. This system of equations (7.10-7.21) is solved over a complete cycle of the waveform (2µs) to determine the ionic current density profile in the electrolyte i.e. CSF.

The time-averaged electrical current densities and overpotentials were used to calculate the heat generated in our model and then used to solve a steady-state heat transfer equation without flow representing a non-draining ventricular catheter in Eqn. (6.22).

$$0 = \vec{\nabla} \cdot \left[k\vec{\nabla}T(\vec{x})\right] + Q_{bulk} + Q_t \quad (6.22)$$

Here, $T(\vec{x})$ is the temperature at position $\vec{x}$, k is the thermal conductivity and Q_{bulk} is the heat generated in the bulk CSF and Q_t is the heat removed by capillary blood perfusion in the tissue layer. Thermal properties of all materials in this model are listed in Table VI.

4. Heat sources

We introduced heat sources that may occur in an electrochemical system in Chapter IV. Here, we use included the following sources in the model.

Heat source in CSF: The energy added to the domain by Joule heating in the bulk electrolyte is given by

$$Q_{bulk} = \vec{\nabla}V(\vec{x}) \cdot \sum_i \left(z_i F \vec{J}_i\right) \quad (6.23)$$

Q_{bulk} is the heat generated per unit volume (Wm^{-3}), $\vec{J}_i$ is the flux in the CSF ($molm^{-2}s^{-1}$) and z_i is the charge number of ionic species *i*, F is Faraday's constant ($Cmol^{-1}$) and $V(\vec{x})$ is the potential field in the CSF (Vm^{-1}).

Heat sources in the tissue: Brain tissues have a dense capillary network and we assume the perfusing blood to behave as an infinite sink that remains at constant temperature (Berjano 2006; Elwassif et al. 2006). Q_t (Wm^{-3}) represents heat withdrawn by capillary blood perfusion in the tissue layer given in Eqn. (6.24)

$$Q_t = -\rho_b w_t C_{p_b}[T(\vec{x}) - T_b] \quad (6.24)$$

where ρ_b is the density of blood (kgm^{-3}), w_t is the volumetric blood perfusion rate in the tissue per unit volume ($mlcm^{-3}s^{-1}$), (in this case for the brain), Cp_b is the specific heat capacity (Jkg^{-}

$^{1}K^{-1}$) of blood and T_b is the temperature of the blood. The negative sign indicates heat is withdrawn by capillary perfusion. Metabolic heat generated in the tissue is neglected.

Heat sources at the electrode surface: These are covered in the boundary conditions.

TABLE VI.
MATERIAL PROPERTIES USED FOR SIMULATIONS IN THE ELECTROCHEMICAL MODEL

Parameter	CSF	Silicone	Brain Tissue	Blood
k (W/m·K)	0.61	0.25	0.52	-
ρ (kg/m^3)	-	-	1079	1057
C_p (J/kg·K)	-	-	-	3600
w_t (ml/s/cm^3)	-	-	0.01	-

k is the thermal conductivity, ρ is the density, ε_r is the relative permittivity, C_p is the specific heat capacity, w_t is the blood perfusion in a tissue.

5. Electrochemical initial and boundary conditions

The initial field potential at all positions in the model was set to 0V.

$$V(\vec{x}) = 0 \tag{6.25}$$

A current distribution initialization step was implemented to enable convergence of the dynamic simulation. The inner surface, Ωi of the tissue layer surrounding the ventricular fluid space is modeled as an insulator with normal current density set to zero.

$$\left[\sum_i z_i F \vec{J}_i\right]|_{\Omega i} = 0 \tag{6.26}$$

The potential at the electrode proximal to the catheter tip is chosen to be the anode and a sinusoidal potential is applied on the electrode boundary, with the other electrode acting as the cathode and ground.

$$V_{anode} = V_0 \sin(2\pi f t) \qquad \text{and}$$

$$V_{cathode} = 0 \tag{6.27}$$

V_0 is the amplitude of the signal which is set to 10V and f is the signal frequency, set to 500kHz. The electrode assignment is reversed in the second half of the cycle.

6. Temperature initial and boundary conditions

The CSF and tissue are initially assumed to be at core body temperature of 310.15K. The external tissue surface is assumed to be an insulating surface

$$\overrightarrow{q}|_{\Omega o} = 0 \tag{6.28}$$

where $\overrightarrow{q}|_{\Omega o}$ is the heat flux normal to the *outer surface* of the tissue layer surrounding the lateral ventricle. Since the temperature elevation was moderate (<10°C), the CSF parameters were assumed independent of temperature.

Heat sources at the electrodes: The electrode surfaces are modeled as boundary heat sources composed of electrochemical reactive and capacitive heating.

Electrochemical reactive heating: This heat is generated because of the overpotential at the interface. A time-averaged value for the heat flux (Wm^{-2}) in a single cycle was used as the heat source, given by Eqn. (6.29)

$$q_{S,rxn} = \frac{\int_0^2 (i_{rxn} \cdot \eta) dt}{2} \tag{6.29}$$

Where i_{rxn} is the current density at the interface due to the reaction (Am^{-2}), and η is the overpotential at the electrode (V), and the integration step provides a time-averaged value over a cycle of 2μs.

Capacitive heating: This component of the boundary heat source is due to the capacitive nature of the double layer at the interface. The heat flux (Wm^{-2}) produced in a non-ideal dielectric of a capacitor (*The Electronics Handbook* 2005) is given by

$$q_{S,cap} = V_{cap}^2 \cdot \omega \cdot C_{dl} \cdot DF \tag{6.30}$$

where V_{cap} is the RMS potential (V) across the interfacial double layer which is found to be 0.23V using the Debye-Huckel formulation (Israelachvili 1992), ω is the frequency of the applied signal, C_{dl} is the specific capacitance (Fm^{-2}) of the double layer and DF is the *dissipation factor* signifying energy dissipated as heat in the dielectric. For the double layer interface, the dielectric is assumed to be water, which has a DF of 0.05 (Von Hippel 1954). A metal surface in contact with an electrolyte typically acquires a charge of $0.2Cm^{-2}$ because of the formation of the electrode-electrolyte interface. Additionally, an external signal is applied to the electrode deposits additional charge on the metal surface given by

$$\sigma_{dep} = C_{dl} \cdot V_{electrode} \tag{6.31}$$

where σ_{dep} is the charge density deposited in Cm^{-2}, C_{dl} and $V_{electrode}$ are as above. At peak amplitude of a 10V sinusoidal signal, σ_{dep} can be calculated to be 0.023 Cm^{-2} for the measured C_{dl} and A_{elec} bringing the total charge density σ_{total} to $0.223Cm^{-2}$. The potential V_{dl} across the double layer can then be calculated to be

$$V_{dl} = \kappa^{-1} \cdot {}^{\sigma_{total}}/_{\varepsilon_r \varepsilon_0} \tag{6.32}$$

where $\varepsilon_r$is the relative permittivity of the medium, ε_0 is the permittivity of free space (Fm^{-1}) and κ^{-1} is the Debye length for the given solution. κ^{-1} depends on the ionic strength of the solution, which for a one-one electrolyte (Na^+ and Cl^-, in our case) is equal to the concentration. The Debye length is calculated according to Eqn. (6.33)

$$\kappa^{-1} = \sqrt{\frac{\varepsilon_r \varepsilon_0 k_B T}{2 N_A e^2 I}} \tag{6.33}$$

k_B is Boltzmann's constant, N_A is Avogadro's constant, e is the elementary charge, T is the temperature in K, and I is the ionic strength in molm^{-3}. κ^{-1} is found to be 0.828 nm, which is consistent with typical values found in literature (~1nm). In our case, V_{dl} is calculated to be 0.32V, with an RMS value of $V_{cap} = 0.23V$.

7. Solver setup

The simulation study in COMSOL is configured as follows:

(i) Step 1: Current Distribution initialization: This step computes the **initial potential distribution** in the CSF domain, without any electrical potential stimulus applied to electrode boundaries. It facilitates solving a dynamic system in an electrochemical model by improving stability and convergence. It solves a steady-state non-linear system using the Newton's method with each linearized iteration solved using a Direct Linear solver from the COMSOL solver library. The solution comprises of a non-zero potential distribution in the CSF domain.

(ii) Step 2: Time-dependent: This is a **dynamic** step, the **potential distribution** and the **ionic distribution** in the CSF domain are computed in response to a time-varying electrical potential applied to the electrode surfaces. We solve for 1 cycle of the applied electric signal. Electrochemical reactions (in this case, water electrolysis by oxygen and hydrogen evolution) are configured using the Electrode Surface nodes on the electrode boundaries. Ions in the bulk CSF undergo electromigration under the electric field induced in the conductive medium. The time-dependent solver used is MUMPS, and it is implemented using the Backward Differentiation Formula method, with the maximum step-size restricted to 0.005μs to avoid large changes in computed variables. Each time-step consists of solving a non-linear system using Newton's method.

(iii) Step 3: Stationary: This step computes the **temperature distribution** in the 2D model by solving the **steady-state** heat conduction equation. The heat sources (described earlier) are computed using time-averaged values obtained from Step 2. The non-linear system is solved using the Newton method, with each linearized iteration solved using a Direct Linear solver from the COMSOL solver library.

E. Results – Electrochemical model

An electrochemical analysis of hyperthermia in a proximal ventricular catheter was conducted to support our experimental observations. We calculated the peak ionic current density induced in the electrolyte for a single cycle of the applied signal and then predicted the spatial temperature distribution at steady state. The maximum temperature in CSF and the ventricular wall are of particular significance, as they indicate the volume influenced by our signal around the catheter and possible thermal damage to the ventricular wall respectively.

For a normal ventricle, the simulations predict that the temperature rise is confined to the region adjacent to the luminal electrodes, as shown in the axial slice in Fig 15A2. 2D heat maps from the planes X′-X″ near a luminal electrode and Y′-Y″ between the luminal electrodes are shown in Figs. 15A3 and 15A4 respectively. Predicted temperature distributions and current density distributions along centerlines Z′-Z″ of the heat maps are plotted adjacent to the heat maps. Elevated temperatures are clearly confined to inside the catheter lumen and around the ports – regions that are frequently obstructed. Inside the lumen, the temperature rise is predicted to a maximum of 50.9°C at the electrodes. In the CSF filled space outside the catheter wall, the temperature rises to a maximum of 48.6°C at a port adjacent to a luminal electrode and does not exceed 38°C at the ventricular wall. The maximum current density inside the lumen is predicted

to be 3320.7mAcm^{-2} at the electrode surface and 1428.3mAcm^{-2} in the CSF outside the catheter.

The current drops to near zero (<10mAcm^{-2}) at the ventricular wall. We also compare the values

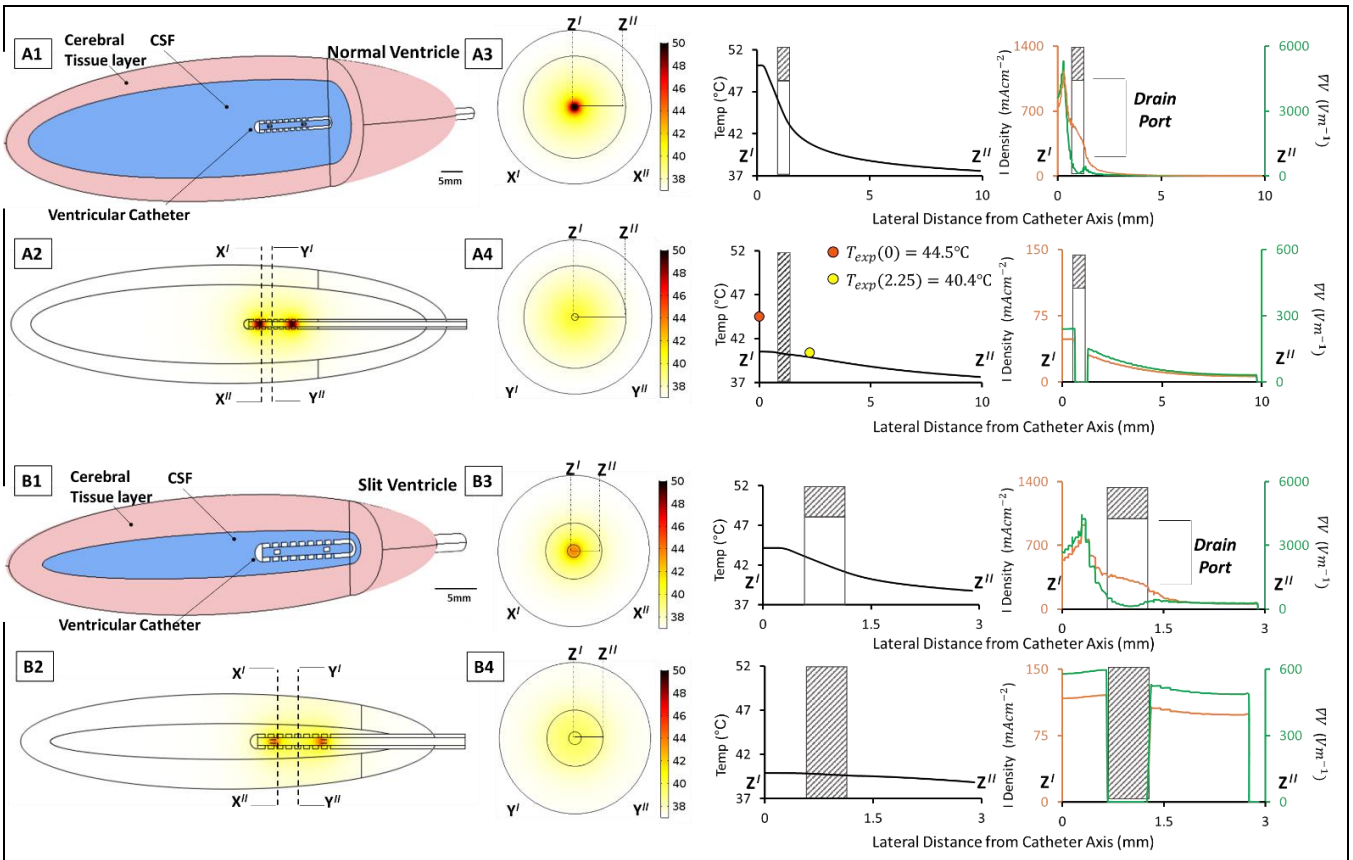

Fig. 15: Solutions of the simulations performed using the electrochemical model. Results are shown for an implanted ventricular catheter suspended in a CSF-filled normal ventricle (A1-A4) and slit ventricle (B1-B4). The lateral ventricle filled with CSF (blue domain) is surrounded by a 5mm layer of tissue (pink domain). An alternating electric signal of 10Vpeak and is applied to a luminal electrode, the other being ground. Panel A represents a "normal ventricle" with a maximum cross-sectional diameter of 10mm (Volume = 20.9 ml) and panel B represent the extreme case of a "slit ventricle" with a maximum cross-sectional diameter of 6mm (Volume = 1.15ml) Panels A2 and B2 show the heat map denoting the temperature distribution on the central cut-plane at steady state in the "normal ventricle" and slit ventricle respectively. Planes X′-X″ near the luminal electrode closer to the catheter proximal tip and Y′-Y″ between the luminal electrodes are marked in panels A1 and B1. 2D heat maps in these planes are shown in panels A3, A4, B3 and B4 Temperatures at steady state predicted by the simulations along the line Z′-Z″ are plotted in panels A3 and A4 for the "normal ventricle" and in panels B3 and B4 for the slit ventricle. The catheter wall is depicted as a grey dashed region, with the drain port found in plane X′-X″ depicted and labelled. Similarly, ionic current density (orange) and the gradient of electrolyte potential (green) at peak applied signal amplitude (0.5μs) is plotted along the same line Z′-Z″.

of heat sources in the bulk as well as at the electrode surfaces to determine their relative contributions to hyperthermia. The heat generated because of the kinetic overpotential at the interface is 3.34×10^{-3}W, the capacitive heat dissipated in the interfacial double layer is 7.39×10^{-5}W and the heat dissipated in a 0.57mm^3 cylindrical envelope of CSF around an electrode is 2.27×10^{-2}W. From this comparison, we can conclude that Joule heating due to bulk ionic motion in is the most important contributor to the temperature elevation.

Our simulation for a slit ventricle (Fig 15B) predicts the temperature distribution for the tissue layers close to the electrodes. The temperature and current density distributions are shown in Fig 15B4 in the planes X′-X″ near a luminal electrode and Y′-Y″ between the two electrodes. Inside the lumen, the maximum temperature is predicted to be 44.8°C near the electrodes, 43.5°C at the port and attains a maximum of 39.2°C at the ventricular wall. The maximum current density inside the lumen is predicted to be 2327.2mAcm^{-2} at the electrode surface, 1063.9mAcm^{-2} in the CSF outside the port near each electrode.

Fig. 16 captures snapshots of the total ionic flux induced in the ventricular CSF by the electric potential applied to luminal electrodes. The magnitude of total flux (in molm^{-2}s^{-1}) in our 2D domain is displayed at various times of a half-cycle of the applied alternating signal. Both sodium and chloride ions migrate under the electrical field induced in the CSF. Higher flux intensities are found at sites of high potential gradients, close to the luminal electrodes. These sites also correspond to largest temperature elevation. A non-zero flux is found in the bulk CSF, which supports our hypothesis that hyperthermia is induced by Joule-heating because of bulk ionic motion.

F. Model Comparison

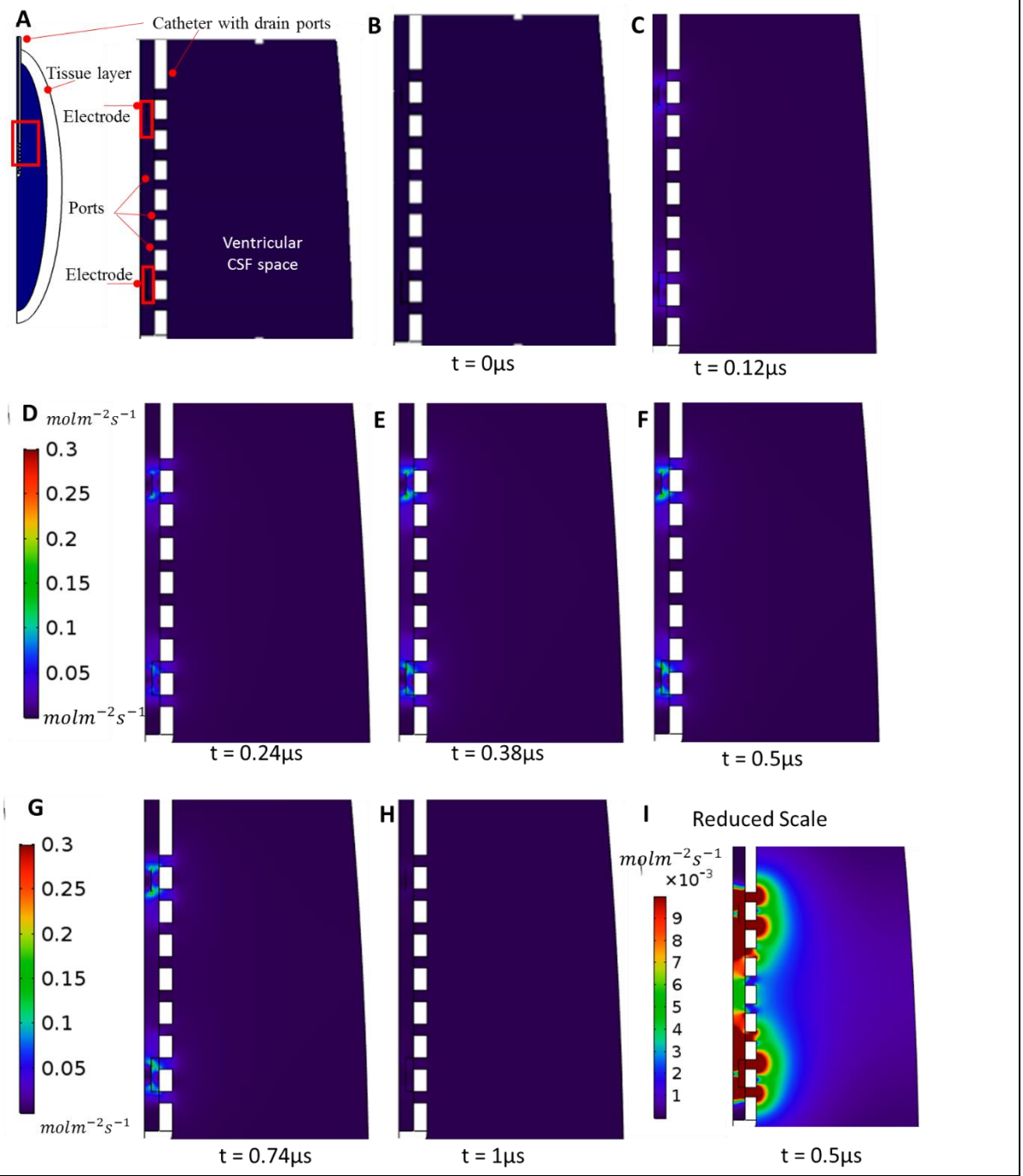

Fig 16: Snapshots of the total ionic flux magnitude at various instances of time. Ion fluxes are induced in the ventricular CSF space during a half-cycle of the applied electrical potential. (A) 2D Model domain, depicting the catheter with drain ports and luminal electrodes submerged in the ventricular CSF space. (B)-(H) Ionic flux magnitude increases with time as the applied potential increases to peak value of 10V at 0.5µs, then falling back to indiscernible values at 1µs. The flux is localized primarily at the electrode surfaces. (I) A non-zero flux in the bulk ventricular CSF space outside the catheter walls, visible by reducing the scale bar.

We used 2 models to validate our experimental results and provide a theoretical framework for our observations. The resistive electrical model assumed the model domains to be ohmic conductors with a bulk isotropic conductivity value. It also assumed that the contact between different material surfaces is lossless and neglects interfacial phenomena such as chemical reactions and electrical double layer capacitive effects. Joule heating in the CSF (the ohmic conductor in our model) due to the propagation of an electric current given by Ohm's law is the only source of heat in this model. We perceive value in our models for the purpose of selecting appropriate electrical signal parameters based on the desired temperature distribution, catheter position and in predicting the risk of injury to the periventricular tissue.

The electrochemical model, on the other hand, models the CSF as an electrolyte with ionic charge carriers. We solve for the motion of ions under the influence of the potential field induced in the electrolyte when an external sinusoidal potential is applied to the electrodes. Instead of a bulk medium conductivity, the ionic concentrations and properties are summed to obtain a solution conductivity value. Interfacial phenomena, including the electrochemical reactions and the capacitive effects of the electrical double layer are incorporated in to the model. Apart from Joule heating in the bulk, two other sources of heat are present – the reactive heating at the electrode surfaces because of the overpotential and the capacitive heating within the electrical double layer because of the dissipation in the dielectric medium.

Computational simulations were performed using both models to predict the temperature and current density distribution in a 3D domain consisting of a catheter ideally located in ventricular CSF. We compare the spatial distribution of both factors in the center-plane of the computational domain at two locations for a normal ventricle –

(i) Near a luminal electrode (line X'–X'')

(ii) Between the luminal electrodes (line Y’ –Y”)

The locations are marked in Fig. 17A1 and B1. Near an electrode, from the catheter axis to the ventricular wall along line X’ – X”, the temperatures are plotted vs distance from the axis in Fig. 17A2, and the ionic current density in Fig. 17A3. In panel B, in the region between the electrodes, from the catheter axis to the ventricular wall along line Y’–Y” the temperatures are plotted vs distance from the axis in Fig. 17B2, and the ionic current density in Fig. 17B3.

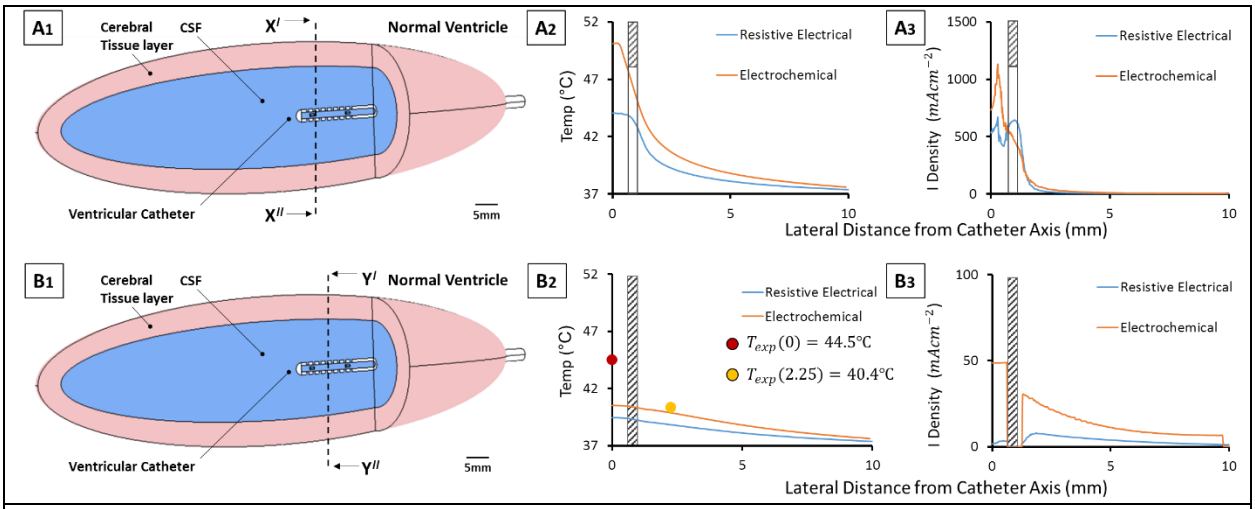

Fig. 17: Comparison between the resistive electrical and electrochemical model solutions. The temperature and current density spatial distributions are compared between the resistive electrical (blue lines) and electrochemical (red lines) model. (A) Near a luminal electrode: the temperature (A2) and the current density (A3) vs lateral distance from catheter axis along the line X’–X”. (B) Between the luminal electrode: the temperature (B2) and the current density (B3) vs lateral distance from catheter axis along the line Y’–Y”. Electrochemical model predictions are found to be consistently greater than those of the resistive electrical model. Experimentally measured temperatures are marked by filled circles in panel B2.

The electrochemical model predictions for the temperature and current density are greater than those of the resistive electrical model. The difference in the predicted values between the models is larger closer to the catheter axis. Experimental temperature measurements, shown in Fig. 15, and reproduced in 17B2, and show that the electrochemical model predictions are closer to experimentally observed values.

The electrochemical model also gives us the advantage of accurately accounting for changes in ionic composition of CSF, in response to physiological conditions in a patient's brain. For instance, edema is a common complication induced in hydrocephalus patients because of underlying conditions such as hypertrophy of the choroid (Hirofumi Hirano et al. 1994) or tumors (Goel 2002). Abnormal CSF osmolarity may change ionic concentrations from the normal CSF range, and may influence the temperature distribution achieved for an applied electric potential signal. In such cases, solving for ionic concentrations rather than a lumped conductivity parameter may improve the predictive qualities of the model.

G. Conclusion

Using computational modeling, we determined that our proposed treatment using 25mA RMS current only reaches the desired temperature close to the electrodes. Although predicted temperatures are well below the threshold at the ventricular wall, the electrode configuration currently used is unable to achieve the desired temperature at all obstruction sites – most prominently, the region between the electrodes. Experimentally, these are found to be clear of cells, likely because of the lengthy exposure time (24 hours) and a more practical treatment duration may leave the catheter partially blocked. Although only *one* unblocked port is sufficient to render the catheter patent, it may be possible to optimize the treatment so as to completely clear all cellular obstruction. One possible alternative is to increase the strength of the applied electrical signal such that sufficient heat is generated in all regions. A more appropriate solution would be to optimize the electrode configuration so as to target all obstruction sites while at the same time minimizing the risk of injury at the ventricular wall. The aim of our research was to determine whether hyperthermia conditions induced by applying the electrical signal would be localized to

affect obstructing tissue without damaging the peripheral brain tissue. With judicious design, it would be possible achieve both objectives.

VII. DISCUSSION

A. Summary

Proximal ventricular catheter obstruction is a major shunt complication leading to shunt failure. Current clinical standards of care rely on costly shunt replacements or invasive clearance procedures. Using in-vitro methods and computational modeling, we show that an alternating electrical signal may be used to clear such obstruction in an effective yet safe manner. In this chapter, we discuss our findings and the limitations of our method, as well as describe how to move forward in converting this new ventricular catheter design into a product.

B. Reviewing our findings

Using cell culture experiments, we demonstrate that cell death can be induced using a low-amplitude AC signal, as shown in Chapter V. We observed cell death using viability assay at the central electrode. Temperature measurements in this region indicate a maximum temperature rise of 8°C. In the regulated biological environment of the mammalian brain where temperatures are maintained at 37°C, this will result in a local temperature in the region of 43°C – 48°C. This temperature range is accepted within the purview of hyperthermia (Mallory et al. 2016). The mechanism of heat generation is likely to be Joule heating in the bulk medium, as well as electrochemical processes at the electrode surfaces. Moreover, through experiments with mock ventricular catheter segments described in Chapter VI, we observed that the low-voltage signal applied to the luminal electrodes caused cell death only inside the lumen and spared the cells outside the catheter. These results show that low-voltage Joule heating to remove cellular obstruction in a proximal ventricular catheter and reestablish CSF flow is feasible.

We also developed 2 computational models to elucidate the temperature and current density spatial profiles in a ventricular catheter implanted in a lateral CSF filled ventricle, as described in Chapter VII. Models were constructed for an implanted catheter in a normal sized ventricle, and an extreme case of a slit ventricle. Simulations were performed to predict the temperature distribution - using a resistive electrical model and also a more comprehensive electrochemical model. The first model approximated the CSF as a simple conductor and neglected any electrode surface phenomena. The second incorporated local ionic motion under the influence of the applied electric potential, and also accounted for the electrochemical reactions at the electrode-electrolyte interface and capacitive heating in the interfacial double layer. We find that a low-to-moderate intensity electric signal (10V-12V OR 10-15mA) applied to luminal electrodes only generates heat locally, in regions adjacent to the electrode surfaces. The ventricular wall remains <40°C at steady state. A literature review reveals that such temperatures at the boundary of the ventricle (Sminia et al. 1994; S. Y. Lee et al. 2000; Haveman et al. 2005) are unlikely to damage the periventricular cell layer. Our preliminary simulations and in-vitro experiments indicate that the effect of low-voltage Joule heating is confined to the shunt lumen and the catheter ports, areas that are prone to obstruction. We believe this method will eliminate or at least lower collateral damage to cerebral tissue. Moreover, there are precedents in the use of thermal methods within the ventricles, particularly endoscopic ventriculostomy and choroid plexus cautery (Scellig S. D. Stone and Benjamin C. Warf 2014; Hellwig et al. 2005).

C. Significance of our work

Proximal obstruction of ventricular catheters is a prominent cause of shunt failure leading to revision. Any method that allows non-surgical removal of the obstruction and reestablishes CSF flow will tremendously improve the Hydrocephalus patients' quality of life by reducing incidences

of shunt failures, and the associated surgical complications, cost of therapy and general morbidity. We propose a preliminary design of a novel ventricular catheter that enables exactly this. Our experiments demonstrate that hyperthermia induced by an AC signal applied to electrodes in the catheter has a locally acting lethal effect on cells. With judicious planning and design, it may be possible to develop a ventricular catheter capable of non-invasive obstruction clearance, and possibly eliminate a severe cause of shunt failure. We perceive several advantages in our proposed method of obstruction clearance, as described below:

(i) Low Power: Hyperthermia is associated with moderate temperature elevations, the final temperature achieved usually falling in the range 43°C - 48°C. This can be easily attained using a low-intensity electrical signal (10V-12V) as demonstrated in experiments and validated by our simulations. The current drawn is also in the range of 10mA-15mA. Such low-intensity signals are easier to generate in an implant device, with minimal risk. Other methods that have been explored for removing obstruction are electrocautery (Pattisapu et al. 1999; Gnanalingham et al. 2005). However, electrocautery is a high power application with complications including sparking, charring due to instantaneous ablation of tissue and vaporization of CSF (Handler 1996). In comparison, a low-power AC signal is inherently safer and eliminates such complications.

(ii) Apoptotic pathway induction: Hyperthermia as a therapy has been found to be an effective adjuvant in combinatorial tumor treatments (Wust et al. 2002; Mallory et al. 2016). Although tumors are more sensitive to the lethal effects of hyperthermia, several animal studies confirm that normal tissue of the CNS is also susceptible to thermal damage (Sminia et al. 1994; Haveman et al. 2005). Various studies indicate that exposure to hyperthermia conditions activates multiple apoptotic cell pathways (Hildebrandt et al.

2002; Harmon et al. 1990) that induce cell death. Other strategies such as mechanical shearing (S. A. Lee et al. 2011) or cauterization (Pattisapu et al. 1999; Gnanalingham et al. 2005) are much more aggressive and typically induce necrotic cell death. Cell death by necrosis often generates an inflammatory cascade that leads to aggregation of glial cells and leukocytes at the site of injury. This carries the risk of repeated obstruction, a feature that has been observed clinically in hydrocephalus surgeries (Lazareff et al. 1998; Sagun Tuli et al. 2000). Cell death by apoptosis (Rock and Kono 2008) may reduce or eliminate this risk as it does not generate an immune response.

(iii) Non-invasive power transfer: Electrical power may be easily transferred to implants by means of electromagnetic radiation (Budgett et al. 2007). Such an approach using capacitively coupled components has been tested and proven to be clinically effective in inducing hyperthermia in intracranial tumors (Tanaka et al. 1987; Fiorentini et al. 2006). It could be possible to adopt this mechanism in order to develop a catheter with non-invasive clearance capability.

D. Limitations and Future Work:

Our objective was to design a self-clearing ventricular catheter system to clear cellular obstruction and eliminate a primary source of shunt failure. We hypothesized that hyperthermia induced by a low-voltage AC electrical signal is a feasible strategy to achieve our objective. Our observations from in-vitro experiments and simulation studies support the feasibility of AC signals as a clearing mechanism. However, our preliminary efforts have some limitations that must be addressed in order to transform our first steps in designing a novel catheter into a commercial medical device. We address these limitations and provide strategies on overcoming them below.

(i) Signal exposure time for cell death: Hyperthermia does not induce cell death in tissues instantaneously. Its mechanisms are not completely elucidated and it has been suggested that it initiates multiple pathways that overloads a cell and promotes an overall cytotoxic effect (Hildebrandt et al. 2002). Scientific literature includes observations of a threshold in the delivered thermal dose to irreparably damage cells, as well as cases of thermotolerance in case of insufficient dose (Dewhirst et al. 2003). Our experiments with glioma cells indicate that a 24 hours exposure was necessary to reliably induce cell death in a plate, for a selected set of AC signal parameters and a 2-electrode configuration. Lowering this exposure time would be a significant improvement and necessary for shortening the total time of therapy.

Future Work: A modification in the electrode configuration may be able to change the temperature distribution so as to reduce the exposure time. Experiments with a 5-electrode configuration in cell plates showed that 4 hours are sufficient to reliably induce cell death. Catheter designs and configurations can be constructed for optimal thermal spread using our computer-aided methods.

It would also be interesting to study whether a periodic heating regime could inhibit the growth of obstructing material and prevent proximal ventricular catheter obstruction in a *prophylactic* way. For this purpose, a follow-up study that investigates cell growth rates with periodic low-voltage Joule heating in a catheter test system as described in (Harris and McAllister 2011) would be very useful. A similar setup has already been adopted by our research group (Basati et al. 2015) for testing an impedance-based obstruction sensor. Combining both systems could be a framework in the design of sensing an obstruction and

automatically selecting an obstruction-specific AC signal parameters for clearance and verify the clearance and catheter patency.

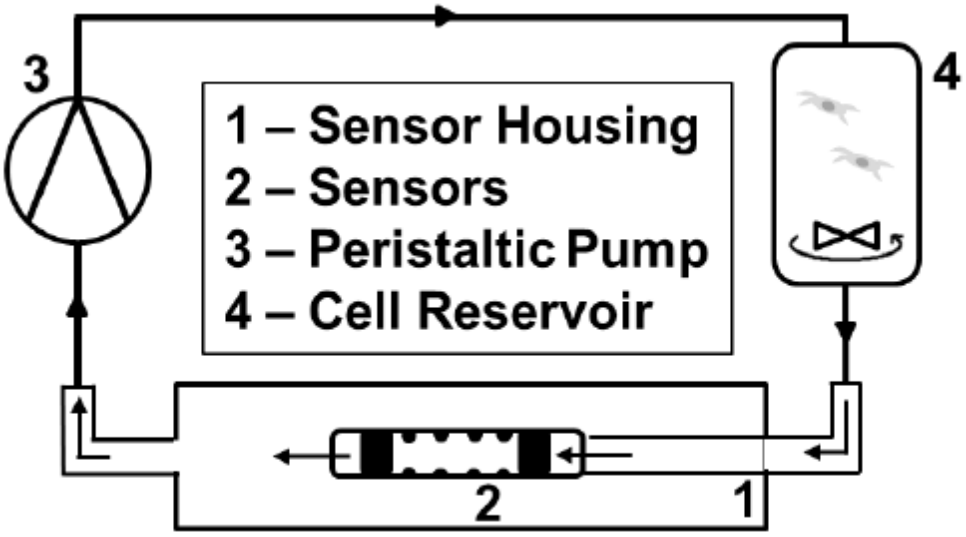

Fig 18: Flow enabled in-vitro benchtop setup used by Basati et. al. to test obstruction sensor. A similar setup may be adopted to test the feasibility of hyperthermia induced by AC signals as a prophylactic measure to prevent proximal obstruction. © 2015, IEEE, Reprinted, with permission, from Basati S. et. al. *Impedance Changes Indicate Proximal Ventriculoperitoneal Shunt Obstruction In Vitro*, IEEE Transactions on Biomedical Engineering, Dec. 2015.

(ii) Static conditions: Our experiments were carried out with the culture medium remaining stationary. Similarly, our simulations did not account for CSF flow. CSF drainage through a partially obstructed catheter, as well as the pulsatile flow dynamics of CSF in the ventricular system will both contribute in removing any heat generated by the applied AC signal. We have already seen how hyperthermia is dose dependent, and an insufficient dose can even lead to thermotolerance.

Future Work: A future step should include experiments and simulations with dynamic flow conditions, to assess its impact on temperature distribution in the catheter lumen and surroundings. A parametric evaluation of the AC signal could elucidate a greater range of

signal parameters that are acceptable for inducing hyperthermia in flow conditions. A setup as shown in Fig. 18 could be constructed for this purpose.

(iii) Choice of cell line: We used a C6 rat glioma cell line in our experiments to ascertain that hyperthermia is a feasible method to clear a cellular monolayer in a mock catheters. These are immortalized tumor cell lines that are resilient and easy to maintain in culture. However, cellular sources of catheter obstruction are typically healthy cell types such as glial cells, astrocytes, choroid layer, etc. that may have different properties and may require different thermal dose than what was achieved in our experiments to be effective. Additionally, the behavior of individual cells as used in our work differs from that of a tissue containing a connective tissue matrix.

Future Work: Further experiments with a cell line such as e19 primary rat astrocytes or even human neurons would be essential to verify that our obstruction clearance strategy is effective in more physiological conditions. Another strategy would be to use in-vivo methods, such as implanting a catheter in the abdominal cavity or transcutaneous muscular tissue of mice or rats and observe the sequential obstruction and clearance, without risking the cerebral structures of the animal.

(iv) MRI-related complications: Hydrocephalus diagnosis and care consists of frequent MRI scans. Therefore, it is important to address the possible risks involved of undesirable thermal response of our shunt design during MRI. Clinical cases in which patients with metallic implants suffer from moderate to severe burns during an MRI have been documented (Chou, McDougall, and Chan 1997; Tronnier et al. 1999; Kovacs et al. 2006).

There are two mechanisms that may generate heat in a metallic implant during an MRI (J. A. Nyenhuis et al. 2005). Time-varying magnetic fields induce eddy currents in

insulated metallic leads or metallic implants with large cross-sectional areas. The linking of the magnetic field with electrode leads is greater in coiled metallic structures. Secondly, electrodes and leads in our catheter may also act as antennas for the RF pulse sequences that are used to excite hydrogen nuclei during an MRI. The risk of RF interaction becomes higher in case of long wires or leads due to resonance, when the antenna length is an odd multiple of half-wavelength of the RF signal. The voltages induced in insulated wires are trapped until they reach an exposed section of the implant such as an electrode. The built-up electrical energy is released forming high-intensity currents at the exposed section, which leads to undesirable and often severe heating.

Future Work: It is imperative to design the new ventricular catheter taking into consideration possible MRI-induced thermal effects. The electrodes and electrode leads will be made of Platinum-Iridium, which is an established biocompatible material for neural implants (Bhavaraju et al. 2002; Georgi et al. 2004; Ciumas et al. 2014). Magnetic linkage to metallic wires may be reduced by preventing any coiled structures along the length of the catheter.

Studies have sought to characterize the effect of RF-field linkage with metallic wire length and diameter (Armenean et al. 2004; Shrivastava et al. 2010). RF linkage in implanted wires is found to be severe when the wire length is a multiple of the half-wavelength of the RF signal frequency. Shortening the length of wire (< 1m) to below that required for resonant behavior is feasible (Darcey et al. 2016). Other design changes such as adding metallic chokes to alter the impedance characteristics of the wires may also be feasible (Ladd and Quick 2000). Such designs may be considered and verified using combined computational studies and benchtop experiments such as described in (Neufeld

et al. 2009). Preliminary guidelines have been established for the safe use of MRI procedures on patients with metallic implants, and may be reviewed for MRI-safety design conditions. For instance, the ACTIVA® Deep brain stimulation system, from Medtronic, Inc. is classified as MRI safe, following certain precautions (Medtronic, MN 2017a).

E. Conclusion

Cellular attachment and in-growth is the primary source of obstruction in ventricular catheters leading to shunt malfunctions in patients suffering from Hydrocephalus. A system built into the ventricular catheter that is capable of clearing cellular obstructions can be beneficial to the patients by reducing or eliminating a major source of shunt failure leading to revisions. In this dissertation, we have proposed a prototype catheter system that can clear such cellular obstruction. Our ventricular catheter induces hyperthermia conditions by applying an alternating electrical signal to luminal electrodes, and we show that it is a feasible strategy to clears obstructed shunts. Based on results from a combination of in-vitro methods and simulations, we demonstrated that this strategy is effective for clearing cellular layers in a catheter lumen and ports thus potentially clearing shunt obstruction without damaging the periventricular cerebral tissue. Such a system may also be integrated with an impedance sensor to detect obstruction any and eliminate it before a complete block occurs. This study lays the foundation for the development of a non-invasive obstruction clearance system that may reduce incidences of shunt failures caused by proximal obstruction, lower shunt failure rates and improve patient welfare in hydrocephalus management.

APPENDICES

APPENDIX A – Table of hydrocephalus shunt technological advances

TABLE VII: HYDROCEPHALUS SHUNT TECHNOLOGICAL ADVANCES

Source	Modification	Benefit
	Shunt Design	
Kehler et. al. (2003)	Peel-away sheath for shunt insertions	Prevents brain parenchyma debris from occluding shunt during insertion
Joseph Corbett (1987), US 4,655,745	Ventricular catheter with an inflatable cuff around the ports	Inflating the cuff by fluid infusion after implantation ensures that the ventricular catheter is sufficiently apart from ventricular wall
Medtronic Inc.	Rivulet Catheter – drain ports increasing in size from tip to valve	Uniform CSF flow achieved by modification of drain port size, confirmed by computational modeling by Galarza et. al., 2014
Microbot Medical Inc.	Self-cleaning shunt	Mechanical shearing of obstructing material by roads using magnetic actuators
Sevrain (2010) US 2010/0222732	Ventricular catheter with a tip made of a porous membrane	Porous membrane tip filters CSF and prevents downstream clogging by tissue or protein deposits
Bruce Banks (1983) US 4,377,169	Perforated microtubules made of fluoropolymers	A large number of small perforations, with the redundancy of multiple microtubules makes unlikely total obstruction of catheter
Eric Leuthardt et. al. (2016) US 9227043 B2	Catheter with Rotating element at proximal tip	Ability to rotate tip enables dislodging of brain tissue adhering to tip and inhibits occlusion
Sotelo et. al. (2005)	Shunt with Continuous Flow, without valves. Flow is controlled by the distal catheter cross-section	Absence of valve allows uninterrupted flow, preventing CSF stagnation in the shunt and ventricles. Studies show the system reduces contamination, obstruction, overall failure
	Sensors	
Linninger et. al. (2009), Basati et. al. (2013)	Impedance sensor to measure lateral ventricular volume and degree of ventricular obstruction	Volume sensor allows monitoring of ventricular volume and status of ventricular compliance. Impedance sensor allows early detection of shunt obstruction and impending shunt failure

TABLE VII (continued)

Source	Modification	Benefit
	Sensor	
Kim et. al. (2016)	Microfabricated patency sensor	Monitoring of shunt patency by impedance measurements
Neurodiagnostic Devices Inc.	ShuntCheck non-invasive thermal technique	Monitor shunt flow for early detection of shunt failure
Clark et. al. (2015)	Multi-Modal piezo-resistive sensor for pressure, temperature and flow measurements in the shunt	Provides multiple parameters to monitor shunt function and detect malfunctions before symptoms manifest
	Material modifications	
Suresh and Black (2015)	Electrospun polyurethane (EPU) as shunt material	EPU is relatively resistant to cell attachment and growth and may reduce complications associated with catheter obstruction
Sciubba et. al. (2005)	Anti-biotic impregnated shunts	Reduces the likelihood of CNS shunt infections
	Obstruction clearance mechanisms	
Fox et. al. (2014)	Transducer to induce vibrations in the shunt	Maintains shunt patency by preventing the adherence of material onto shunt
Lee et. al. (2006), (2008), (2011)	Microfabricated Magnetic Actuators built into shunt	Mechanically sweeps away biological tissue at shunt ports
Koullick et. al. US 7,582,068 B2	Shunt incorporated with inserts containing an anti-occluding agent at the proximal and/or distal tip	The anti-occluding agent can be released in a controlled manner to prevent occlusion and maintain catheter patency
	Shunt Valves	
Portnoy et. al. (1973), Gruber et. al. (2010)	Anti-siphon device	Prevents hydrostatic suction experienced due to a sudden postural changes and avoids overdrainage
Ludin and Mauge (2012) US 8,123,714	Programmable shunt with an electromechanical valve actuator	Programmable shunt valves enables adaptation of CSF flow rates based on patient's need and health

TABLE VII (continued)

Source	Modification	Benefit
	Shunt Valves	
proSA™ valve (Aesculap and MIETHKE)	Non-invasively programmable anti-siphon valve using an external magnetic device	Adjustable unit prevents the siphoning of CSF for various degrees of postural changes
Sophysa Polaris®	MRI-stable adjustable valve	Non-invasive adjustment of valve settings to control CSF flow-rate, with a magnetic lock to prevent unwanted adjustment during MRI scans
	Miscellaneous	
Oh et. al. (2011)	Microfabricated valve to act as a surrogate for arachnoid villi	Replaces arachnoid villi functionally to manage CSF reabsorption and maintains ICP.

APPENDIX B – Table of clearance area in cell plate experiments

TABLE VIII. AREA OF CLEARANCE ZONE FOR CELLS IN CULTURE

Date of expt.	Expt. Duration (hour)	Area (# sq.)	Area (mm^2)
04/03/2016	2	8*	2
04/13/2016	2	5*	1.25
04/13/2016	2	2*	0.5
10/02/2016	2	4*	1
10/05/2016	2	0	0
10/05/2016	2	0	0
10/04/2016	4	8	8
10/04/2016	4	6	6
10/04/2016	4	6	6
10/07/2016	4	12	12
10/09/2016	4	8	8
04/19/2016	8	21	21
04/27/2016	8	17	17
09/26/2016	8	22	22
10/09/2016	8	19	19
10/07/2016	8	42	42
10/17/2016	8	28	28
04/28/2016	24	64	64
10/18/2016	24	59	59
10/18/2016	24	57	57
9/28/2016	24	62	62
09/26/2016	24	38	38
11/15/2016	24	39	39

* denotes a $0.25mm^2$ grid was used to quantify the clearance zone

APPENDIX C – Verifying hyperthermia for cells in culture

TABLE IX. AREA OF CLEARANCE ZONE WITH TEMPERATURE CONTROL (USING A WATER BATH)

Date of expt.	Duration of Expt. (hours)	Area (# squares)	Area (mm^2)
02/11/2016	24	7	7
10/22/2016	24	10*	2.5
10/26/2016	24	9*	2.25
15/11/2016	24	9	9
11/30/2016	24	15	15
12/05/2016	24	11	11

* denotes a $0.25mm^2$ grid was used to quantify the clearance zone

TABLE X: TEMPERATURE ELEVATION MEASURED AT THE CENTRAL ELECTRODE

Time (min)	1	2	3	Average	Max	Min	+d	-d
0	0	0	0	0	0	0	0	0
2	4.4	2.6	4.6	3.9	4.5	2.6	0.8	1.3
4	5.8	4.8	5.9	5.5	5.9	4.8	0.4	0.7
6	6.3	5.1	6.3	5.9	6.3	5.1	0.4	0.8
8	6.5	5.2	6.7	6.2	6.7	5.2	0.5	1.0
10	6.9	5.5	6.9	6.4	6.9	5.4	0.5	1.0
15	7.0	5.8	7.1	6.6	7.2	5.8	0.6	0.8
20	7.1	6.0	7.7	6.9	7.7	5.9	0.8	1.0
25	7.1	6.0	7.8	7.0	7.8	5.9	0.8	1.1
30	7.2	6.0	8.1	7.1	8.1	6.0	1.0	1.1

TABLE XI: TEMPERATURE ELEVATION AT THE CENTRAL ELECTRODE WITH TEMPERATURE CONTROL

Time (min)	1	2	3	Average	Max	Min	+d	-d
0	0	0	0	0	0	0	0	0
2	2.7	3.8	3.3	3.3	3.8	2.7	0.5	0.6
4	3.4	4.5	3.9	3.9	4.5	3.4	0.6	0.5
6	3.6	4.9	4.2	4.2	4.9	3.6	0.7	0.6
8	3.8	5.1	4.3	4.4	5.1	3.8	0.7	0.6
10	3.9	5.2	4.5	4.6	5.2	3.9	0.6	0.7
15	4.2	5.3	4.6	4.7	5.3	4.2	0.6	0.5
20	4.3	5.4	4.7	4.8	5.4	4.3	0.6	0.5
25	4.3	5.5	4.8	4.9	5.5	4.3	0.6	0.6
30	4.4	5.5	5.1	5.0	5.5	4.4	0.5	0.6

APPENDIX D – Hyperthermia localized to shunt lumen

TABLE XII: TEMPERATURE ELEVATION INSIDE SHUNT LUMEN								
Time (min)	1	2	3	Average	Max	Min	+d	-d
0	0	0	0	0	0	0	0	0
2	3.6	4.7	5.1	4.5	5.1	3.6	0.6	0.9
4	4.9	5.7	6.0	5.5	6.0	4.9	0.5	0.6
6	6.0	6.1	6.4	6.2	6.4	6.0	0.2	0.2
8	6.7	6.3	6.7	6.6	6.7	6.3	0.1	0.3
10	7.4	6.5	6.8	6.9	7.4	6.5	0.5	0.5
15	7.8	6.7	7.1	7.2	7.8	6.7	0.6	0.5
20	8.1	6.8	7.1	7.3	8.1	6.8	0.8	0.5
25	8.2	6.9	7.2	7.4	8.2	6.9	0.8	0.5
30	8.3	6.9	7.2	7.5	8.3	6.9	0.8	0.6

TABLE XIII: TEMPERATURE ELEVATION OUTSIDE SHUNT LUMEN								
Time (min)	1	2	3	Average	Max	Min	+d	-d
0	0	0	0	0	0	0	0	0
2	1.7	1.2	0.7	1.2	1.7	0.7	0.5	0.5
4	2.8	1.8	0.9	1.8	2.8	0.9	1.0	0.9
6	3.6	1.9	1.5	2.3	3.6	1.5	1.3	0.8
8	4.1	2.1	1.6	2.6	4.1	1.6	1.5	1.0
10	4.5	2.2	1.9	2.9	4.5	1.9	1.6	1.0
15	4.8	2.4	2.1	3.1	4.8	2.1	1.7	1.0
20	4.9	2.5	2.1	3.2	4.9	2.1	1.7	1.1
25	5.0	2.6	2.2	3.3	5.0	2.2	1.7	1.1
30	5.3	2.6	2.3	3.4	5.3	2.3	1.9	1.0

APPENDIX E – COMSOL solver log for a Normal ventricle case

Stationary Solver 1 in Study 1/Solution 1 (sol1) started at 25-Oct-2017 16:30:43.
Nonlinear solver
Number of degrees of freedom solved for: 41266 (plus 2308 internal DOFs).
Symmetric matrices found.
Scales for dependent variables:
Electrolyte potential (comp2.phil): 1
Orthonormal null-space function used.

Iter	SolEst	ResEst	Damping	Stepsize	#Res	#Jac	#Sol	LinErr	LinRes
1	0.038	1.5e+004	1.0000000	0.1	2	1	2	3e-016	1.9e-016
2	0.058	1.2e+004	0.5819767	0.1	3	2	4	2.6e-016	2e-016
3	0.05	5.9e+003	0.7370783	0.1	4	3	6	2.1e-016	1.2e-016
4	0.053	3e+003	0.6763298	0.1	5	4	8	3.1e-016	1.5e-016
5	0.052	1.5e+003	0.6996661	0.1	6	5	10	3.3e-016	2e-016
6	0.052	7.5e+002	0.6906323	0.1	7	6	12	4e-016	3.1e-016
7	0.052	3.7e+002	0.6941192	0.1	8	7	14	2.9e-016	2.2e-016
8	0.052	1.9e+002	0.6927718	0.1	9	8	16	3.8e-016	2.3e-016
9	0.052	93	0.6932922	0.1	10	9	18	3.8e-016	1.5e-016
10	0.052	47	0.6930912	0.1	11	10	20	5.5e-016	2.2e-016
11	0.052	23	0.6931688	0.1	12	11	22	4.4e-016	1.5e-016
12	0.052	12	0.6931388	0.1	13	12	24	4.5e-016	1.4e-016
13	0.052	5.8	0.6931504	0.1	14	13	26	6e-016	1.6e-016
14	0.05	2.9	0.6931459	0.1	15	14	28	8.6e-016	1.4e-016
15	0.047	1.5	0.6931477	0.094	16	15	30	1.1e-015	1.7e-016
16	0.044	0.73	0.6931470	0.088	17	16	32	1.4e-015	2.1e-016
17	0.042	0.36	0.6931473	0.083	18	17	34	2e-015	1.7e-016
18	0.039	0.18	0.6931472	0.079	19	18	36	2.5e-015	2.1e-016
19	0.037	0.091	0.6931472	0.075	20	19	38	5e-015	2.1e-016
20	0.035	0.046	0.6931472	0.071	21	20	40	7e-015	1.7e-016
21	0.034	0.023	0.6931472	0.068	22	21	42	9.5e-015	2.1e-016
22	0.032	0.011	0.6931472	0.065	23	22	44	1.5e-014	2.7e-016
23	0.031	0.0057	0.6931472	0.062	24	23	46	2.6e-014	2.5e-016
24	0.03	0.0028	0.6931472	0.059	25	24	48	3.7e-014	1.6e-016
25	0.028	0.0014	0.6931472	0.057	26	25	50	4.5e-014	1.9e-016
26	0.027	0.00071	0.6931472	0.055	27	26	52	5.8e-014	1.9e-016
27	0.026	0.00036	0.6931472	0.053	28	27	54	8.1e-014	1.7e-016
28	0.025	0.00018	0.6931472	0.051	29	28	56	1.2e-013	2.1e-016
29	0.025	8.9e-005	0.6931472	0.049	30	29	58	1.4e-013	2.2e-016
30	0.024	4.5e-005	0.6931472	0.048	31	30	60	2.4e-013	2.5e-016
31	0.023	2.2e-005	0.6931472	0.046	32	31	62	2.2e-013	2.2e-016
32	0.022	1.1e-005	0.6931472	0.045	33	32	64	4.1e-013	2.6e-016
33	0.022	5.6e-006	0.6931472	0.043	34	33	66	7.2e-013	1.6e-016
34	0.021	2.8e-006	0.6931472	0.042	35	34	68	8.8e-013	2.3e-016
35	0.02	1.4e-006	0.6931472	0.041	36	35	70	9.6e-013	2.8e-016
36	0.02	7e-007	0.6931472	0.04	37	36	72	1.7e-012	2e-016
37	0.019	3.5e-007	0.6931472	0.039	38	37	74	2.4e-012	2.5e-016
38	0.019	1.7e-007	0.6931472	0.038	39	38	76	2.8e-012	1.9e-016
39	0.018	8.7e-008	0.6931472	0.037	40	39	78	3.6e-012	2.2e-016

APPENDIX E (continued)

40	0.018	4.3e-008	0.6931472	0.036	41	40	80	3.5e-012	2.5e-016
41	0.017	2.2e-008	0.6931472	0.035	42	41	82	3.5e-012	3e-016
42	0.017	1.1e-008	0.6931472	0.034	43	42	84	5.7e-012	3.8e-016
43	0.017	5.4e-009	0.6931472	0.033	44	43	86	3.5e-012	4.5e-016
44	0.016	2.7e-009	0.6931472	0.033	45	44	88	4.2e-012	6.5e-016
45	0.016	1.4e-009	0.6931472	0.032	46	45	90	3.8e-012	8.8e-016
46	0.016	6.8e-010	0.6931472	0.031	47	46	92	3.9e-012	1.2e-015
47	0.015	3.4e-010	0.6931472	0.03	48	47	94	6e-012	1.8e-015
48	0.015	1.7e-010	0.6931472	0.03	49	48	96	4.1e-012	2.5e-015
49	0.015	8.5e-011	0.6931472	0.029	50	49	98	5.2e-012	3.6e-015
50	0.014	4.2e-011	0.6931474	0.029	51	50	100	3.4e-012	5.1e-015
51	0.014	2.1e-011	0.6931479	0.028	52	51	102	4.2e-012	7.7e-015
52	0.014	1.1e-011	0.6931502	0.028	53	52	104	4.9e-012	1.2e-014
53	0.014	5.3e-012	0.6931593	0.027	54	53	106	5.1e-012	1.9e-014
54	0.013	2.7e-012	0.6931956	0.027	55	54	108	5.2e-012	3.3e-014
55	0.013	1.3e-012	0.6933410	0.026	56	55	110	3.5e-012	6.1e-014
56	0.013	6.6e-013	0.6939227	0.026	57	56	112	4.4e-012	1.2e-013
57	0.012	3.3e-013	0.6962561	0.025	58	57	114	5.8e-012	2.3e-013
58	0.012	1.6e-013	0.7056920	0.024	59	58	116	7.3e-012	4.7e-013
59	0.011	7.3e-014	0.7451403	0.023	60	59	118	1.7e-011	9.4e-013
60	0.0057	2.1e-014	0.9351176	0.02	61	60	120	1.2e-011	1.8e-012
61	0.00052	1.1e-015	1.0000000	0.0096	62	61	122	2.7e-011	3e-012

Stationary Solver 1 in Study 1/Solution 1 (sol1): Solution time: 152 s (2 minutes, 32 seconds)
Physical memory: 1.16 GB
Virtual memory: 1.37 GB

Time-dependent solver (BDF)
Number of degrees of freedom solved for: 69400 (plus 6140 internal DOFs).
Nonsymmetric matrix found.
Scales for dependent variables:
Electrolyte potential (comp2.phil): 0.44
Concentration (comp2.cOH): 0.00025
Concentration (comp2.cH): 4e-005
Concentration (comp2.cNa): 1.5e+002

Step	Time	Stepsize	Res	Jac	Sol	Order	Tfail	NLfail	LinErr	LinRes
0	0	- out	4	3	4			0	1.2e-008	6.4e-013
1	1e-009	1e-009	6	4	6	1	0	0	4.7e-010	2.8e-016
2	2e-009	1e-009	8	5	8	1	0	0	1.4e-010	3.2e-016
3	3.2502e-009	1.2502e-009	12	7	12	2	1	0	4.5e-010	6.9e-015
4	4.3754e-009	1.1252e-009	14	8	14	2	1	0	3.1e-010	2e-015
5	5.5006e-009	1.1252e-009	16	9	16	2	1	0	2e-010	9.5e-016
6	6.6258e-009	1.1252e-009	18	10	18	2	1	0	5.5e-011	1e-015
7	8.8762e-009	2.2504e-009	20	11	20	2	1	0	6.4e-011	1e-015
8	1.1127e-008	2.2504e-009	22	12	22	2	1	0	8.9e-011	9.7e-016
9	1.5627e-008	4.5008e-009	24	13	24	2	1	0	3.9e-010	4.7e-016
10	2.0627e-008	5e-009	26	14	26	2	1	0	4.1e-010	1e-015

APPENDIX E (continued)

11	2.5627e-008	5e-009	28	15	28	2	1	0	2e-010	9.7e-016
12	3.0627e-008	5e-009	30	16	30	2	1	0	1.4e-010	6.8e-016
13	3.5627e-008	5e-009	32	17	32	2	1	0	2e-010	7.2e-016
14	4.0627e-008	5e-009	34	18	34	3	1	0	1.9e-010	7.8e-016
15	4.5627e-008	5e-009	36	19	36	3	1	0	5.3e-011	7.4e-016
-	5e-008	- out								
16	5.0627e-008	5e-009	38	20	38	3	1	0	1.5e-011	1e-015
17	5.5627e-008	5e-009	40	21	40	3	1	0	1.7e-010	1.2e-015
18	6.0627e-008	5e-009	42	22	42	3	1	0	2.5e-010	9.5e-016
19	6.5627e-008	5e-009	44	23	44	3	1	0	2.5e-010	9.2e-016
20	7.0627e-008	5e-009	46	24	46	3	1	0	2.9e-010	1.2e-015
21	7.5627e-008	5e-009	48	25	48	4	1	0	2.7e-010	1.1e-015
22	8.0627e-008	5e-009	50	26	50	4	1	0	7e-011	9.5e-016
23	8.5627e-008	5e-009	52	27	52	4	1	0	4.8e-011	5.8e-016
24	9.0627e-008	5e-009	54	28	54	4	1	0	2.6e-011	5.6e-016
25	9.5627e-008	5e-009	56	29	56	4	1	0	1e-010	3.6e-016
-	1e-007	- out								
26	1.0063e-007	5e-009	58	30	58	4	1	0	5.7e-011	3.8e-016
27	1.0563e-007	5e-009	60	31	60	5	1	0	1.5e-010	4.4e-016
APPENDIX A (continued)										
28	1.1063e-007	5e-009	62	32	62	5	1	0	8.8e-012	1.6e-016
29	1.1563e-007	5e-009	64	33	64	5	1	0	4.5e-012	8.2e-017
30	1.2063e-007	5e-009	66	34	66	5	1	0	1.1e-012	7.6e-017
31	1.2563e-007	5e-009	68	35	68	5	1	0	1.6e-012	3.4e-016
32	1.3063e-007	5e-009	70	36	70	5	1	0	8.8e-014	1.7e-016
33	1.3563e-007	5e-009	72	37	72	5	1	0	5.4e-014	1.2e-016
34	1.4063e-007	5e-009	74	38	74	5	1	0	2.7e-013	1.1e-016
35	1.4563e-007	5e-009	76	39	76	5	1	0	2.2e-013	3.5e-016
-	1.5e-007	- out								
36	1.5063e-007	5e-009	78	40	78	5	1	0	1.5e-013	3.6e-016
37	1.5563e-007	5e-009	80	41	80	5	1	0	5.5e-013	2.9e-016
38	1.6063e-007	5e-009	82	42	82	5	1	0	1.1e-013	1.4e-016
39	1.6563e-007	5e-009	84	43	84	5	1	0	9.5e-014	1.4e-016
40	1.7063e-007	5e-009	86	44	86	5	1	0	2.1e-013	1.7e-016
41	1.7563e-007	5e-009	88	45	88	5	1	0	2.4e-013	2.2e-016
42	1.8063e-007	5e-009	90	46	90	5	1	0	2.4e-013	3.9e-016
43	1.8563e-007	5e-009	92	47	92	5	1	0	1.7e-013	2.4e-016
44	1.9063e-007	5e-009	94	48	94	5	1	0	1.9e-013	3.6e-016
45	1.9563e-007	5e-009	96	49	96	5	1	0	1.3e-013	2.9e-016
-	2e-007	- out								
46	2.0063e-007	5e-009	98	50	98	5	1	0	1.2e-013	3.2e-016
47	2.0563e-007	5e-009	100	51	100	5	1	0	1.5e-013	3.4e-016
48	2.1063e-007	5e-009	102	52	102	5	1	0	1.1e-013	2.4e-016
49	2.1563e-007	5e-009	104	53	104	5	1	0	8.2e-014	1.9e-016
50	2.2063e-007	5e-009	106	54	106	5	1	0	7.4e-014	1.9e-016
51	2.2563e-007	5e-009	108	55	108	5	1	0	1.1e-013	3.2e-016
52	2.3063e-007	5e-009	110	56	110	5	1	0	4.3e-014	8.9e-017

APPENDIX E (continued)

53	2.3563e-007	5e-009	112	57	112	5	1	0	7e-014	1.6e-016
54	2.4063e-007	5e-009	114	58	114	5	1	0	1.2e-013	2.2e-016
55	2.4563e-007	5e-009	116	59	116	5	1	0	8.6e-014	2.3e-016
-	2.5e-007	- out								
56	2.5063e-007	5e-009	118	60	118	5	1	0	7.2e-014	1.6e-016
57	2.5563e-007	5e-009	120	61	120	5	1	0	1e-013	2.3e-016
58	2.6063e-007	5e-009	122	62	122	5	1	0	1e-013	2.3e-016
59	2.6563e-007	5e-009	124	63	124	5	1	0	8.6e-014	2e-016
60	2.7063e-007	5e-009	126	64	126	5	1	0	1e-013	2.7e-016
61	2.7563e-007	5e-009	128	65	128	5	1	0	1e-013	2.8e-016
62	2.8063e-007	5e-009	130	66	130	5	1	0	3.4e-012	2.9e-016
63	2.8563e-007	5e-009	132	67	132	5	1	0	2.6e-011	4.7e-016
64	2.9063e-007	5e-009	134	68	134	5	1	0	3.6e-011	8.3e-016
65	2.9563e-007	5e-009	136	69	136	5	1	0	1.1e-011	1.4e-016
-	3e-007	- out								
66	3.0063e-007	5e-009	138	70	138	5	1	0	2.5e-011	1.6e-015
67	3.0563e-007	5e-009	140	71	140	4	1	0	8.4e-011	1.5e-015
68	3.1063e-007	5e-009	142	72	142	4	1	0	2.2e-010	1e-015
69	3.1563e-007	5e-009	144	73	144	4	1	0	1.8e-010	1.1e-015
70	3.2063e-007	5e-009	146	74	146	3	1	0	1.7e-010	5.1e-016
71	3.2563e-007	5e-009	148	75	148	3	1	0	5.3e-011	6.3e-016
72	3.3063e-007	5e-009	150	76	150	3	1	0	1.9e-011	3e-016
73	3.3563e-007	5e-009	152	77	152	3	1	0	2.2e-011	3.5e-016
74	3.4063e-007	5e-009	154	78	154	3	1	0	1.1e-010	3e-016
75	3.4563e-007	5e-009	156	79	156	2	1	0	6.2e-011	4.8e-016
-	3.5e-007	- out								
76	3.5063e-007	5e-009	158	80	158	2	1	0	1.5e-011	7.5e-016
77	3.5563e-007	5e-009	160	81	160	2	1	0	2.2e-012	5.8e-016
78	3.6063e-007	5e-009	162	82	162	2	1	0	2.6e-011	1.4e-016
79	3.6563e-007	5e-009	164	83	164	3	1	0	7.8e-011	2.1e-016
80	3.7063e-007	5e-009	166	84	166	3	1	0	2e-012	1.5e-016
81	3.7563e-007	5e-009	168	85	168	2	1	0	7.1e-011	4.4e-016
82	3.8063e-007	5e-009	170	86	170	2	1	0	6.9e-011	2.2e-016
83	3.8563e-007	5e-009	172	87	172	2	1	0	3.4e-011	3.9e-016
84	3.9063e-007	5e-009	174	88	174	2	1	0	4.1e-011	6.3e-016
85	3.9563e-007	5e-009	176	89	176	3	1	0	2.9e-011	2.5e-016
-	4e-007	- out								
86	4.0063e-007	5e-009	178	90	178	3	1	0	5.5e-012	2.6e-016
87	4.0563e-007	5e-009	180	91	180	2	1	0	1.3e-011	4.2e-016
88	4.1063e-007	5e-009	182	92	182	2	1	0	2.5e-012	1.8e-016
89	4.1563e-007	5e-009	184	93	184	2	1	0	7.1e-012	1.8e-016
90	4.2063e-007	5e-009	186	94	186	2	1	0	1.7e-012	3.7e-016
91	4.2563e-007	5e-009	188	95	188	2	1	0	4e-012	2.3e-016
92	4.3063e-007	5e-009	190	96	190	2	1	0	5e-012	1.9e-016
93	4.3563e-007	5e-009	192	97	192	3	1	0	7.2e-012	4.3e-016
94	4.4063e-007	5e-009	194	98	194	3	1	0	2.2e-012	3e-016
95	4.4563e-007	5e-009	196	99	196	3	1	0	1.4e-012	1.6e-016

APPENDIX E (continued)

- 4.5e-007 - out
96 4.5063e-007 5e-009 198 100 198 3 1 0 1.5e-012 1.7e-016
97 4.5563e-007 5e-009 200 101 200 3 1 0 1.3e-012 2.5e-016
98 4.6063e-007 5e-009 202 102 202 2 1 0 3.5e-012 2e-016
99 4.6563e-007 5e-009 204 103 204 2 1 0 2.4e-012 1.4e-016
100 4.7063e-007 5e-009 206 104 206 2 1 0 3.5e-012 3.9e-016
101 4.7563e-007 5e-009 208 105 208 2 1 0 1.6e-012 1.5e-016
102 4.8063e-007 5e-009 210 106 210 3 1 0 1.8e-012 2.1e-016
103 4.8563e-007 5e-009 212 107 212 3 1 0 4e-012 4.2e-016
104 4.9063e-007 5e-009 214 108 214 3 1 0 5.1e-012 3.2e-016
105 4.9563e-007 5e-009 216 109 216 3 1 0 1.7e-012 3.7e-016
- 5e-007 - out
106 5.0063e-007 5e-009 218 110 218 3 1 0 8e-012 3.1e-016
107 5.0563e-007 5e-009 220 111 220 3 1 0 3.7e-013 3e-016
108 5.1063e-007 5e-009 222 112 222 2 1 0 3.9e-012 2.3e-016
109 5.1563e-007 5e-009 224 113 224 2 1 0 9.9e-013 2.7e-016
110 5.2063e-007 5e-009 226 114 226 2 1 0 1.2e-011 2.3e-016
111 5.2563e-007 5e-009 228 115 228 2 1 0 2.1e-012 2.6e-016
112 5.3063e-007 5e-009 230 116 230 3 1 0 1.1e-013 1.8e-016
113 5.3563e-007 5e-009 232 117 232 3 1 0 1.3e-012 3.5e-016
114 5.4063e-007 5e-009 234 118 234 3 1 0 7.9e-013 2.6e-016
115 5.4563e-007 5e-009 236 119 236 3 1 0 1.5e-012 2.5e-016
- 5.5e-007 - out
116 5.5063e-007 5e-009 238 120 238 3 1 0 9.4e-014 1.7e-016
117 5.5563e-007 5e-009 240 121 240 4 1 0 2e-013 3.8e-016
118 5.6063e-007 5e-009 242 122 242 4 1 0 2e-012 2.5e-016
119 5.6563e-007 5e-009 244 123 244 4 1 0 9.6e-013 1.9e-016
120 5.7063e-007 5e-009 246 124 246 4 1 0 3.7e-013 2.1e-016
121 5.7563e-007 5e-009 248 125 248 4 1 0 2.1e-013 2.7e-016
122 5.8063e-007 5e-009 250 126 250 4 1 0 3.5e-013 2.8e-016
123 5.8563e-007 5e-009 252 127 252 4 1 0 7.8e-013 3.1e-016
124 5.9063e-007 5e-009 254 128 254 4 1 0 6.8e-013 2.6e-016
125 5.9563e-007 5e-009 256 129 256 5 1 0 8.9e-014 2e-016
- 6e-007 - out
126 6.0063e-007 5e-009 258 130 258 5 1 0 1.2e-013 3.1e-016
127 6.0563e-007 5e-009 260 131 260 5 1 0 5.9e-013 4.5e-016
128 6.1063e-007 5e-009 262 132 262 5 1 0 4.2e-014 1.5e-016
129 6.1563e-007 5e-009 264 133 264 5 1 0 1.4e-013 1.2e-016
130 6.2063e-007 5e-009 266 134 266 5 1 0 2.3e-013 2.6e-016
131 6.2563e-007 5e-009 268 135 268 5 1 0 1.7e-013 1.8e-016
132 6.3063e-007 5e-009 270 136 270 5 1 0 3.6e-013 3.9e-016
133 6.3563e-007 5e-009 272 137 272 5 1 0 2e-013 2.6e-016
134 6.4063e-007 5e-009 274 138 274 5 1 0 6e-013 2.3e-016
135 6.4563e-007 5e-009 276 139 276 5 1 0 3.1e-013 5.4e-016
- 6.5e-007 - out
136 6.5063e-007 5e-009 278 140 278 5 1 0 7.4e-014 2.4e-016
137 6.5563e-007 5e-009 280 141 280 5 1 0 6.3e-013 1.5e-016

APPENDIX E (continued)

138	6.6063e-007	5e-009	282	142	282	5	1	0	5.7e-013	8.4e-016
139	6.6563e-007	5e-009	284	143	284	5	1	0	3.7e-013	3e-016
140	6.7063e-007	5e-009	286	144	286	5	1	0	4.5e-013	3.3e-016
141	6.7563e-007	5e-009	288	145	288	5	1	0	7.8e-013	6.7e-016
142	6.8063e-007	5e-009	290	146	290	5	1	0	3.4e-013	2.4e-016
143	6.8563e-007	5e-009	292	147	292	5	1	0	2.4e-013	1.7e-016
144	6.9063e-007	5e-009	294	148	294	5	1	0	2e-013	4.3e-016
145	6.9563e-007	5e-009	296	149	296	5	1	0	2.5e-013	4.8e-016
-	7e-007	- out								
146	7.0063e-007	5e-009	298	150	298	5	1	0	1.9e-013	4.8e-016
147	7.0563e-007	5e-009	300	151	300	5	1	0	2.8e-013	5.2e-016
148	7.1063e-007	5e-009	302	152	302	5	1	0	3e-013	4e-016
149	7.1563e-007	5e-009	304	153	304	5	1	0	1.5e-013	8.4e-017
150	7.2063e-007	5e-009	306	154	306	5	1	0	2.9e-013	5.5e-016
151	7.2563e-007	5e-009	308	155	308	5	1	0	4.7e-013	1.1e-015
152	7.3063e-007	5e-009	310	156	310	5	1	0	1.6e-013	3.3e-016
153	7.3563e-007	5e-009	312	157	312	5	1	0	1.3e-013	1e-016
154	7.4063e-007	5e-009	314	158	314	5	1	0	6.7e-014	1.4e-016
155	7.4563e-007	5e-009	316	159	316	5	1	0	1.6e-013	1.6e-016
-	7.5e-007	- out								
156	7.5063e-007	5e-009	318	160	318	5	1	0	1.6e-013	4.1e-016
157	7.5563e-007	5e-009	320	161	320	5	1	0	2.3e-013	2.8e-016
158	7.6063e-007	5e-009	322	162	322	5	1	0	1.5e-013	3.7e-016
159	7.6563e-007	5e-009	324	163	324	5	1	0	1.9e-013	1e-016
160	7.7063e-007	5e-009	326	164	326	5	1	0	1.5e-013	3.1e-016
161	7.7563e-007	5e-009	328	165	328	5	1	0	1.6e-013	3.9e-016
162	7.8063e-007	5e-009	330	166	330	5	1	0	6.4e-014	8.5e-017
163	7.8563e-007	5e-009	332	167	332	5	1	0	4.5e-014	8.4e-017
164	7.9063e-007	5e-009	334	168	334	5	1	0	1.3e-013	3.7e-016
165	7.9563e-007	5e-009	336	169	336	5	1	0	1.1e-013	2.6e-016
-	8e-007	- out								
166	8.0063e-007	5e-009	338	170	338	5	1	0	1.7e-013	4e-016
167	8.0563e-007	5e-009	340	171	340	5	1	0	2.1e-013	4.7e-016
168	8.1063e-007	5e-009	342	172	342	5	1	0	9.9e-014	1.7e-016
169	8.1563e-007	5e-009	344	173	344	5	1	0	9.9e-014	1.9e-016
170	8.2063e-007	5e-009	346	174	346	5	1	0	2.9e-013	1.3e-016
171	8.2563e-007	5e-009	348	175	348	5	1	0	3.4e-013	1.6e-016
172	8.3063e-007	5e-009	350	176	350	5	1	0	2.1e-013	3.3e-016
173	8.3563e-007	5e-009	352	177	352	5	1	0	7.7e-013	4.4e-016
174	8.4063e-007	5e-009	354	178	354	5	1	0	9.8e-013	3.6e-016
175	8.4563e-007	5e-009	356	179	356	5	1	0	1.2e-012	2.9e-016
-	8.5e-007	- out								
176	8.5063e-007	5e-009	358	180	358	5	1	0	2.8e-012	2.4e-016
177	8.5563e-007	5e-009	360	181	360	5	1	0	1.3e-012	2.6e-016
178	8.6063e-007	5e-009	362	182	362	5	1	0	1.6e-012	3.4e-016
179	8.6563e-007	5e-009	364	183	364	5	1	0	1.3e-011	3.1e-016
180	8.7063e-007	5e-009	366	184	366	5	1	0	1.7e-011	3.4e-016

APPENDIX E (continued)

181 8.7563e-007 5e-009 368 185 368 5 1 0 1.9e-011 2.4e-016
182 8.8063e-007 5e-009 370 186 370 5 1 0 2.5e-011 4.8e-016
183 8.8563e-007 5e-009 372 187 372 5 1 0 5.6e-011 4.6e-016
184 8.9063e-007 5e-009 374 188 374 5 1 0 1.2e-010 6e-016
185 8.9563e-007 5e-009 376 189 376 5 1 0 1.4e-010 3.2e-016
- 9e-007 - out
186 9.0063e-007 5e-009 378 190 378 5 1 0 1.8e-010 3.4e-016
187 9.0563e-007 5e-009 380 191 380 5 1 0 8.6e-011 3.3e-016
188 9.1063e-007 5e-009 382 192 382 5 1 0 1.4e-010 3.3e-016
189 9.1563e-007 5e-009 384 193 384 5 1 0 1.4e-011 2.6e-016
190 9.2063e-007 5e-009 386 194 386 5 1 0 1e-010 4.3e-016
191 9.2563e-007 5e-009 388 195 388 5 1 0 2.4e-010 7.5e-016
192 9.3063e-007 5e-009 390 196 390 5 1 0 5.6e-011 7.9e-016
193 9.3563e-007 5e-009 392 197 392 5 1 0 1.3e-010 7.6e-016
194 9.4063e-007 5e-009 394 198 394 5 1 0 1e-010 3.3e-016
195 9.4563e-007 5e-009 396 199 396 5 1 0 8.2e-011 4.2e-016
- 9.5e-007 - out
196 9.5063e-007 5e-009 398 200 398 5 1 0 7.8e-011 5.9e-016
197 9.5563e-007 5e-009 400 201 400 5 1 0 4.3e-011 3.5e-016
198 9.6063e-007 5e-009 402 202 402 5 1 0 1.1e-010 3.5e-016
199 9.6563e-007 5e-009 404 203 404 5 1 0 1.9e-010 4.2e-016
200 9.7063e-007 5e-009 406 204 406 4 1 0 1.6e-010 6.7e-016
201 9.7563e-007 5e-009 408 205 408 4 1 0 8.6e-011 6.8e-016
202 9.8063e-007 5e-009 410 206 410 4 1 0 1.4e-010 7.9e-016
203 9.8563e-007 5e-009 412 207 412 4 1 0 2.6e-010 7.5e-016
204 9.9063e-007 5e-009 414 208 414 4 1 0 2.1e-010 1.3e-015
205 9.9188e-007 1.25e-009 431 210 417 4 1 1 3.5e-010 8.3e-016
206 9.9334e-007 1.4614e-009 440 216 430 4 2 1 5.2e-010 2.2e-015
207 9.9353e-007 1.9078e-010 450 223 444 4 4 1 6.6e-010 1.5e-015
208 9.9391e-007 3.8156e-010 452 224 446 4 4 1 2.9e-010 1.5e-015
209 9.9423e-007 3.2237e-010 457 227 452 4 5 1 1.7e-010 1.3e-015
210 9.9448e-007 2.5086e-010 461 229 456 4 6 1 7.1e-010 1.4e-015
211 9.9452e-007 3.7847e-011 468 233 464 4 8 1 1.2e-010 1.2e-015
212 9.946e-007 7.5695e-011 470 234 466 4 8 1 2.9e-010 3.2e-015
213 9.9467e-007 7.5695e-011 472 235 468 4 8 1 2e-010 2.1e-015
214 9.9475e-007 7.5695e-011 474 236 470 4 8 1 3.5e-010 2e-015
215 9.9482e-007 6.8125e-011 476 237 472 4 8 1 3.7e-010 7.5e-015
216 9.9486e-007 4.4003e-011 481 240 478 4 9 1 2.1e-010 1.8e-014
217 9.9491e-007 4.4003e-011 483 241 480 4 9 1 2.3e-010 7.3e-014
218 9.9495e-007 4.4003e-011 485 242 482 4 9 1 4.3e-010 3.6e-014
219 9.9499e-007 4.4003e-011 488 244 486 4 9 1 2.7e-010 4.6e-014
220 9.9502e-007 3.1345e-011 492 246 490 3 10 1 5.1e-010 5.2e-014
221 9.9506e-007 3.1345e-011 500 253 504 3 10 1 4.8e-010 9.3e-014
222 9.9508e-007 2.1381e-011 512 263 524 2 11 1 5.2e-010 6.8e-014
223 9.951e-007 2.1381e-011 514 264 526 2 11 1 5.3e-011 7.5e-014
224 9.9512e-007 2.1381e-011 516 265 528 2 11 1 7e-010 8.7e-014
225 9.9514e-007 2.1381e-011 518 266 530 2 11 1 1.7e-010 1.1e-013

APPENDIX E (continued)

226 9.9516e-007 2.1381e-011 520 267 532 3 11 1 7.8e-010 1e-013
227 9.9521e-007 4.2762e-011 522 268 534 2 11 1 2.5e-010 3.8e-014
228 9.9524e-007 3.6728e-011 524 269 536 2 11 1 9.7e-010 4.6e-014
229 9.9528e-007 3.6728e-011 526 270 538 2 11 1 7.4e-010 2e-013
230 9.9531e-007 3.5075e-011 536 278 554 2 12 1 1.1e-010 6.6e-014
231 9.9535e-007 3.5075e-011 538 279 556 2 12 1 9.8e-010 7.7e-014
232 9.9538e-007 3.5075e-011 540 280 558 2 12 1 7.7e-011 9.6e-014
233 9.9542e-007 3.5075e-011 542 281 560 2 12 1 2.6e-010 1.3e-013
234 9.9545e-007 3.5075e-011 544 282 562 3 12 1 7.9e-010 5.5e-014
APPENDIX A (continued)
235 9.9549e-007 3.5075e-011 546 283 564 2 12 1 9.3e-010 4.6e-014
236 9.9552e-007 3.5075e-011 548 284 566 2 12 1 4.9e-010 1e-013
237 9.9556e-007 3.5075e-011 550 285 568 2 12 1 9e-010 9.5e-014
238 9.9559e-007 3.5075e-011 552 286 570 2 12 1 6.5e-010 1.8e-013
239 9.9563e-007 3.5075e-011 554 287 572 2 12 1 7.1e-010 1.1e-013
240 9.9567e-007 3.5075e-011 556 288 574 2 12 1 1.2e-010 1e-013
241 9.957e-007 3.5075e-011 558 289 576 2 12 1 8.9e-010 7.5e-014
242 9.9574e-007 3.5075e-011 560 290 578 2 12 1 8e-010 8.5e-014
243 9.9581e-007 7.0151e-011 562 291 580 2 12 1 1.6e-009 4.7e-014
244 9.9595e-007 1.403e-010 564 292 582 2 12 1 3.7e-009 1.2e-013
245 9.9609e-007 1.403e-010 566 293 584 2 12 1 2.4e-009 1.8e-013
246 9.9637e-007 2.806e-010 568 294 586 2 12 1 1.4e-009 1.1e-013
247 9.9693e-007 5.6121e-010 570 295 588 2 12 1 9.4e-010 6.8e-014
248 9.9749e-007 5.6121e-010 576 298 596 2 12 1 4.1e-010 1.7e-014
249 9.9805e-007 5.6121e-010 578 299 598 2 12 1 4.3e-010 2.6e-014
250 9.9917e-007 1.1224e-009 582 301 603 2 12 1 3.8e-010 1.5e-014
251 9.997e-007 5.2725e-010 595 311 624 2 13 1 4.2e-010 3.8e-014
252 9.9978e-007 8.057e-011 611 324 650 2 15 1 3e-010 5.2e-014
253 9.9994e-007 1.6114e-010 614 326 654 2 15 1 1.4e-009 6.7e-014
- 1e-006 - out
254 1.0001e-006 1.6114e-010 623 333 669 2 15 1 6.5e-008 2e-012
255 1.0002e-006 7.0744e-011 638 346 695 2 16 1 3.7e-008 2.6e-012
256 1.0002e-006 7.0744e-011 640 347 697 2 16 1 2.3e-008 2.4e-012
257 1.0003e-006 7.0744e-011 642 348 699 2 16 1 2.7e-008 1.5e-012
258 1.0004e-006 7.0744e-011 644 349 701 2 16 1 3.2e-008 1.4e-012
259 1.0005e-006 7.0744e-011 646 350 703 2 16 1 3e-008 5.7e-013
260 1.0006e-006 1.4149e-010 648 351 705 2 16 1 2.3e-009 4.1e-014
261 1.0009e-006 2.8298e-010 650 352 707 2 16 1 5.1e-010 5.4e-015
262 1.0014e-006 5.6596e-010 652 353 709 2 16 1 7.5e-011 6.6e-016
263 1.002e-006 5.6596e-010 654 354 711 2 16 1 4.4e-010 2.1e-015
264 1.0031e-006 1.1319e-009 656 355 713 2 16 1 3.1e-010 6e-016
265 1.0043e-006 1.1319e-009 658 356 715 2 16 1 3e-010 1.6e-015
266 1.0053e-006 1.0187e-009 660 357 717 2 16 1 2.6e-010 1.5e-015
267 1.0063e-006 1.0187e-009 662 358 719 2 16 1 4e-010 1.6e-015
268 1.0073e-006 1.0187e-009 664 359 721 2 16 1 3.6e-010 5.4e-016
269 1.0094e-006 2.0374e-009 666 360 723 2 16 1 1.7e-010 1.8e-015
270 1.0114e-006 2.0374e-009 668 361 725 2 16 1 1.7e-010 1.7e-015

APPENDIX E (continued)

271 1.0155e-006 4.0749e-009 670 362 727 2 16 1 3.6e-010 2.1e-015
272 1.0205e-006 5e-009 672 363 729 2 16 1 4.2e-010 1.8e-015
273 1.0255e-006 5e-009 674 364 731 2 16 1 3.5e-010 1.9e-015
274 1.0305e-006 5e-009 676 365 733 2 16 1 1.6e-010 1.9e-015
275 1.0355e-006 5e-009 678 366 735 2 16 1 4.1e-010 2.2e-015
276 1.0405e-006 5e-009 680 367 737 2 16 1 2.4e-010 1.7e-015
277 1.0455e-006 5e-009 682 368 739 3 16 1 3e-010 1.9e-015
- 1.05e-006 - out
278 1.0505e-006 5e-009 684 369 741 3 16 1 7.9e-011 1.5e-015
279 1.0555e-006 5e-009 686 370 743 3 16 1 2.2e-010 1.4e-015
280 1.0605e-006 5e-009 688 371 745 3 16 1 4.3e-010 1.8e-015
281 1.0655e-006 5e-009 690 372 747 3 16 1 3.5e-010 1.6e-015
282 1.0705e-006 5e-009 692 373 749 4 16 1 1.6e-010 1.6e-015
283 1.0755e-006 5e-009 694 374 751 4 16 1 5.6e-011 8.8e-016
284 1.0805e-006 5e-009 696 375 753 4 16 1 2.3e-010 1e-015
285 1.0855e-006 5e-009 698 376 755 4 16 1 6.1e-011 9.4e-016
286 1.0905e-006 5e-009 700 377 757 4 16 1 5.8e-011 7e-016
287 1.0955e-006 5e-009 702 378 759 4 16 1 3.5e-011 6.4e-016
- 1.1e-006 - out
288 1.1005e-006 5e-009 704 379 761 5 16 1 2.6e-010 7.4e-016
289 1.1055e-006 5e-009 706 380 763 5 16 1 1.7e-010 7.6e-016
290 1.1105e-006 5e-009 708 381 765 5 16 1 3.5e-010 7e-016
291 1.1155e-006 5e-009 710 382 767 5 16 1 4e-010 7.2e-016
292 1.1205e-006 5e-009 712 383 769 5 16 1 2.4e-011 7.8e-016
293 1.1255e-006 5e-009 714 384 771 5 16 1 4.8e-011 5.8e-016
294 1.1305e-006 5e-009 716 385 773 5 16 1 9.4e-011 6e-016
295 1.1355e-006 5e-009 718 386 775 5 16 1 9.2e-011 7.6e-016
296 1.1405e-006 5e-009 720 387 777 5 16 1 2.3e-011 5.5e-016
297 1.1455e-006 5e-009 722 388 779 5 16 1 1.3e-010 5.5e-016
- 1.15e-006 - out
298 1.1505e-006 5e-009 724 389 781 5 16 1 2.3e-011 5.8e-016
299 1.1555e-006 5e-009 726 390 783 5 16 1 4.2e-011 5.6e-016
300 1.1605e-006 5e-009 728 391 785 5 16 1 1.4e-010 4.8e-016
301 1.1655e-006 5e-009 730 392 787 5 16 1 4.5e-011 5e-016
302 1.1705e-006 5e-009 732 393 789 5 16 1 3.3e-011 3.1e-016
303 1.1755e-006 5e-009 734 394 791 5 16 1 6.7e-011 3.6e-016
304 1.1805e-006 5e-009 736 395 793 5 16 1 1.2e-010 6.2e-016
305 1.1855e-006 5e-009 738 396 795 5 16 1 8.7e-011 4.9e-016
306 1.1905e-006 5e-009 740 397 797 5 16 1 5.5e-011 4e-016
307 1.1955e-006 5e-009 742 398 799 5 16 1 1.3e-010 2.8e-016
- 1.2e-006 - out
308 1.2005e-006 5e-009 744 399 801 4 16 1 8.6e-011 3.3e-016
309 1.2055e-006 5e-009 746 400 803 4 16 1 5.8e-011 2.4e-016
310 1.2105e-006 5e-009 748 401 805 4 16 1 1.2e-011 2.5e-016
311 1.2155e-006 5e-009 750 402 807 4 16 1 2.6e-011 1.4e-016
312 1.2205e-006 5e-009 752 403 809 4 16 1 1.6e-011 3.2e-016
313 1.2255e-006 5e-009 754 404 811 4 16 1 3.6e-012 3.2e-016

APPENDIX E (continued)

314	1.2305e-006	5e-009	756	405	813	5	16	1	4.1e-012	2.7e-016
315	1.2355e-006	5e-009	758	406	815	5	16	1	3.4e-012	2.6e-016
316	1.2405e-006	5e-009	760	407	817	5	16	1	7.5e-012	1.7e-016
317	1.2455e-006	5e-009	762	408	819	5	16	1	5.6e-012	6.8e-017
-	1.25e-006	- out								
318	1.2505e-006	5e-009	764	409	821	5	16	1	2.4e-010	1.6e-015
319	1.2555e-006	5e-009	766	410	823	5	16	1	9.5e-011	1.9e-015
320	1.2605e-006	5e-009	768	411	825	5	16	1	1.7e-010	1.7e-015
321	1.2655e-006	5e-009	770	412	827	5	16	1	1.5e-010	1.7e-015
322	1.2705e-006	5e-009	772	413	829	5	16	1	6.1e-011	1.8e-015
323	1.2755e-006	5e-009	774	414	831	5	16	1	8.1e-011	1.5e-015
324	1.2805e-006	5e-009	776	415	833	4	16	1	1.4e-010	1.7e-015
325	1.2855e-006	5e-009	778	416	835	3	16	1	3.3e-010	1.5e-015
326	1.2905e-006	5e-009	780	417	837	2	16	1	1.9e-010	1.4e-015
327	1.2955e-006	5e-009	782	418	839	2	16	1	3.3e-010	1.5e-015
-	1.3e-006	- out								
328	1.3005e-006	5e-009	784	419	841	2	16	1	3.9e-010	1.3e-015
329	1.3055e-006	5e-009	786	420	843	2	16	1	5.9e-010	1.5e-015
330	1.3105e-006	5e-009	788	421	845	2	16	1	3.3e-010	2e-015
331	1.3155e-006	5e-009	790	422	847	3	16	1	2e-010	1.7e-015
332	1.3205e-006	5e-009	792	423	849	3	16	1	2e-010	1.6e-015
333	1.3255e-006	5e-009	794	424	851	3	16	1	2.9e-010	1.6e-015
334	1.3305e-006	5e-009	796	425	853	3	16	1	3.3e-010	1.4e-015
335	1.3355e-006	5e-009	798	426	855	3	16	1	1.5e-010	8.7e-016
336	1.3405e-006	5e-009	800	427	857	3	16	1	2.3e-010	1.4e-015
337	1.3455e-006	5e-009	802	428	859	2	16	1	3.7e-010	1.3e-015
-	1.35e-006	- out								
338	1.3505e-006	5e-009	804	429	861	2	16	1	8.1e-011	7.8e-016
339	1.3555e-006	5e-009	806	430	863	2	16	1	2e-010	1e-015
340	1.3605e-006	5e-009	808	431	865	2	16	1	2e-010	8.3e-016
341	1.3655e-006	5e-009	810	432	867	3	16	1	1.7e-010	9.6e-016
342	1.3705e-006	5e-009	812	433	869	3	16	1	2.6e-010	6.4e-016
343	1.3755e-006	5e-009	814	434	871	3	16	1	1.4e-010	7.1e-016
344	1.3805e-006	5e-009	816	435	873	3	16	1	1.2e-010	6.1e-016
345	1.3855e-006	5e-009	818	436	875	3	16	1	1.2e-011	7.1e-016
346	1.3905e-006	5e-009	820	437	877	3	16	1	1.3e-010	5.1e-016
347	1.3955e-006	5e-009	822	438	879	3	16	1	1.8e-010	6.2e-016
-	1.4e-006	- out								
348	1.4005e-006	5e-009	824	439	881	4	16	1	7.3e-011	5.2e-016
349	1.4055e-006	5e-009	826	440	883	4	16	1	1.8e-010	5.9e-016
350	1.4105e-006	5e-009	828	441	885	4	16	1	8.5e-011	7.2e-016
351	1.4155e-006	5e-009	830	442	887	4	16	1	1.2e-010	6e-016
352	1.4205e-006	5e-009	832	443	889	4	16	1	4.2e-011	4.7e-016
353	1.4255e-006	5e-009	834	444	891	4	16	1	2.4e-010	5.8e-016
354	1.4305e-006	5e-009	836	445	893	5	16	1	1.9e-011	4.5e-016
355	1.4355e-006	5e-009	838	446	895	5	16	1	1.1e-010	5.3e-016
356	1.4405e-006	5e-009	840	447	897	5	16	1	1.1e-010	5.5e-016

APPENDIX E (continued)

357	1.4455e-006	5e-009	842	448	899	5	16	1	1.6e-010	7.5e-016
-	1.45e-006	- out								
358	1.4505e-006	5e-009	844	449	901	5	16	1	1.3e-010	4.1e-016
359	1.4555e-006	5e-009	846	450	903	5	16	1	1.2e-010	4.5e-016
360	1.4605e-006	5e-009	848	451	905	5	16	1	9.3e-011	5.5e-016
361	1.4655e-006	5e-009	850	452	907	5	16	1	4.6e-011	5e-016
362	1.4705e-006	5e-009	852	453	909	5	16	1	4.4e-011	6.7e-016
363	1.4755e-006	5e-009	854	454	911	5	16	1	1.6e-010	5.7e-016
364	1.4805e-006	5e-009	856	455	913	5	16	1	1.1e-010	5.3e-016
365	1.4855e-006	5e-009	858	456	915	5	16	1	1.1e-011	5.8e-016
366	1.4905e-006	5e-009	860	457	917	5	16	1	1.4e-010	5.5e-016
367	1.4955e-006	5e-009	862	458	919	5	16	1	6.9e-011	5.7e-016
-	1.5e-006	- out								
368	1.5005e-006	5e-009	864	459	921	5	16	1	7.9e-011	5.3e-016
369	1.5055e-006	5e-009	866	460	923	5	16	1	2.5e-011	5e-016
370	1.5105e-006	5e-009	868	461	925	5	16	1	3.9e-011	4.4e-016
371	1.5155e-006	5e-009	870	462	927	5	16	1	2.6e-011	5.8e-016
372	1.5205e-006	5e-009	872	463	929	5	16	1	3.6e-011	4.5e-016
373	1.5255e-006	5e-009	874	464	931	5	16	1	1.9e-010	6e-016
374	1.5305e-006	5e-009	876	465	933	5	16	1	1.3e-010	4.7e-016
375	1.5355e-006	5e-009	878	466	935	5	16	1	1.2e-010	5.3e-016
376	1.5405e-006	5e-009	880	467	937	5	16	1	1.5e-010	6e-016
377	1.5455e-006	5e-009	882	468	939	4	16	1	1.1e-010	4.8e-016
-	1.55e-006	- out								
378	1.5505e-006	5e-009	884	469	941	4	16	1	8.6e-011	5.9e-016
379	1.5555e-006	5e-009	886	470	943	4	16	1	2.8e-011	5.7e-016
380	1.5605e-006	5e-009	888	471	945	4	16	1	4.1e-011	5.4e-016
381	1.5655e-006	5e-009	890	472	947	4	16	1	1.1e-010	7e-016
382	1.5705e-006	5e-009	892	473	949	4	16	1	1.1e-010	4.2e-016
383	1.5755e-006	5e-009	894	474	951	5	16	1	1e-010	5.5e-016
384	1.5805e-006	5e-009	896	475	953	5	16	1	4.1e-011	4.1e-016
385	1.5855e-006	5e-009	898	476	955	5	16	1	1.4e-010	5.7e-016
386	1.5905e-006	5e-009	900	477	957	5	16	1	4e-011	4.5e-016
387	1.5955e-006	5e-009	902	478	959	5	16	1	1.5e-010	4e-016
-	1.6e-006	- out								
388	1.6005e-006	5e-009	904	479	961	5	16	1	2.2e-010	4.1e-016
389	1.6055e-006	5e-009	906	480	963	5	16	1	7e-011	3.6e-016
390	1.6105e-006	5e-009	908	481	965	5	16	1	2.6e-010	3.7e-016
391	1.6155e-006	5e-009	910	482	967	5	16	1	8.1e-011	5.2e-016
392	1.6205e-006	5e-009	912	483	969	5	16	1	5.5e-011	5e-016
393	1.6255e-006	5e-009	914	484	971	5	16	1	1.5e-010	4.3e-016
394	1.6305e-006	5e-009	916	485	973	5	16	1	8.2e-011	3.2e-016
395	1.6355e-006	5e-009	918	486	975	5	16	1	5.1e-011	3.1e-016
396	1.6405e-006	5e-009	920	487	977	5	16	1	1.1e-010	3.2e-016
397	1.6455e-006	5e-009	922	488	979	5	16	1	1.6e-010	4e-016
-	1.65e-006	- out								
398	1.6505e-006	5e-009	924	489	981	5	16	1	2e-011	3.1e-016

APPENDIX E (continued)

399 1.6555e-006 5e-009 926 490 983 5 16 1 1.6e-010 3.8e-016
400 1.6605e-006 5e-009 928 491 985 5 16 1 1.3e-010 3e-016
401 1.6655e-006 5e-009 930 492 987 5 16 1 1.6e-010 3.6e-016
402 1.6705e-006 5e-009 932 493 989 5 16 1 8.8e-011 3.8e-016
403 1.6755e-006 5e-009 934 494 991 5 16 1 1.4e-010 3.4e-016
404 1.6805e-006 5e-009 936 495 993 5 16 1 1.3e-010 3.1e-016
405 1.6855e-006 5e-009 938 496 995 5 16 1 2.7e-010 2.8e-016
406 1.6905e-006 5e-009 940 497 997 5 16 1 2.6e-010 3.7e-016
407 1.6955e-006 5e-009 942 498 999 5 16 1 2.2e-010 3.9e-016
- 1.7e-006 - out
408 1.7005e-006 5e-009 944 499 1001 5 16 1 1.4e-010 3.1e-016
409 1.7055e-006 5e-009 946 500 1003 5 16 1 1e-010 6.3e-016
410 1.7105e-006 5e-009 948 501 1005 5 16 1 2.2e-010 4.3e-016
411 1.7155e-006 5e-009 950 502 1007 5 16 1 6.9e-011 3.9e-016
412 1.7205e-006 5e-009 952 503 1009 5 16 1 1e-010 5.6e-016
413 1.7255e-006 5e-009 954 504 1011 5 16 1 1.2e-010 2.6e-016
414 1.7305e-006 5e-009 956 505 1013 5 16 1 6.1e-011 4.2e-016
415 1.7355e-006 5e-009 958 506 1015 5 16 1 9.9e-011 3.5e-016
416 1.7405e-006 5e-009 960 507 1017 5 16 1 2.7e-010 3.7e-016
417 1.7455e-006 5e-009 962 508 1019 5 16 1 5.7e-011 3.9e-016
- 1.75e-006 - out
418 1.7505e-006 5e-009 964 509 1021 5 16 1 7e-011 3e-016
419 1.7555e-006 5e-009 966 510 1023 5 16 1 1.2e-010 3.1e-016
420 1.7605e-006 5e-009 968 511 1025 5 16 1 1.5e-010 2.6e-016
421 1.7655e-006 5e-009 970 512 1027 5 16 1 1.8e-010 4.2e-016
422 1.7705e-006 5e-009 972 513 1029 5 16 1 2.9e-010 5.2e-016
423 1.7755e-006 5e-009 974 514 1031 5 16 1 6.9e-011 2.5e-016
424 1.7805e-006 5e-009 976 515 1033 5 16 1 1.5e-010 4.1e-016
425 1.7855e-006 5e-009 978 516 1035 5 16 1 2.6e-011 2.5e-016
426 1.7905e-006 5e-009 980 517 1037 5 16 1 2.2e-010 2.2e-016
427 1.7955e-006 5e-009 982 518 1039 5 16 1 1.8e-010 4.3e-016
- 1.8e-006 - out
428 1.8005e-006 5e-009 984 519 1041 5 16 1 8.9e-011 2.8e-016
429 1.8055e-006 5e-009 986 520 1043 5 16 1 5.2e-011 3.3e-016
430 1.8105e-006 5e-009 988 521 1045 5 16 1 6.5e-011 3.2e-016
431 1.8155e-006 5e-009 990 522 1047 5 16 1 8.1e-011 2.5e-016
432 1.8205e-006 5e-009 992 523 1049 5 16 1 4.9e-011 2.2e-016
433 1.8255e-006 5e-009 994 524 1051 5 16 1 7.5e-011 5.1e-016
434 1.8305e-006 5e-009 996 525 1053 5 16 1 2.3e-011 1.6e-016
435 1.8355e-006 5e-009 998 526 1055 5 16 1 6.3e-011 5.3e-016
436 1.8405e-006 5e-009 1000 527 1057 5 16 1 1.2e-010 3.8e-016
437 1.8455e-006 5e-009 1002 528 1059 5 16 1 7.9e-011 3.6e-016
- 1.85e-006 - out
438 1.8505e-006 5e-009 1004 529 1061 5 16 1 3.8e-011 3.2e-016
439 1.8555e-006 5e-009 1006 530 1063 5 16 1 1e-011 2.4e-016
440 1.8605e-006 5e-009 1008 531 1065 5 16 1 7.9e-011 1.7e-016
441 1.8655e-006 5e-009 1010 532 1067 5 16 1 8.2e-011 2.7e-016

442 1.8705e-006 5e-009 1012 533 1069 5 16 1 3.1e-011 4e-016
443 1.8755e-006 5e-009 1014 534 1071 5 16 1 1.6e-010 3.3e-016
444 1.8805e-006 5e-009 1016 535 1073 5 16 1 2e-011 4.2e-016
445 1.8855e-006 5e-009 1018 536 1075 5 16 1 6.4e-011 6e-016
446 1.8905e-006 5e-009 1020 537 1077 5 16 1 9.1e-011 8.9e-016
447 1.8955e-006 5e-009 1022 538 1079 5 16 1 2.3e-010 1.3e-015
- 1.9e-006 - out
448 1.9005e-006 5e-009 1024 539 1081 5 16 1 1.6e-010 1.5e-015
449 1.9055e-006 5e-009 1026 540 1083 5 16 1 4.8e-011 1.7e-015
450 1.9105e-006 5e-009 1028 541 1085 5 16 1 2.4e-010 1.8e-015
451 1.9155e-006 5e-009 1030 542 1087 5 16 1 1.7e-010 1.9e-015
452 1.9205e-006 5e-009 1032 543 1089 5 16 1 1.1e-010 2e-015
453 1.9255e-006 5e-009 1034 544 1091 5 16 1 1.5e-010 1.9e-015
454 1.9305e-006 5e-009 1036 545 1093 5 16 1 4.8e-011 1.9e-015
455 1.9355e-006 5e-009 1038 546 1095 5 16 1 7.8e-011 1.8e-015
456 1.9405e-006 5e-009 1040 547 1097 5 16 1 1.2e-010 2e-015
457 1.9455e-006 5e-009 1042 548 1099 5 16 1 4.9e-011 1.7e-015
- 1.95e-006 - out
458 1.9505e-006 5e-009 1044 549 1101 5 16 1 2.4e-010 8.8e-016
459 1.9555e-006 5e-009 1046 550 1103 5 16 1 7.3e-011 1.9e-015
460 1.9605e-006 5e-009 1048 551 1105 5 16 1 1.7e-010 2.1e-015
461 1.9655e-006 5e-009 1050 552 1107 5 16 1 1.5e-010 2e-015
462 1.9705e-006 5e-009 1052 553 1109 5 16 1 1.5e-010 2.1e-015
463 1.9755e-006 5e-009 1054 554 1111 5 16 1 3e-011 1.2e-015
464 1.9805e-006 5e-009 1056 555 1113 5 16 1 7.9e-011 1.6e-015
465 1.9855e-006 5e-009 1058 556 1115 5 16 1 2.7e-010 2.4e-015
466 1.9905e-006 5e-009 1060 557 1117 5 16 1 3.4e-010 1.7e-015
467 1.9955e-006 5e-009 1062 558 1119 5 16 1 2.6e-010 7.6e-016
- 2e-006 - out
468 2.0005e-006 5e-009 1064 559 1121 5 16 1 4.9e-011 2e-015
Time-stepping completed.
Time-Dependent Solver 1 in Study 1/Solution 1 (sol1): Solution time: 1334 s (22 minutes, 14 seconds)
Physical memory: 1.3 GB
Virtual memory: 1.54 GB

Stationary Solver 1 in Study 2/Solution 3 (sol3) started at 26-Oct-2017 16:23:19.
Linear solver
Number of degrees of freedom solved for: 21137 (plus 2689 internal DOFs).
Symmetric matrices found.
Scales for dependent variables:
Temperature (comp2.T): 3.1e+002
Orthonormal null-space function used.
Iter SolEst Damping Stepsize #Res #Jac #Sol LinErr LinRes
1 0.011 1.0000000 0.011 1 1 1 8.4e-012 1.5e-013
Stationary Solver 1 in Study 2/Solution 3 (sol3): Solution time: 517 s (8 minutes, 37 seconds)
Physical memory: 4.55 GB
Virtual memory: 4.72 GB

CITED LITERATURE

Appelgren, Tobias, Sofia Zetterstrand, Jorgen Elfversson, and Daniel Nilsson. 2010. "Long-Term Outcome after Treatment of Hydrocephalus in Children." *Pediatric Neurosurgery* 46 (3):221–26. https://doi.org/10.1159/000319365.

Armenean, Cristina, Emmanuel Perrin, Mircea Armenean, Olivier Beuf, Frank Pilleul, and Herve Saint-Jalmes. 2004. "RF-Induced Temperature Elevation along Metallic Wires in Clinical Magnetic Resonance Imaging: Influence of Diameter and Length." *Magnetic Resonance in Medicine* 52 (5):1200–1206. https://doi.org/10.1002/mrm.20246.

Bañobre-López, Manuel, Antonio Teijeiro, and Jose Rivas. 2013. "Magnetic Nanoparticle-Based Hyperthermia for Cancer Treatment." *Reports of Practical Oncology & Radiotherapy* 18 (6):397–400. https://doi.org/http://dx.doi.org/10.1016/j.rpor.2013.09.011.

Basati, Sukhraaj, Kevin Tangen, Ying Hsu, Hanna Lin, David Frim, and Andreas Linninger. 2015. "Impedance Changes Indicate Proximal Ventriculoperitoneal Shunt Obstruction In Vitro." *IEEE Transactions on Bio-Medical Engineering* 62 (12):2787–93. https://doi.org/10.1109/TBME.2014.2335171.

Baştuğ, Turgut, and Serdar Kuyucak. 2005. "Temperature Dependence of the Transport Coefficients of Ions from Molecular Dynamics Simulations." *Chemical Physics Letters* 408 (1):84–88. https://doi.org/http://dx.doi.org/10.1016/j.cplett.2005.04.012.

Berjano, Enrique J. 2006. "Theoretical Modeling for Radiofrequency Ablation: State-of-the-Art and Challenges for the Future." *BioMedical Engineering OnLine* 5:24. https://doi.org/10.1186/1475-925X-5-24.

Bhavaraju, N. C., V. Nagaraddi, S. R. Chetlapalli, and I. Osorio. 2002. "Electrical and Thermal Behavior of Non-Ferrous Noble Metal Electrodes Exposed to MRI Fields." *Magnetic Resonance Imaging* 20 (4):351–57.

Blegvad, C., A. D. Skjolding, H. Broholm, H. Laursen, and M. Juhler. 2013. "Pathophysiology of Shunt Dysfunction in Shunt Treated Hydrocephalus." *Acta Neurochirurgica* 155 (9):1763–1772. https://doi.org/10.1007/s00701-013-1729-6.

Browd, Samuel R., Oren N. Gottfried, Brian T. Ragel, and John R. W. Kestle. 2006b. "Failure of Cerebrospinal Fluid Shunts: Part II: Overdrainage, Loculation, and Abdominal Complications." *Pediatric Neurology* 34 (3):171–76. https://doi.org/http://dx.doi.org/10.1016/j.pediatrneurol.2005.05.021.

Browd, Samuel R., Brian T. Ragel, Oren N. Gottfried, and John R. W. Kestle. 2006a. "Failure of Cerebrospinal Fluid Shunts: Part I: Obstruction and Mechanical Failure." *Pediatric Neurology* 34 (2):83–92. https://doi.org/http://dx.doi.org/10.1016/j.pediatrneurol.2005.05.020.

Budgett, David M., Aiguo Patrick Hu, Ping Si, Wayne T. Pallas, Mark G. Donnelly, Jared W. T. Broad, Carolyn J. Barrett, Sarah-Jane Guild, and Simon C. Malpas. 2007. "Novel Technology for the Provision of Power to Implantable Physiological Devices." *Journal of Applied Physiology* 102 (4):1658–1663. https://doi.org/10.1152/japplphysiol.00105.2006.

Bulat, Marin, and Marijan Klarica. 2011. "Recent Insights into a New Hydrodynamics of the Cerebrospinal Fluid." *Brain Research Reviews* 65 (2):99–112. https://doi.org/https://doi.org/10.1016/j.brainresrev.2010.08.002.

Cherukuri, Paul, Evan S. Glazer, and Steven A. Curley. 2010. “Targeted Hyperthermia Using Metal Nanoparticles.” *Advanced Drug Delivery Reviews* 62 (3):339–45. https://doi.org/http://dx.doi.org/10.1016/j.addr.2009.11.006.

Chi, John, Heather Fullerton, and Nalin Gupta. 2005. “Time Trends and Demographics of Deaths from Congenital Hydrocephalus in Children in the United States: National Center for Health Statistics Data, 1979 to 1998.” *Journal of Neurosurgery: Pediatrics* 103 (2):113–18. https://doi.org/10.3171/ped.2005.103.2.0113.

Chicheł, Adam, Janusz Skowronek, Magda Kubaszewska, and Marek Kanikowski. 2007. “Hyperthermia – Description of a Method and a Review of Clinical Applications.” *Reports of Practical Oncology & Radiotherapy* 12 (5):267–75. https://doi.org/10.1016/S1507-1367(10)60065-X.

Chou, C. K., J. A. McDougall, and K. W. Chan. 1997. “RF Heating of Implanted Spinal Fusion Stimulator during Magnetic Resonance Imaging.” *IEEE Transactions on Bio-Medical Engineering* 44 (5):367–73. https://doi.org/10.1109/10.568912.

Ciumas, Carolina, Gregor Schaefers, Sandrine Bouvard, Emmeline Tailhades, Emmanuel Perrin, Jean-Christophe Comte, Emmanuelle Canet-Soulas, et al. 2014. “A Phantom and Animal Study of Temperature Changes during fMRI with Intracerebral Depth Electrodes.” *Epilepsy Research* 108 (1):57–65. https://doi.org/http://dx.doi.org/10.1016/j.eplepsyres.2013.10.016.

Cui, Daan, and Mojie Cheng. 2009. “Numerical Analysis of Thermal and Electrochemical Phenomena for Anode Supported Microtubular SOFC.” *AIChE Journal* 55 (3):771–782. https://doi.org/10.1002/aic.11697.

Darcey, Terrance M., Erik J. Kobylarz, Michael A. Pearl, Patricia J. Krauss, Stephanie A. Ferri, David W. Roberts, and David F. Bauer. 2016. “Safe Use of Subdermal Needles for Intraoperative Monitoring with MRI.” *Neurosurgical Focus* 40 (3):E19. https://doi.org/10.3171/2015.12.FOCUS15555.

Davalos, R. V., L. M. Mir, and B. Rubinsky. 2005. “Tissue Ablation with Irreversible Electroporation.” *Annals of Biomedical Engineering* 33 (2):223. https://doi.org/10.1007/s10439-005-8981-8.

Davies, Angela M., Uri Weinberg, and Yoram Palti. 2013. “Tumor Treating Fields: A New Frontier in Cancer Therapy.” *Annals of the New York Academy of Sciences* 1291 (1):86–95. https://doi.org/10.1111/nyas.12112.

Del Bigio, M. R. 1998. “Biological Reactions to Cerebrospinal Fluid Shunt Devices: A Review of the Cellular Pathology.” *Neurosurgery* 42 (2):319-25; discussion 325-326.

Dewhirst, M. W., B. L. Viglianti, M. Lora-Michiels, M. Hanson, and P. J. Hoopes. 2003. “Basic Principles of Thermal Dosimetry and Thermal Thresholds for Tissue Damage from Hyperthermia.” *International Journal of Hyperthermia : The Official Journal of European Society for Hyperthermic Oncology, North American Hyperthermia Group* 19 (3):267–94. https://doi.org/10.1080/0265673031000119006.

Elwassif, Maged M., Qingjun Kong, Maribel Vazquez, and Marom Bikson. 2006. “Bio-Heat Transfer Model of Deep Brain Stimulation Induced Temperature Changes.” *Conference Proceedings : ... Annual International Conference of the IEEE Engineering in Medicine and Biology Society. IEEE Engineering in Medicine and Biology Society. Annual Conference* 1:3580–83. https://doi.org/10.1109/IEMBS.2006.259425.

Fiorentini, Giammaria, Petros Giovanis, Susanna Rossi, Patrizia Dentico, Raffaele Paola, Gina Turrisi, and Paolo Bernardeschi. 2006. “A Phase II Clinical Study on Relapsed Malignant Gliomas Treated with Electro-Hyperthermia.” *In Vivo* 20 (6):721–724.

Gebert, Anna-Felicitas, Matthias Schulz, Karin Schwarz, and Ulrich-Wilhelm Thomale. 2016. "Long-Term Survival Rates of Gravity-Assisted, Adjustable Differential Pressure Valves in Infants with Hydrocephalus." *Journal of Neurosurgery: Pediatrics* 17 (5):544–51. https://doi.org/10.3171/2015.10.PEDS15328.

Georgi, J.-C., C. Stippich, V.M. Tronnier, and S. Heiland. 2004. "Active Deep Brain Stimulation during MRI: A Feasibility Study." *Magnetic Resonance in Medicine* 51 (2):380–388. https://doi.org/10.1002/mrm.10699.

Ginsberg, Howard J., James M. Drake, Thomas M. Peterson, and Richard S. C. Cobbold. 2006. "Recanalization of Obstructed Cerebrospinal Fluid Ventricular Catheters Using Ultrasonic Cavitation." *Neurosurgery* 59 (4 Suppl 2):ONS403–412; discussion ONS412. https://doi.org/10.1227/01.NEU.0000233968.80352.25.

Gnanalingham, Kanna K., Jesus Lafuente, Stefan Brew, Dominic Thompson, William Harkness, and Richard Hayward. 2005. "Percutaneous Coagulation of Choroid Plexus to Unblock the Ventricular Catheter Using the Seldinger Technique: Preliminary Report." *Surgical Neurology* 64 (5):440–43. https://doi.org/http://dx.doi.org/10.1016/j.surneu.2005.06.015.

Goel, A. 2002. "Tumour Induced Hydrocephalus and Oedema: Pathology or Natural Defence." *Journal of Postgraduate Medicine* 48 (2):153–54.

Golberg, Alexander, and Martin L. Yarmush. 2013. "Nonthermal Irreversible Electroporation: Fundamentals, Applications, and Challenges." *IEEE Transactions on Bio-Medical Engineering* 60 (3):707–14. https://doi.org/10.1109/TBME.2013.2238672.

Gruber, Rolf W., and Bernd Roehrig. 2010. "Prevention of Ventricular Catheter Obstruction and Slit Ventricle Syndrome by the Prophylactic Use of the Integra Antisiphon Device in Shunt Therapy for Pediatric Hypertensive Hydrocephalus: A 25-Year Follow-up Study." *Journal of Neurosurgery: Pediatrics* 5 (1):4–16. https://doi.org/10.3171/2008.7.17690.

Hanak, Brian W., Emily F. Ross, Carolyn A. Harris, Samuel R. Browd, and William Shain. 2016. "Toward a Better Understanding of the Cellular Basis for Cerebrospinal Fluid Shunt Obstruction: Report on the Construction of a Bank of Explanted Hydrocephalus Devices." *Journal of Neurosurgery: Pediatrics* 18 (2):213–23. https://doi.org/10.3171/2016.2.PEDS15531.

Handler, M.H. 1996. "A Complication in Removing a Retained Ventricular Catheter Using Electrocautery." *Pediatric Neurosurgery* 25 (5):276–276.

Harmon, B. V., A. M. Corder, R. J. Collins, G. C. Gobe, J. Allen, D. J. Allan, and J. F. Kerr. 1990. "Cell Death Induced in a Murine Mastocytoma by 42-47 Degrees C Heating in Vitro: Evidence That the Form of Death Changes from Apoptosis to Necrosis above a Critical Heat Load." *International Journal of Radiation Biology* 58 (5):845–58.

Harris, Carolyn A., and James P. McAllister. 2011. "Does Drainage Hole Size Influence Adhesion on Ventricular Catheters?" *Child's Nervous System* 27 (8):1221–1232. https://doi.org/10.1007/s00381-011-1430-0.

Harris, Carolyn A., and James P. 2nd McAllister. 2012. "What We Should Know about the Cellular and Tissue Response Causing Catheter Obstruction in the Treatment of Hydrocephalus." *Neurosurgery* 70 (6):1589-601; discussion 1601-1602. https://doi.org/10.1227/NEU.0b013e318244695f.

Haveman, J., P. Sminia, J. Wondergem, J. van der Zee, and M. C. C. M. Hulshof. 2005. "Effects of Hyperthermia on the Central Nervous System: What Was Learnt from Animal Studies?" *International Journal of Hyperthermia : The Official Journal of European Society for*

Hyperthermic Oncology, North American Hyperthermia Group 21 (5):473–87. https://doi.org/10.1080/02656730500159079.

Hellwig, Dieter, Joachim Andreas Grotenhuis, Wuttipong Tirakotai, Thomas Riegel, Dirk Michael Schulte, Bernhard Ludwig Bauer, and Helmut Bertalanffy. 2005. "Endoscopic Third Ventriculostomy for Obstructive Hydrocephalus." *Neurosurgical Review* 28 (1):1–34. https://doi.org/10.1007/s10143-004-0365-2.

Hideki Ogiwara, Kodai Uematsu, and Nobuhito Morota. 2014. "Obliteration of the Choroid Plexus after Endoscopic Coagulation." *Journal of Neurosurgery: Pediatrics* 14 (3):230–33. https://doi.org/10.3171/2014.6.PEDS1438.

Hildebrandt, Bert, Peter Wust, Olaf Ahlers, Annette Dieing, Geetha Sreenivasa, Thoralf Kerner, Roland Felix, and Hanno Riess. 2002. "The Cellular and Molecular Basis of Hyperthermia." *Critical Reviews in Oncology/Hematology* 43 (1):33–56. https://doi.org/http://dx.doi.org/10.1016/S1040-8428(01)00179-2.

Hirofumi Hirano, Kazuho Hirahara, Tetsuhiko Asakura, Tetsuro Shimozuru, Koki Kadota, Shizuya Kasamo, Masaru Shimohonji, Kanetaka Kimotsuki, and Masamichi Goto. 1994. "Hydrocephalus due to Villous Hypertrophy of the Choroid Plexus in the Lateral Ventricles." *Journal of Neurosurgery* 80 (2):321–23. https://doi.org/10.3171/jns.1994.80.2.0321.

Horsman, M. R., and J. Overgaard. 2007. "Hyperthermia: A Potent Enhancer of Radiotherapy." *Clinical Oncology* 19 (6):418–26. https://doi.org/http://dx.doi.org/10.1016/j.clon.2007.03.015.

Hudgins, R. J., and W. R. Boydston. 1998. "Shunt Revision by Coagulation with Retention of the Ventricular Catheter." *Pediatric Neurosurgery* 29 (2):57–59.

Huyette, David R., Benjamin J. Turnbow, Christian Kaufman, Dale F. Vaslow, Benjamin B. Whiting, and Michael Y. Oh. 2008. "Accuracy of the Freehand Pass Technique for Ventriculostomy Catheter Placement: Retrospective Assessment Using Computed Tomography Scans." *Journal of Neurosurgery* 108 (1):88–91. https://doi.org/10.3171/JNS/2008/108/01/0088.

Iglesias, Sara, Bienvenido Ros, Álvaro Martín, Antonio Carrasco, Miguel Segura, Andrea Delgado, Francisca Rius, and Miguel Ángel Arráez. 2016. "Surgical Outcome of the Shunt: 15-Year Experience in a Single Institution." *Child's Nervous System*, 1–9. https://doi.org/10.1007/s00381-016-3206-z.

Israelachvili, Jacob N. 1992. "Electrostatic Forces between Surfaces in Liquids." In *Intermolecular and Surface Forces*, Second, 213–60. Academic Press.

J. A. Nyenhuis, Sung-Min Park, R. Kamondetdacha, A. Amjad, F. G. Shellock, and A. R. Rezai. 2005. "MRI and Implanted Medical Devices: Basic Interactions with an Emphasis on Heating." *IEEE Transactions on Device and Materials Reliability* 5 (3):467–80. https://doi.org/10.1109/TDMR.2005.859033.

Jung, Nayoung, and Dongwon Kim. 2013. "Effect of Electromagnetic Navigated Ventriculoperitoneal Shunt Placement on Failure Rates." *Journal of Korean Neurosurgical Society* 53 (3):150–54. https://doi.org/10.3340/jkns.2013.53.3.150.

Kast, J., D. Duong, F. Nowzari, W. M. Chadduck, and S. J. Schiff. 1994. "Time-Related Patterns of Ventricular Shunt Failure." *Child's Nervous System : ChNS : Official Journal of the International Society for Pediatric Neurosurgery* 10 (8):524–28.

Kaufman, B. A., and T. S. Park. 1999. "Ventricular Anatomy and Shunt Catheters." *Pediatric Neurosurgery* 31 (1):1–6. https://doi.org/28823.

Kehler, Uwe, A. Klöhn, O. Heese, and J. Gliemroth. 2003. "Hydrocephalus Therapy: Reduction of Shunt Occlusions Using a Peel-Away Sheath." *Clinical Neurology and Neurosurgery* 105 (4):253–55. https://doi.org/10.1016/S0303-8467(03)00041-6.

Kehler, Uwe, Niels Langer, Jan Gliemroth, Ullrich Meier, Johannes Lemcke, Christian Sprung, Hans-Georg Schlosser, Michael Kiefer, Regina Eymann, and Oliver Heese. 2012. "Reduction of Shunt Obstructions by Using a Peel-Away Sheath Technique? A Multicenter Prospective Randomized Trial." *Clinical Neurology and Neurosurgery* 114 (4):381–84. https://doi.org/10.1016/j.clineuro.2011.11.020.

Kestle, J., J. Drake, R. Milner, C. Sainte-Rose, G. Cinalli, F. Boop, J. Piatt, et al. 2000. "Long-Term Follow-up Data from the Shunt Design Trial." *Pediatric Neurosurgery* 33 (5):230–36. https://doi.org/55960.

Kim, Yong Bae, Jae Whan Lee, Kyu Sung Lee, and Kyu Chang Lee. 2006. "Image-Guided Placement of Ventricular Shunt Catheter." *Journal of Clinical Neuroscience* 13 (1):50–54. https://doi.org/10.1016/j.jocn.2004.12.010.

Kirson, Eilon D., Vladimír Dbalý, František Tovaryš, Josef Vymazal, Jean F. Soustiel, Aviran Itzhaki, Daniel Mordechovich, et al. 2007. "Alternating Electric Fields Arrest Cell Proliferation in Animal Tumor Models and Human Brain Tumors." *Proceedings of the National Academy of Sciences* 104 (24):10152–57. https://doi.org/10.1073/pnas.0702916104.

Kirson, Eilon D., Zoya Gurvich, Rosa Schneiderman, Erez Dekel, Aviran Itzhaki, Yoram Wasserman, Rachel Schatzberger, and Yoram Palti. 2004. "Disruption of Cancer Cell Replication by Alternating Electric Fields." *Cancer Research* 64 (9):3288–3295. https://doi.org/10.1158/0008-5472.CAN-04-0083.

Kossovsky, Nir, and Robert B. Snow. 1989. "Clinical-Pathological Analysis of Failed Central Nervous System Fluid Shunts." *Journal of Biomedical Materials Research* 23 (S13):73–86. https://doi.org/10.1002/jbm.820231308.

Kousi, Maria, and Nicholas Katsanis. 2016. "The Genetic Basis of Hydrocephalus." *Annual Review of Neuroscience* 39 (July):409–35. https://doi.org/10.1146/annurev-neuro-070815-014023.

Kovacs, Norbert, Ferenc Nagy, Ferenc Kover, Adam Feldmann, Carlos Llumiguano, Jozsef Janszky, Gyula Kotek, Tamas Doczi, and Istvan Balas. 2006. "Implanted Deep Brain Stimulator and 1.0-Tesla Magnetic Resonance Imaging." *Journal of Magnetic Resonance Imaging : JMRI* 24 (6):1409–12. https://doi.org/10.1002/jmri.20779.

Krauss, Joachim K., Jens P. Regel, Werner Vach, Dirk W. Droste, Jan J. Borremans, and Thomas Mergner. 1996. "Vascular Risk Factors and Arteriosclerotic Disease in Idiopathic Normal-Pressure Hydrocephalus of the Elderly." *Stroke* 27 (1):24–29. https://doi.org/10.1161/01.STR.27.1.24.

Ladd, Mark E., and Harald H. Quick. 2000. "Reduction of Resonant RF Heating in Intravascular Catheters Using Coaxial Chokes." *Magnetic Resonance in Medicine* 43 (4):615–619. https://doi.org/10.1002/(SICI)1522-2594(200004)43:4<615::AID-MRM19>3.0.CO;2-B.

Lazareff, J. A., W. Peacock, L. Holly, J. Ver Halen, A. Wong, and C. Olmstead. 1998. "Multiple Shunt Failures: An Analysis of Relevant Factors." *Child's Nervous System : ChNS : Official Journal of the International Society for Pediatric Neurosurgery* 14 (6):271–75.

Lee, H., K. Kolahi, M. Bergsneider, and J. W. Judy. 2014. "Mechanical Evaluation of Unobstructing Magnetic Microactuators for Implantable Ventricular Catheters." *Journal of Microelectromechanical Systems* 23 (4):795–802. https://doi.org/10.1109/JMEMS.2014.2321377.

Lee, S. Y., S. H. Lee, K. Akuta, M. Uda, and C. W. Song. 2000. "Acute Histological Effects of Interstitial Hyperthermia on Normal Rat Brain." *International Journal of Hyperthermia : The Official Journal of European Society for Hyperthermic Oncology, North American Hyperthermia Group* 16 (1):73–83.

Lee, Selene A., Hyowon Lee, James R. Pinney, Elvira Khialeeva, Marvin Bergsneider, and Jack W. Judy. 2011. "Development of Microfabricated Magnetic Actuators for Removing Cellular Occlusion." *Journal of Micromechanics and Microengineering : Structures, Devices, and Systems* 21 (5):54006. https://doi.org/10.1088/0960-1317/21/5/054006.

Lew, Sean M., Anne E. Matthews, Adam L. Hartman, and Neil Haranhalli. 2013. "Post-Hemispherectomy Hydrocephalus: Results of a Comprehensive, Multi-Institutional Review." *Epilepsia* 54 (2):383–89. https://doi.org/10.1111/epi.12010.

Linninger, Andreas A., Cristian Tsakiris, David C. Zhu, Michalis Xenos, Peter Roycewicz, Zachary Danziger, and Richard Penn. 2005. "Pulsatile Cerebrospinal Fluid Dynamics in the Human Brain." *IEEE Transactions on Bio-Medical Engineering* 52 (4):557–65. https://doi.org/10.1109/TBME.2005.844021.

Linninger, Andreas, Sukhraaj Basati, Robert Dawe, and Richard Penn. 2009. "An Impedance Sensor to Monitor and Control Cerebral Ventricular Volume." *Medical Engineering & Physics* 31 (7):838–45. https://doi.org/10.1016/j.medengphy.2009.03.011.

Mallory, Matthew, Emile Gogineni, Guy C. Jones, Lester Greer, and Charles B. Simone II. 2016. "Therapeutic Hyperthermia: The Old, the New, and the Upcoming." *Critical Reviews in Oncology/Hematology* 97:56–64. https://doi.org/http://dx.doi.org/10.1016/j.critrevonc.2015.08.003.

Martínez-Lage, F. J., Francisco López, Máximo Poza, and Mayte Hernández. 1998. "Prevention of Intraventricular Hemorrhage during CSF Shunt Revisions by Means of a Flexible Coagulating electrodeA Preliminary Report." *Child's Nervous System* 14 (4):203–206. https://doi.org/10.1007/s003810050211.

Medtronic, MN. 2017a. "ActivaTM Medtronic." http://professional.medtronic.com/mri/clinicians/mri-dbs-systems/index.htm.

———. 2017b. "Medtronic Neurosurgery." http://www.medtronic.com/us-en/businesses/neurosurgery.html.

"Microbot Medical Inc." 2017. http://www.microbotmedical.com/product/self-cleaning-shunt-scs/.

Nelson, D. A., and S. A. Nunneley. 1998. "Brain Temperature and Limits on Transcranial Cooling in Humans: Quantitative Modeling Results." *European Journal of Applied Physiology and Occupational Physiology* 78 (4):353–59.

Neufeld, E., S. Kuhn, G. Szekely, and N. Kuster. 2009. "Measurement, Simulation and Uncertainty Assessment of Implant Heating during MRI." *Physics in Medicine and Biology* 54 (13):4151–69. https://doi.org/10.1088/0031-9155/54/13/012.

Nielsen, Nadine, and Amanda Breedt. 2017. "Hydrocephalus." In *Nursing Care of the Pediatric Neurosurgery Patient*, 3rd ed. Springer International Publishing.

Nulsen, F. E., and E. B. Spitz. 1952. "Treatment of Hydrocephalus by Direct Shunt from Ventricle to Jugular Vain." *Surgical Forum*, 399–403.

Oi, Shizuo. 2005. "Classification and Definition of Hydrocephalus: Origin, Controversy, and Assignment Ofthe Terminology." In *Pediatric Hydrocephalus*, 95–112. Springer-Verlag Italia.

Orešković, D., and M. Klarica. 2011. “Development of Hydrocephalus and Classical Hypothesis of Cerebrospinal Fluid Hydrodynamics: Facts and Illusions.” *Progress in Neurobiology* 94 (3):238–58. https://doi.org/http://dx.doi.org/10.1016/j.pneurobio.2011.05.005.

Pattisapu, J. V., E. R. Trumble, K. R. Taylor, P. D. Howard, and T. M. Kovach. 1999. “Percutaneous Endoscopic Recanalization of the Catheter: A New Technique of Proximal Shunt Revision.” *Neurosurgery* 45 (6):1361-6; discussion 1366-1367.

Patwardhan, Ravish V., and Anil Nanda. 2005. “Implanted Ventricular Shunts in the United States: The Billion-Dollar-a-Year Cost of Hydrocephalus Treatment.” *Neurosurgery* 56 (1):139-44; discussion 144-145.

Piatt, J. H. Jr. 1995. “Cerebrospinal Fluid Shunt Failure: Late Is Different from Early.” *Pediatric Neurosurgery* 23 (3):133–39.

Pople, Ian K. 2002. “Hydrocephalus and Shunts: What the Neurologist Should Know.” *Journal of Neurology, Neurosurgery & Psychiatry* 73 (suppl 1):i17–i22. https://doi.org/10.1136/jnnp.73.suppl_1.i17.

Reddy, G. Kesava, Papireddy Bollam, and Gloria Caldito. 2014. “Long-Term Outcomes of Ventriculoperitoneal Shunt Surgery in Patients with Hydrocephalus.” *World Neurosurgery* 81 (2):404–10. https://doi.org/10.1016/j.wneu.2013.01.096.

Redzic, Zoran B., and Malcolm B. Segal. 2004. “The Structure of the Choroid Plexus and the Physiology of the Choroid Plexus Epithelium.” *Advanced Drug Delivery Reviews* 56 (12):1695–1716. https://doi.org/http://dx.doi.org/10.1016/j.addr.2004.07.005.

Rekate, Harold L. 2009. “A Contemporary Definition and Classification of Hydrocephalus.” *Seminars in Pediatric Neurology* 16 (1):9–15. https://doi.org/10.1016/j.spen.2009.01.002.

Rock, Kenneth L., and Hajime Kono. 2008. “The Inflammatory Response to Cell Death.” *Annual Review of Pathology* 3:99–126. https://doi.org/10.1146/annurev.pathmechdis.3.121806.151456.

Rossmeisl Jr, John H., Paulo A. Garcia, Theresa E. Pancotto, John L. Robertson, Natalia Henao-Guerrero, Robert E. Neal II, Thomas L. Ellis, and Rafael V. Davalos. 2015. “Safety and Feasibility of the NanoKnife System for Irreversible Electroporation Ablative Treatment of Canine Spontaneous Intracranial Gliomas.” *Journal of Neurosurgery* 123 (4):1008–25. https://doi.org/10.3171/2014.12.JNS141768.

Sakka, L., G. Coll, and J. Chazal. 2011. “Anatomy and Physiology of Cerebrospinal Fluid.” *European Annals of Otorhinolaryngology, Head and Neck Diseases* 128 (6):309–16. https://doi.org/10.1016/j.anorl.2011.03.002.

Scellig S. D. Stone, and Benjamin C. Warf. 2014. “Combined Endoscopic Third Ventriculostomy and Choroid Plexus Cauterization as Primary Treatment for Infant Hydrocephalus: A Prospective North American Series.” *Journal of Neurosurgery: Pediatrics* 14 (5):439–46. https://doi.org/10.3171/2014.7.PEDS14152.

Segal, M. B. 1993. “Extracellular and Cerebrospinal Fluids.” *Journal of Inherited Metabolic Disease* 16 (4):617–38.

Sekhar, Laligam N., John Moossy, and Norman A. Guthkelch. 1982. “Malfunctioning Ventriculoperitoneal Shunts.” *Journal of Neurosurgery* 56 (3):411–16. https://doi.org/10.3171/jns.1982.56.3.0411.

Shrivastava, Devashish, Aviva Abosch, Timothy Hanson, Jinfeng Tian, Akshay Gupte, Paul A. Iaizzo, and J. Thomas Vaughan. 2010. “Effect of the Extra-Cranial DBS Lead on Radiofrequency Heating at 9.4T (400.2 MHz).” *Journal of Magnetic Resonance Imaging : JMRI* 32 (3):600–607. https://doi.org/10.1002/jmri.22292.

Simon, Tamara, Jay Riva-Cambrin, Raj Srivastava, Susan L. Bratton, J. Michael Dean, and John R. W. Kestle. 2008. "Hospital Care for Children with Hydrocephalus in the United States: Utilization, Charges, Comorbidities, and Deaths." *Journal of Neurosurgery: Pediatrics* 1 (2):131–37. https://doi.org/10.3171/PED/2008/1/2/131.

Singh, Daljit, Anurag Saxena, Anita Jagetia, Hukum Singh, Monica S. Tandon, and Pragati Ganjoo. 2012. "Endoscopic Observations of Blocked Ventriculoperitoneal (VP) Shunt: A Step toward Better Understanding of Shunt Obstruction and Its Removal." *British Journal of Neurosurgery* 26 (5):747–53. https://doi.org/10.3109/02688697.2012.690908.

Singh, Meenesh R., Kimberly Papadantonakis, Chengxiang Xiang, and Nathan S. Lewis. 2015. "An Electrochemical Engineering Assessment of the Operational Conditions and Constraints for Solar-Driven Water-Splitting Systems at near-Neutral pH." *Energy Environ. Sci.* 8 (9):2760–67. https://doi.org/10.1039/C5EE01721A.

Sivagnanam, Milani, and Neilank Jha. 2012. "Hydrocephalus: An Overview." In *Hydrocephalus*, 1–18. InTech.

Sminia, P., J. van der Zee, J. Wondergem, and J. Haveman. 1994. "Effect of Hyperthermia on the Central Nervous System: A Review." *International Journal of Hyperthermia : The Official Journal of European Society for Hyperthermic Oncology, North American Hyperthermia Group* 10 (1):1–30.

Smith, Katisha D., and Liang Zhu. 2010. "Brain Hypothermia Induced by Cold Spinal Fluid Using a Torso Cooling Pad: Theoretical Analyses." *Medical & Biological Engineering & Computing* 48 (8):783–791. https://doi.org/10.1007/s11517-010-0635-9.

Spector, Reynold, Richard F. Keep, S. Robert Snodgrass, Quentin R. Smith, and Conrad E. Johanson. 2015. "A Balanced View of Choroid Plexus Structure and Function: Focus on Adult Humans." *Experimental Neurology* 267:78–86. https://doi.org/http://dx.doi.org/10.1016/j.expneurol.2015.02.032.

Stein, Sherman C., and Wensheng Guo. 2008. "Have We Made Progress in Preventing Shunt Failure? A Critical Analysis." *Journal of Neurosurgery: Pediatrics* 1 (1):40–47. https://doi.org/10.3171/PED-08/01/040.

———. 2009. "The Prevalence of Shunt-Treated Hydrocephalus: A Mathematical Model." *Surgical Neurology* 72 (2):131–37. https://doi.org/10.1016/j.surneu.2008.07.012.

Stone, Jonathan, Corey Walker, Maxwell Jacobson, Valerie Phillips, and Howard Silberstein. 2013. "Revision Rate of Pediatric Ventriculoperitoneal Shunts after 15 Years." *Journal of Neurosurgery: Pediatrics* 11 (1):15–19. https://doi.org/10.3171/2012.9.PEDS1298.

Symss, Nigel Peter, and Shizuo Oi. 2015. "Is There an Ideal Shunt? A Panoramic View of 110 Years in CSF Diversions and Shunt Systems Used for the Treatment of Hydrocephalus: From Historical Events to Current Trends." *Child's Nervous System* 31 (2):191–202. https://doi.org/10.1007/s00381-014-2608-z.

Tanaka, R., C. H. Kim, N. Yamada, and Y. Saito. 1987. "Radiofrequency Hyperthermia for Malignant Brain Tumors: Preliminary Results of Clinical Trials." *Neurosurgery* 21 (4):478–83.

The Electronics Handbook. 2005. Second ed. Boca Raton, FL: CRC Press.

Thompson, Dominic N.P. 2009. "Hydrocephalus." *Surgery - Oxford International Edition* 27 (3):130–34. https://doi.org/10.1016/j.mpsur.2009.02.005.

Tronnier, V. M., A. Staubert, S. Hahnel, and A. Sarem-Aslani. 1999. "Magnetic Resonance Imaging with Implanted Neurostimulators: An in Vitro and in Vivo Study." *Neurosurgery* 44 (1):118-25; discussion 125-126.

Tuli, S., B. O'Hayon, J. Drake, M. Clarke, and J. Kestle. 1999. "Change in Ventricular Size and Effect of Ventricular Catheter Placement in Pediatric Patients with Shunted Hydrocephalus." *Neurosurgery* 45 (6):1329-33; discussion 1333-1335.

Tuli, Sagun, James M. Drake, Jerry Lawless, Melanie Wigg, and Maria Lamberti-Pasculli. 2000. "Risk Factors for Repeated Cerebrospinal Shunt Failures in Pediatric Patients with Hydrocephalus." *Journal of Neurosurgery* 92 (1):31–38. https://doi.org/10.3171/jns.2000.92.1.0031.

Tully, Hannah M., and William B. Dobyns. 2014. "Infantile Hydrocephalus: A Review of Epidemiology, Classification and Causes." *European Journal of Medical Genetics* 57 (8):359–68. https://doi.org/10.1016/j.ejmg.2014.06.002.

Vanysek, Petr. 2003. "Electrochemical Series." In *CRC Handbook of Chemistry and Physics*, 84th ed., 8-21 to 8-31. CRC Press.

Villavicencio, Alan T., Jean-Christophe Leveque, Matthew J. McGirt, John S. Hopkins, Herbert E. Fuchs, and Timothy M. George. 2003. "Comparison of Revision Rates Following Endoscopically versus Nonendoscopically Placed Ventricular Shunt Catheters." *Surgical Neurology* 59 (5):375–79. https://doi.org/http://dx.doi.org/10.1016/S0090-3019(03)00070-3.

Vinchon, Matthieu, Marc Baroncini, and Isabelle Delestret. 2012. "Adult Outcome of Pediatric Hydrocephalus." *Child's Nervous System* 28 (6):847–54. https://doi.org/10.1007/s00381-012-1723-y.

Von Hippel, Arthur. 1954. "Water Loss Tangent." In *Dielectric Materials and Applications*, 361–62. MIT Press.

Weisenberg, Sofy H., Stephanie C. TerMaath, Chad E. Seaver, and James A. Killeffer. 2016. "Ventricular Catheter Development: Past, Present, and Future." *Journal of Neurosurgery* 125 (6):1504–12. https://doi.org/10.3171/2015.12.JNS151181.

Wust, P., B. Hildebrandt, G. Sreenivasa, B. Rau, J. Gellermann, H. Riess, R. Felix, and P. M. Schlag. 2002. "Hyperthermia in Combined Treatment of Cancer." *The Lancet Oncology* 3 (8):487–97. https://doi.org/http://dx.doi.org/10.1016/S1470-2045(02)00818-5.

Yamada, Shinya, and Erin Kelly. 2016. "Cerebrospinal Fluid Dynamics and the Pathophysiology of Hydrocephalus: New Concepts." *Seminars in Ultrasound, CT and MRI* 37 (2):84–91. https://doi.org/https://doi.org/10.1053/j.sult.2016.01.001.

Appelgren, Tobias, Sofia Zetterstrand, Jorgen Elfversson, and Daniel Nilsson. 2010. "Long-Term Outcome after Treatment of Hydrocephalus in Children." *Pediatric Neurosurgery* 46 (3):221–26. https://doi.org/10.1159/000319365.

Armenean, Cristina, Emmanuel Perrin, Mircea Armenean, Olivier Beuf, Frank Pilleul, and Herve Saint-Jalmes. 2004. "RF-Induced Temperature Elevation along Metallic Wires in Clinical Magnetic Resonance Imaging: Influence of Diameter and Length." *Magnetic Resonance in Medicine* 52 (5):1200–1206. https://doi.org/10.1002/mrm.20246.

Bañobre-López, Manuel, Antonio Teijeiro, and Jose Rivas. 2013. "Magnetic Nanoparticle-Based Hyperthermia for Cancer Treatment." *Reports of Practical Oncology & Radiotherapy* 18 (6):397–400. https://doi.org/http://dx.doi.org/10.1016/j.rpor.2013.09.011.

Basati, Sukhraaj, Kevin Tangen, Ying Hsu, Hanna Lin, David Frim, and Andreas Linninger. 2015. "Impedance Changes Indicate Proximal Ventriculoperitoneal Shunt Obstruction In Vitro." *IEEE Transactions on Bio-Medical Engineering* 62 (12):2787–93. https://doi.org/10.1109/TBME.2014.2335171.

Baştuğ, Turgut, and Serdar Kuyucak. 2005. "Temperature Dependence of the Transport Coefficients of Ions from Molecular Dynamics Simulations." *Chemical Physics Letters* 408 (1):84–88. https://doi.org/http://dx.doi.org/10.1016/j.cplett.2005.04.012.

Berjano, Enrique J. 2006. "Theoretical Modeling for Radiofrequency Ablation: State-of-the-Art and Challenges for the Future." *BioMedical Engineering OnLine* 5:24. https://doi.org/10.1186/1475-925X-5-24.

Bhavaraju, N. C., V. Nagaraddi, S. R. Chetlapalli, and I. Osorio. 2002. "Electrical and Thermal Behavior of Non-Ferrous Noble Metal Electrodes Exposed to MRI Fields." *Magnetic Resonance Imaging* 20 (4):351–57.

Blegvad, C., A. D. Skjolding, H. Broholm, H. Laursen, and M. Juhler. 2013. "Pathophysiology of Shunt Dysfunction in Shunt Treated Hydrocephalus." *Acta Neurochirurgica* 155 (9):1763–1772. https://doi.org/10.1007/s00701-013-1729-6.

Browd, Samuel R., Oren N. Gottfried, Brian T. Ragel, and John R. W. Kestle. 2006b. "Failure of Cerebrospinal Fluid Shunts: Part II: Overdrainage, Loculation, and Abdominal Complications." *Pediatric Neurology* 34 (3):171–76. https://doi.org/http://dx.doi.org/10.1016/j.pediatrneurol.2005.05.021.

Browd, Samuel R., Brian T. Ragel, Oren N. Gottfried, and John R. W. Kestle. 2006a. "Failure of Cerebrospinal Fluid Shunts: Part I: Obstruction and Mechanical Failure." *Pediatric Neurology* 34 (2):83–92. https://doi.org/http://dx.doi.org/10.1016/j.pediatrneurol.2005.05.020.

Budgett, David M., Aiguo Patrick Hu, Ping Si, Wayne T. Pallas, Mark G. Donnelly, Jared W. T. Broad, Carolyn J. Barrett, Sarah-Jane Guild, and Simon C. Malpas. 2007. "Novel Technology for the Provision of Power to Implantable Physiological Devices." *Journal of Applied Physiology* 102 (4):1658–1663. https://doi.org/10.1152/japplphysiol.00105.2006.

Bulat, Marin, and Marijan Klarica. 2011. "Recent Insights into a New Hydrodynamics of the Cerebrospinal Fluid." *Brain Research Reviews* 65 (2):99–112. https://doi.org/https://doi.org/10.1016/j.brainresrev.2010.08.002.

Cherukuri, Paul, Evan S. Glazer, and Steven A. Curley. 2010. "Targeted Hyperthermia Using Metal Nanoparticles." *Advanced Drug Delivery Reviews* 62 (3):339–45. https://doi.org/http://dx.doi.org/10.1016/j.addr.2009.11.006.

Chi, John, Heather Fullerton, and Nalin Gupta. 2005. "Time Trends and Demographics of Deaths from Congenital Hydrocephalus in Children in the United States: National Center for Health Statistics Data, 1979 to 1998." *Journal of Neurosurgery: Pediatrics* 103 (2):113–18. https://doi.org/10.3171/ped.2005.103.2.0113.

Chicheł, Adam, Janusz Skowronek, Magda Kubaszewska, and Marek Kanikowski. 2007. "Hyperthermia – Description of a Method and a Review of Clinical Applications." *Reports of Practical Oncology & Radiotherapy* 12 (5):267–75. https://doi.org/10.1016/S1507-1367(10)60065-X.

Chou, C. K., J. A. McDougall, and K. W. Chan. 1997. "RF Heating of Implanted Spinal Fusion Stimulator during Magnetic Resonance Imaging." *IEEE Transactions on Bio-Medical Engineering* 44 (5):367–73. https://doi.org/10.1109/10.568912.

Ciumas, Carolina, Gregor Schaefers, Sandrine Bouvard, Emmeline Tailhades, Emmanuel Perrin, Jean-Christophe Comte, Emmanuelle Canet-Soulas, et al. 2014. "A Phantom and Animal Study of Temperature Changes during fMRI with Intracerebral Depth Electrodes." *Epilepsy Research* 108 (1):57–65. https://doi.org/http://dx.doi.org/10.1016/j.eplepsyres.2013.10.016.

Cui, Daan, and Mojie Cheng. 2009. “Numerical Analysis of Thermal and Electrochemical Phenomena for Anode Supported Microtubular SOFC.” *AIChE Journal* 55 (3):771–782. https://doi.org/10.1002/aic.11697.

Darcey, Terrance M., Erik J. Kobylarz, Michael A. Pearl, Patricia J. Krauss, Stephanie A. Ferri, David W. Roberts, and David F. Bauer. 2016. “Safe Use of Subdermal Needles for Intraoperative Monitoring with MRI.” *Neurosurgical Focus* 40 (3):E19. https://doi.org/10.3171/2015.12.FOCUS15555.

Davalos, R. V., L. M. Mir, and B. Rubinsky. 2005. “Tissue Ablation with Irreversible Electroporation.” *Annals of Biomedical Engineering* 33 (2):223. https://doi.org/10.1007/s10439-005-8981-8.

Davies, Angela M., Uri Weinberg, and Yoram Palti. 2013. “Tumor Treating Fields: A New Frontier in Cancer Therapy.” *Annals of the New York Academy of Sciences* 1291 (1):86–95. https://doi.org/10.1111/nyas.12112.

Del Bigio, M. R. 1998. “Biological Reactions to Cerebrospinal Fluid Shunt Devices: A Review of the Cellular Pathology.” *Neurosurgery* 42 (2):319-25; discussion 325-326.

Dewhirst, M. W., B. L. Viglianti, M. Lora-Michiels, M. Hanson, and P. J. Hoopes. 2003. “Basic Principles of Thermal Dosimetry and Thermal Thresholds for Tissue Damage from Hyperthermia.” *International Journal of Hyperthermia : The Official Journal of European Society for Hyperthermic Oncology, North American Hyperthermia Group* 19 (3):267–94. https://doi.org/10.1080/0265673031000119006.

Elwassif, Maged M., Qingjun Kong, Maribel Vazquez, and Marom Bikson. 2006. “Bio-Heat Transfer Model of Deep Brain Stimulation Induced Temperature Changes.” *Conference Proceedings : ... Annual International Conference of the IEEE Engineering in Medicine and Biology Society. IEEE Engineering in Medicine and Biology Society. Annual Conference* 1:3580–83. https://doi.org/10.1109/IEMBS.2006.259425.

Fiorentini, Giammaria, Petros Giovanis, Susanna Rossi, Patrizia Dentico, Raffaele Paola, Gina Turrisi, and Paolo Bernardeschi. 2006. “A Phase II Clinical Study on Relapsed Malignant Gliomas Treated with Electro-Hyperthermia.” *In Vivo* 20 (6):721–724.

Gebert, Anna-Felicitas, Matthias Schulz, Karin Schwarz, and Ulrich-Wilhelm Thomale. 2016. “Long-Term Survival Rates of Gravity-Assisted, Adjustable Differential Pressure Valves in Infants with Hydrocephalus.” *Journal of Neurosurgery: Pediatrics* 17 (5):544–51. https://doi.org/10.3171/2015.10.PEDS15328.

Georgi, J.-C., C. Stippich, V.M. Tronnier, and S. Heiland. 2004. “Active Deep Brain Stimulation during MRI: A Feasibility Study.” *Magnetic Resonance in Medicine* 51 (2):380–388. https://doi.org/10.1002/mrm.10699.

Ginsberg, Howard J., James M. Drake, Thomas M. Peterson, and Richard S. C. Cobbold. 2006. “Recanalization of Obstructed Cerebrospinal Fluid Ventricular Catheters Using Ultrasonic Cavitation.” *Neurosurgery* 59 (4 Suppl 2):ONS403–412; discussion ONS412. https://doi.org/10.1227/01.NEU.0000233968.80352.25.

Gnanalingham, Kanna K., Jesus Lafuente, Stefan Brew, Dominic Thompson, William Harkness, and Richard Hayward. 2005. “Percutaneous Coagulation of Choroid Plexus to Unblock the Ventricular Catheter Using the Seldinger Technique: Preliminary Report.” *Surgical Neurology* 64 (5):440–43. https://doi.org/http://dx.doi.org/10.1016/j.surneu.2005.06.015.

Goel, A. 2002. “Tumour Induced Hydrocephalus and Oedema: Pathology or Natural Defence.” *Journal of Postgraduate Medicine* 48 (2):153–54.

Golberg, Alexander, and Martin L. Yarmush. 2013. "Nonthermal Irreversible Electroporation: Fundamentals, Applications, and Challenges." *IEEE Transactions on Bio-Medical Engineering* 60 (3):707–14. https://doi.org/10.1109/TBME.2013.2238672.

Gruber, Rolf W., and Bernd Roehrig. 2010. "Prevention of Ventricular Catheter Obstruction and Slit Ventricle Syndrome by the Prophylactic Use of the Integra Antisiphon Device in Shunt Therapy for Pediatric Hypertensive Hydrocephalus: A 25-Year Follow-up Study." *Journal of Neurosurgery: Pediatrics* 5 (1):4–16. https://doi.org/10.3171/2008.7.17690.

Hanak, Brian W., Emily F. Ross, Carolyn A. Harris, Samuel R. Browd, and William Shain. 2016. "Toward a Better Understanding of the Cellular Basis for Cerebrospinal Fluid Shunt Obstruction: Report on the Construction of a Bank of Explanted Hydrocephalus Devices." *Journal of Neurosurgery: Pediatrics* 18 (2):213–23. https://doi.org/10.3171/2016.2.PEDS15531.

Handler, M.H. 1996. "A Complication in Removing a Retained Ventricular Catheter Using Electrocautery." *Pediatric Neurosurgery* 25 (5):276–276.

Harmon, B. V., A. M. Corder, R. J. Collins, G. C. Gobe, J. Allen, D. J. Allan, and J. F. Kerr. 1990. "Cell Death Induced in a Murine Mastocytoma by 42-47 Degrees C Heating in Vitro: Evidence That the Form of Death Changes from Apoptosis to Necrosis above a Critical Heat Load." *International Journal of Radiation Biology* 58 (5):845–58.

Harris, Carolyn A., and James P. McAllister. 2011. "Does Drainage Hole Size Influence Adhesion on Ventricular Catheters?" *Child's Nervous System* 27 (8):1221–1232. https://doi.org/10.1007/s00381-011-1430-0.

Harris, Carolyn A., and James P. 2nd McAllister. 2012. "What We Should Know about the Cellular and Tissue Response Causing Catheter Obstruction in the Treatment of Hydrocephalus." *Neurosurgery* 70 (6):1589-601; discussion 1601-1602. https://doi.org/10.1227/NEU.0b013e318244695f.

Haveman, J., P. Sminia, J. Wondergem, J. van der Zee, and M. C. C. M. Hulshof. 2005. "Effects of Hyperthermia on the Central Nervous System: What Was Learnt from Animal Studies?" *International Journal of Hyperthermia : The Official Journal of European Society for Hyperthermic Oncology, North American Hyperthermia Group* 21 (5):473–87. https://doi.org/10.1080/02656730500159079.

Hellwig, Dieter, Joachim Andreas Grotenhuis, Wuttipong Tirakotai, Thomas Riegel, Dirk Michael Schulte, Bernhard Ludwig Bauer, and Helmut Bertalanffy. 2005. "Endoscopic Third Ventriculostomy for Obstructive Hydrocephalus." *Neurosurgical Review* 28 (1):1–34. https://doi.org/10.1007/s10143-004-0365-2.

Hideki Ogiwara, Kodai Uematsu, and Nobuhito Morota. 2014. "Obliteration of the Choroid Plexus after Endoscopic Coagulation." *Journal of Neurosurgery: Pediatrics* 14 (3):230–33. https://doi.org/10.3171/2014.6.PEDS1438.

Hildebrandt, Bert, Peter Wust, Olaf Ahlers, Annette Dieing, Geetha Sreenivasa, Thoralf Kerner, Roland Felix, and Hanno Riess. 2002. "The Cellular and Molecular Basis of Hyperthermia." *Critical Reviews in Oncology/Hematology* 43 (1):33–56. https://doi.org/http://dx.doi.org/10.1016/S1040-8428(01)00179-2.

Hirofumi Hirano, Kazuho Hirahara, Tetsuhiko Asakura, Tetsuro Shimozuru, Koki Kadota, Shizuya Kasamo, Masaru Shimohonji, Kanetaka Kimotsuki, and Masamichi Goto. 1994. "Hydrocephalus due to Villous Hypertrophy of the Choroid Plexus in the Lateral Ventricles." *Journal of Neurosurgery* 80 (2):321–23. https://doi.org/10.3171/jns.1994.80.2.0321.

Horsman, M. R., and J. Overgaard. 2007. “Hyperthermia: A Potent Enhancer of Radiotherapy.” *Clinical Oncology* 19 (6):418–26. https://doi.org/http://dx.doi.org/10.1016/j.clon.2007.03.015.

Hudgins, R. J., and W. R. Boydston. 1998. “Shunt Revision by Coagulation with Retention of the Ventricular Catheter.” *Pediatric Neurosurgery* 29 (2):57–59.

Huyette, David R., Benjamin J. Turnbow, Christian Kaufman, Dale F. Vaslow, Benjamin B. Whiting, and Michael Y. Oh. 2008. “Accuracy of the Freehand Pass Technique for Ventriculostomy Catheter Placement: Retrospective Assessment Using Computed Tomography Scans.” *Journal of Neurosurgery* 108 (1):88–91. https://doi.org/10.3171/JNS/2008/108/01/0088.

Iglesias, Sara, Bienvenido Ros, Álvaro Martín, Antonio Carrasco, Miguel Segura, Andrea Delgado, Francisca Rius, and Miguel Ángel Arráez. 2016. “Surgical Outcome of the Shunt: 15-Year Experience in a Single Institution.” *Child’s Nervous System*, 1–9. https://doi.org/10.1007/s00381-016-3206-z.

Israelachvili, Jacob N. 1992. “Electrostatic Forces between Surfaces in Liquids.” In *Intermolecular and Surface Forces*, Second, 213–60. Academic Press.

J. A. Nyenhuis, Sung-Min Park, R. Kamondetdacha, A. Amjad, F. G. Shellock, and A. R. Rezai. 2005. “MRI and Implanted Medical Devices: Basic Interactions with an Emphasis on Heating.” *IEEE Transactions on Device and Materials Reliability* 5 (3):467–80. https://doi.org/10.1109/TDMR.2005.859033.

Jung, Nayoung, and Dongwon Kim. 2013. “Effect of Electromagnetic Navigated Ventriculoperitoneal Shunt Placement on Failure Rates.” *Journal of Korean Neurosurgical Society* 53 (3):150–54. https://doi.org/10.3340/jkns.2013.53.3.150.

Kast, J., D. Duong, F. Nowzari, W. M. Chadduck, and S. J. Schiff. 1994. “Time-Related Patterns of Ventricular Shunt Failure.” *Child’s Nervous System : ChNS : Official Journal of the International Society for Pediatric Neurosurgery* 10 (8):524–28.

Kaufman, B. A., and T. S. Park. 1999. “Ventricular Anatomy and Shunt Catheters.” *Pediatric Neurosurgery* 31 (1):1–6. https://doi.org/28823.

Kehler, Uwe, A. Klöhn, O. Heese, and J. Gliemroth. 2003. “Hydrocephalus Therapy: Reduction of Shunt Occlusions Using a Peel-Away Sheath.” *Clinical Neurology and Neurosurgery* 105 (4):253–55. https://doi.org/10.1016/S0303-8467(03)00041-6.

Kehler, Uwe, Niels Langer, Jan Gliemroth, Ullrich Meier, Johannes Lemcke, Christian Sprung, Hans-Georg Schlosser, Michael Kiefer, Regina Eymann, and Oliver Heese. 2012. “Reduction of Shunt Obstructions by Using a Peel-Away Sheath Technique? A Multicenter Prospective Randomized Trial.” *Clinical Neurology and Neurosurgery* 114 (4):381–84. https://doi.org/10.1016/j.clineuro.2011.11.020.

Kestle, J., J. Drake, R. Milner, C. Sainte-Rose, G. Cinalli, F. Boop, J. Piatt, et al. 2000. “Long-Term Follow-up Data from the Shunt Design Trial.” *Pediatric Neurosurgery* 33 (5):230–36. https://doi.org/55960.

Kim, Yong Bae, Jae Whan Lee, Kyu Sung Lee, and Kyu Chang Lee. 2006. “Image-Guided Placement of Ventricular Shunt Catheter.” *Journal of Clinical Neuroscience* 13 (1):50–54. https://doi.org/10.1016/j.jocn.2004.12.010.

Kirson, Eilon D., Vladimír Dbalý, František Tovaryš, Josef Vymazal, Jean F. Soustiel, Aviran Itzhaki, Daniel Mordechovich, et al. 2007. “Alternating Electric Fields Arrest Cell Proliferation in Animal Tumor Models and Human Brain Tumors.” *Proceedings of the National Academy of Sciences* 104 (24):10152–57. https://doi.org/10.1073/pnas.0702916104.

Kirson, Eilon D., Zoya Gurvich, Rosa Schneiderman, Erez Dekel, Aviran Itzhaki, Yoram Wasserman, Rachel Schatzberger, and Yoram Palti. 2004. “Disruption of Cancer Cell Replication by Alternating Electric Fields.” *Cancer Research* 64 (9):3288–3295. https://doi.org/10.1158/0008-5472.CAN-04-0083.

Kossovsky, Nir, and Robert B. Snow. 1989. “Clinical-Pathological Analysis of Failed Central Nervous System Fluid Shunts.” *Journal of Biomedical Materials Research* 23 (S13):73–86. https://doi.org/10.1002/jbm.820231308.

Kousi, Maria, and Nicholas Katsanis. 2016. “The Genetic Basis of Hydrocephalus.” *Annual Review of Neuroscience* 39 (July):409–35. https://doi.org/10.1146/annurev-neuro-070815-014023.

Kovacs, Norbert, Ferenc Nagy, Ferenc Kover, Adam Feldmann, Carlos Llumiguano, Jozsef Janszky, Gyula Kotek, Tamas Doczi, and Istvan Balas. 2006. “Implanted Deep Brain Stimulator and 1.0-Tesla Magnetic Resonance Imaging.” *Journal of Magnetic Resonance Imaging : JMRI* 24 (6):1409–12. https://doi.org/10.1002/jmri.20779.

Krauss, Joachim K., Jens P. Regel, Werner Vach, Dirk W. Droste, Jan J. Borremans, and Thomas Mergner. 1996. “Vascular Risk Factors and Arteriosclerotic Disease in Idiopathic Normal-Pressure Hydrocephalus of the Elderly.” *Stroke* 27 (1):24–29. https://doi.org/10.1161/01.STR.27.1.24.

Ladd, Mark E., and Harald H. Quick. 2000. “Reduction of Resonant RF Heating in Intravascular Catheters Using Coaxial Chokes.” *Magnetic Resonance in Medicine* 43 (4):615–619. https://doi.org/10.1002/(SICI)1522-2594(200004)43:4<615::AID-MRM19>3.0.CO;2-B.

Lazareff, J. A., W. Peacock, L. Holly, J. Ver Halen, A. Wong, and C. Olmstead. 1998. “Multiple Shunt Failures: An Analysis of Relevant Factors.” *Child’s Nervous System : ChNS : Official Journal of the International Society for Pediatric Neurosurgery* 14 (6):271–75.

Lee, H., K. Kolahi, M. Bergsneider, and J. W. Judy. 2014. “Mechanical Evaluation of Unobstructing Magnetic Microactuators for Implantable Ventricular Catheters.” *Journal of Microelectromechanical Systems* 23 (4):795–802. https://doi.org/10.1109/JMEMS.2014.2321377.

Lee, S. Y., S. H. Lee, K. Akuta, M. Uda, and C. W. Song. 2000. “Acute Histological Effects of Interstitial Hyperthermia on Normal Rat Brain.” *International Journal of Hyperthermia : The Official Journal of European Society for Hyperthermic Oncology, North American Hyperthermia Group* 16 (1):73–83.

Lee, Selene A., Hyowon Lee, James R. Pinney, Elvira Khialeeva, Marvin Bergsneider, and Jack W. Judy. 2011. “Development of Microfabricated Magnetic Actuators for Removing Cellular Occlusion.” *Journal of Micromechanics and Microengineering : Structures, Devices, and Systems* 21 (5):54006. https://doi.org/10.1088/0960-1317/21/5/054006.

Lew, Sean M., Anne E. Matthews, Adam L. Hartman, and Neil Haranhalli. 2013. “Post-Hemispherectomy Hydrocephalus: Results of a Comprehensive, Multi-Institutional Review.” *Epilepsia* 54 (2):383–89. https://doi.org/10.1111/epi.12010.

Linninger, Andreas A., Cristian Tsakiris, David C. Zhu, Michalis Xenos, Peter Roycewicz, Zachary Danziger, and Richard Penn. 2005. “Pulsatile Cerebrospinal Fluid Dynamics in the Human Brain.” *IEEE Transactions on Bio-Medical Engineering* 52 (4):557–65. https://doi.org/10.1109/TBME.2005.844021.

Linninger, Andreas, Sukhraaj Basati, Robert Dawe, and Richard Penn. 2009. “An Impedance Sensor to Monitor and Control Cerebral Ventricular Volume.” *Medical Engineering & Physics* 31 (7):838–45. https://doi.org/10.1016/j.medengphy.2009.03.011.

Mallory, Matthew, Emile Gogineni, Guy C. Jones, Lester Greer, and Charles B. Simone II. 2016. "Therapeutic Hyperthermia: The Old, the New, and the Upcoming." *Critical Reviews in Oncology/Hematology* 97:56–64. https://doi.org/http://dx.doi.org/10.1016/j.critrevonc.2015.08.003.

Martínez-Lage, F. J., Francisco López, Máximo Poza, and Mayte Hernández. 1998. "Prevention of Intraventricular Hemorrhage during CSF Shunt Revisions by Means of a Flexible Coagulating electrodeA Preliminary Report." *Child's Nervous System* 14 (4):203–206. https://doi.org/10.1007/s003810050211.

Medtronic, MN. 2017a. "ActivaTM Medtronic." http://professional.medtronic.com/mri/clinicians/mri-dbs-systems/index.htm.

———. 2017b. "Medtronic Neurosurgery." http://www.medtronic.com/us-en/businesses/neurosurgery.html.

"Microbot Medical Inc." 2017. http://www.microbotmedical.com/product/self-cleaning-shunt-scs/.

Nelson, D. A., and S. A. Nunneley. 1998. "Brain Temperature and Limits on Transcranial Cooling in Humans: Quantitative Modeling Results." *European Journal of Applied Physiology and Occupational Physiology* 78 (4):353–59.

Neufeld, E., S. Kuhn, G. Szekely, and N. Kuster. 2009. "Measurement, Simulation and Uncertainty Assessment of Implant Heating during MRI." *Physics in Medicine and Biology* 54 (13):4151–69. https://doi.org/10.1088/0031-9155/54/13/012.

Nielsen, Nadine, and Amanda Breedt. 2017. "Hydrocephalus." In *Nursing Care of the Pediatric Neurosurgery Patient*, 3rd ed. Springer International Publishing.

Nulsen, F. E., and E. B. Spitz. 1952. "Treatment of Hydrocephalus by Direct Shunt from Ventricle to Jugular Vain." *Surgical Forum*, 399–403.

Oi, Shizuo. 2005. "Classification and Definition of Hydrocephalus: Origin, Controversy, and Assignment Ofthe Terminology." In *Pediatric Hydrocephalus*, 95–112. Springer-Verlag Italia.

Orešković, D., and M. Klarica. 2011. "Development of Hydrocephalus and Classical Hypothesis of Cerebrospinal Fluid Hydrodynamics: Facts and Illusions." *Progress in Neurobiology* 94 (3):238–58. https://doi.org/http://dx.doi.org/10.1016/j.pneurobio.2011.05.005.

Pattisapu, J. V., E. R. Trumble, K. R. Taylor, P. D. Howard, and T. M. Kovach. 1999. "Percutaneous Endoscopic Recanalization of the Catheter: A New Technique of Proximal Shunt Revision." *Neurosurgery* 45 (6):1361-6; discussion 1366-1367.

Patwardhan, Ravish V., and Anil Nanda. 2005. "Implanted Ventricular Shunts in the United States: The Billion-Dollar-a-Year Cost of Hydrocephalus Treatment." *Neurosurgery* 56 (1):139-44; discussion 144-145.

Piatt, J. H. Jr. 1995. "Cerebrospinal Fluid Shunt Failure: Late Is Different from Early." *Pediatric Neurosurgery* 23 (3):133–39.

Pople, Ian K. 2002. "Hydrocephalus and Shunts: What the Neurologist Should Know." *Journal of Neurology, Neurosurgery & Psychiatry* 73 (suppl 1):i17–i22. https://doi.org/10.1136/jnnp.73.suppl_1.i17.

Reddy, G. Kesava, Papireddy Bollam, and Gloria Caldito. 2014. "Long-Term Outcomes of Ventriculoperitoneal Shunt Surgery in Patients with Hydrocephalus." *World Neurosurgery* 81 (2):404–10. https://doi.org/10.1016/j.wneu.2013.01.096.

Redzic, Zoran B., and Malcolm B. Segal. 2004. “The Structure of the Choroid Plexus and the Physiology of the Choroid Plexus Epithelium.” *Advanced Drug Delivery Reviews* 56 (12):1695–1716. https://doi.org/http://dx.doi.org/10.1016/j.addr.2004.07.005.

Rekate, Harold L. 2009. “A Contemporary Definition and Classification of Hydrocephalus.” *Seminars in Pediatric Neurology* 16 (1):9–15. https://doi.org/10.1016/j.spen.2009.01.002.

Rock, Kenneth L., and Hajime Kono. 2008. “The Inflammatory Response to Cell Death.” *Annual Review of Pathology* 3:99–126. https://doi.org/10.1146/annurev.pathmechdis.3.121806.151456.

Rossmeisl Jr, John H., Paulo A. Garcia, Theresa E. Pancotto, John L. Robertson, Natalia Henao-Guerrero, Robert E. Neal II, Thomas L. Ellis, and Rafael V. Davalos. 2015. “Safety and Feasibility of the NanoKnife System for Irreversible Electroporation Ablative Treatment of Canine Spontaneous Intracranial Gliomas.” *Journal of Neurosurgery* 123 (4):1008–25. https://doi.org/10.3171/2014.12.JNS141768.

Sakka, L., G. Coll, and J. Chazal. 2011. “Anatomy and Physiology of Cerebrospinal Fluid.” *European Annals of Otorhinolaryngology, Head and Neck Diseases* 128 (6):309–16. https://doi.org/10.1016/j.anorl.2011.03.002.

Scellig S. D. Stone, and Benjamin C. Warf. 2014. “Combined Endoscopic Third Ventriculostomy and Choroid Plexus Cauterization as Primary Treatment for Infant Hydrocephalus: A Prospective North American Series.” *Journal of Neurosurgery: Pediatrics* 14 (5):439–46. https://doi.org/10.3171/2014.7.PEDS14152.

Segal, M. B. 1993. “Extracellular and Cerebrospinal Fluids.” *Journal of Inherited Metabolic Disease* 16 (4):617–38.

Sekhar, Laligam N., John Moossy, and Norman A. Guthkelch. 1982. “Malfunctioning Ventriculoperitoneal Shunts.” *Journal of Neurosurgery* 56 (3):411–16. https://doi.org/10.3171/jns.1982.56.3.0411.

Shrivastava, Devashish, Aviva Abosch, Timothy Hanson, Jinfeng Tian, Akshay Gupte, Paul A. Iaizzo, and J. Thomas Vaughan. 2010. “Effect of the Extra-Cranial DBS Lead on Radiofrequency Heating at 9.4T (400.2 MHz).” *Journal of Magnetic Resonance Imaging : JMRI* 32 (3):600–607. https://doi.org/10.1002/jmri.22292.

Simon, Tamara, Jay Riva-Cambrin, Raj Srivastava, Susan L. Bratton, J. Michael Dean, and John R. W. Kestle. 2008. “Hospital Care for Children with Hydrocephalus in the United States: Utilization, Charges, Comorbidities, and Deaths.” *Journal of Neurosurgery: Pediatrics* 1 (2):131–37. https://doi.org/10.3171/PED/2008/1/2/131.

Singh, Daljit, Anurag Saxena, Anita Jagetia, Hukum Singh, Monica S. Tandon, and Pragati Ganjoo. 2012. “Endoscopic Observations of Blocked Ventriculoperitoneal (VP) Shunt: A Step toward Better Understanding of Shunt Obstruction and Its Removal.” *British Journal of Neurosurgery* 26 (5):747–53. https://doi.org/10.3109/02688697.2012.690908.

Singh, Meenesh R., Kimberly Papadantonakis, Chengxiang Xiang, and Nathan S. Lewis. 2015. “An Electrochemical Engineering Assessment of the Operational Conditions and Constraints for Solar-Driven Water-Splitting Systems at near-Neutral pH.” *Energy Environ. Sci.* 8 (9):2760–67. https://doi.org/10.1039/C5EE01721A.

Sivagnanam, Milani, and Neilank Jha. 2012. “Hydrocephalus: An Overview.” In *Hydrocephalus*, 1–18. InTech.

Sminia, P., J. van der Zee, J. Wondergem, and J. Haveman. 1994. “Effect of Hyperthermia on the Central Nervous System: A Review.” *International Journal of Hyperthermia : The Official Journal of European Society for Hyperthermic Oncology, North American Hyperthermia Group* 10 (1):1–30.

Smith, Katisha D., and Liang Zhu. 2010. “Brain Hypothermia Induced by Cold Spinal Fluid Using a Torso Cooling Pad: Theoretical Analyses.” *Medical & Biological Engineering & Computing* 48 (8):783–791. https://doi.org/10.1007/s11517-010-0635-9.

Spector, Reynold, Richard F. Keep, S. Robert Snodgrass, Quentin R. Smith, and Conrad E. Johanson. 2015. “A Balanced View of Choroid Plexus Structure and Function: Focus on Adult Humans.” *Experimental Neurology* 267:78–86. https://doi.org/http://dx.doi.org/10.1016/j.expneurol.2015.02.032.

Stein, Sherman C., and Wensheng Guo. 2008. “Have We Made Progress in Preventing Shunt Failure? A Critical Analysis.” *Journal of Neurosurgery: Pediatrics* 1 (1):40–47. https://doi.org/10.3171/PED-08/01/040.

———. 2009. “The Prevalence of Shunt-Treated Hydrocephalus: A Mathematical Model.” *Surgical Neurology* 72 (2):131–37. https://doi.org/10.1016/j.surneu.2008.07.012.

Stone, Jonathan, Corey Walker, Maxwell Jacobson, Valerie Phillips, and Howard Silberstein. 2013. “Revision Rate of Pediatric Ventriculoperitoneal Shunts after 15 Years.” *Journal of Neurosurgery: Pediatrics* 11 (1):15–19. https://doi.org/10.3171/2012.9.PEDS1298.

Symss, Nigel Peter, and Shizuo Oi. 2015. “Is There an Ideal Shunt? A Panoramic View of 110 Years in CSF Diversions and Shunt Systems Used for the Treatment of Hydrocephalus: From Historical Events to Current Trends.” *Child’s Nervous System* 31 (2):191–202. https://doi.org/10.1007/s00381-014-2608-z.

Tanaka, R., C. H. Kim, N. Yamada, and Y. Saito. 1987. “Radiofrequency Hyperthermia for Malignant Brain Tumors: Preliminary Results of Clinical Trials.” *Neurosurgery* 21 (4):478–83.

The Electronics Handbook. 2005. Second ed. Boca Raton, FL: CRC Press.

Thompson, Dominic N.P. 2009. “Hydrocephalus.” *Surgery - Oxford International Edition* 27 (3):130–34. https://doi.org/10.1016/j.mpsur.2009.02.005.

Tronnier, V. M., A. Staubert, S. Hahnel, and A. Sarem-Aslani. 1999. “Magnetic Resonance Imaging with Implanted Neurostimulators: An in Vitro and in Vivo Study.” *Neurosurgery* 44 (1):118-25; discussion 125-126.

Tuli, S., B. O’Hayon, J. Drake, M. Clarke, and J. Kestle. 1999. “Change in Ventricular Size and Effect of Ventricular Catheter Placement in Pediatric Patients with Shunted Hydrocephalus.” *Neurosurgery* 45 (6):1329-33; discussion 1333-1335.

Tuli, Sagun, James M. Drake, Jerry Lawless, Melanie Wigg, and Maria Lamberti-Pasculli. 2000. “Risk Factors for Repeated Cerebrospinal Shunt Failures in Pediatric Patients with Hydrocephalus.” *Journal of Neurosurgery* 92 (1):31–38. https://doi.org/10.3171/jns.2000.92.1.0031.

Tully, Hannah M., and William B. Dobyns. 2014. “Infantile Hydrocephalus: A Review of Epidemiology, Classification and Causes.” *European Journal of Medical Genetics* 57 (8):359–68. https://doi.org/10.1016/j.ejmg.2014.06.002.

Vanysek, Petr. 2003. “Electrochemical Series.” In *CRC Handbook of Chemistry and Physics*, 84th ed., 8-21 to 8-31. CRC Press.

Villavicencio, Alan T., Jean-Christophe Leveque, Matthew J. McGirt, John S. Hopkins, Herbert E. Fuchs, and Timothy M. George. 2003. “Comparison of Revision Rates Following Endoscopically versus Nonendoscopically Placed Ventricular Shunt Catheters.” *Surgical Neurology* 59 (5):375–79. https://doi.org/http://dx.doi.org/10.1016/S0090-3019(03)00070-3.

Vinchon, Matthieu, Marc Baroncini, and Isabelle Delestret. 2012. “Adult Outcome of Pediatric Hydrocephalus.” *Child’s Nervous System* 28 (6):847–54. https://doi.org/10.1007/s00381-012-1723-y.

Von Hippel, Arthur. 1954. “Water Loss Tangent.” In *Dielectric Materials and Applications*, 361–62. MIT Press.

Weisenberg, Sofy H., Stephanie C. TerMaath, Chad E. Seaver, and James A. Killeffer. 2016. “Ventricular Catheter Development: Past, Present, and Future.” *Journal of Neurosurgery* 125 (6):1504–12. https://doi.org/10.3171/2015.12.JNS151181.

Wust, P., B. Hildebrandt, G. Sreenivasa, B. Rau, J. Gellermann, H. Riess, R. Felix, and P. M. Schlag. 2002. “Hyperthermia in Combined Treatment of Cancer.” *The Lancet Oncology* 3 (8):487–97. https://doi.org/http://dx.doi.org/10.1016/S1470-2045(02)00818-5.

Yamada, Shinya, and Erin Kelly. 2016. “Cerebrospinal Fluid Dynamics and the Pathophysiology of Hydrocephalus: New Concepts.” *Seminars in Ultrasound, CT and MRI* 37 (2):84–91. https://doi.org/https://doi.org/10.1053/j.sult.2016.01.001.

VITA

Proficient in product design, 3D CAD, FEA modeling, LabVIEW systems and programming
Experienced in protocol writing and technical documentation with strong communication skills
Working knowledge of FDA guidelines and 21 CFR for medical device design
Initial Training in Six Sigma and GD&T, familiar with GMP

Education

M.S. in **Bioengineering**, GPA - 3.52 Aug. 2013 – Mar 2017
University of Illinois at Chicago (UIC)

B.Tech in **Pharmaceutical Chemistry**, First Class with Distinction Jun. 2007 – May 2011
Institute of Chemical Technology (ICT), University of Mumbai.

Skills

FEA and CAD	–	COMSOL Multiphysics, ANSYS, SOLIDWORKS, Salome
Programming	–	LabVIEW, Python 3.x, MATLAB, R
Medical Devices	–	In-vitro methods, benchtop assembly experimentation and testing
Laboratory work	–	Cell culture, organic synthesis, spectroscopy methods, HPLC

Master's Thesis Dissertation Jan. 2015 – Nov. 2017

New design and prototyping of ventricular catheter with built-in cellular obstruction clearance mechanism. Validation of feasibility and efficiency of prototype with in-vitro methods

- **Prototype 3D design** in SOLIDWORKS
- Conceptual **design** and **implementation** of tests for **design verification**
- **Computational modeling** of device operation using FEA tools - COMSOL Multiphysics and ANSYS Based on electrochemical theory and CFD analysis

Work Experience

DAQ Engineer: Larson Research Group, University of Illinois at Chicago May 2015 – Current

- Design and implementation of a DAQ system using **LabVIEW**, for **synchronized stimulation and recording** of electrical signals from biological tissue.
- **System design verification** using test cases
- Upgrading existing DAQ system - simplified user interface, robust system with multiple operative modes,
- Implemented **new features** - real-time **statistical analysis** and **displaying trends**
- Conducting **training sessions** on DAQ system operations and troubleshooting

Laboratory Intern: System Science Inc., Chicago Feb. 2014 – Aug. 2014

- **Conducting verification tests** on prototype ventricular catheter with an integrated pressure and volume sensor as a compliance monitor.
- Preparing technical documentation – test results, SOPs and technical summaries

Industrial Intern: Lupin Ltd., Aurangabad, India May 2010 – Jun. 2010

- Studied large-scale manufacturing processes for pharmaceuticals including tablets, capsules and liquid oral formulations.
- Overview of regulatory requirements for pharmaceuticals in Indian Market, Quality management systems and Analytical methods validation.

Publications

- *Electrolyte transport pathways induced in the midgut epithelium of Drosophila melanogaster larvae by commensal gut microbiota and pathogens.* Shanbhag SR, Vazhappilly AT, **Sane A**, D'Silva NM, Tripathi S., J Physiol. 2016 Jul 4. doi: 10.1113/JP272617
- *Cellular obstruction clearance in proximal ventricular catheters using low-voltage Joule heating,* IEEE Transactions on Biomedical Engineering (under review)

Research Experience

Junior Research Fellow Nov. 2012 – Mar. 2013

International Center for Genetic Engineering and Biotechnology (ICGEB), New Delhi, India

- Performed routine **Short Peptide synthesis** using chemical conjugation techniques
- Routine analysis using **HPLC**
- **Nanoparticle characterization** of self-assembled dipeptides using Dynamic light Scattering and Zeta potential measurement techniques
- **Folate Conjugation** to peptide nanoparticles for tumor targeted therapy

Research Trainee Jul. 2011 – May 2012

Tata Institute of Fundamental Research (TIFR), Mumbai, India

- Studied and measured water transport across ion channels under an osmotic gradient
- **Assembled custom apparatus** and performed experiments to **study water transport** properties of ion channels in **black lipid membranes** (<10 nm thick)
- Performed voltage-clamped ion channel recordings

Undergraduate Research Jan. 2011 – Apr. 2011

Self-microemulsifying drug delivery system (SMEDDS) for a poorly water-soluble drug to achieve rapid onset of action

- Developed a formulation for rapid dissolution (<15 min) at intestinal pH (6 – 8)
- Tested and optimized composition of formulation for **maximum drug uptake capacity** by constructing pseudoternary phase diagrams
- Characterization by **UV-vis Spectroscopy** and **Dynamic light scattering** methods
- **Preliminary Plant Layout** for a small-scale manufacturing facility for new formulation

ELSEVIER LICENSE
TERMS AND CONDITIONS

Mar 08, 2017

This Agreement between Abhay Sane ("You") and Elsevier ("Elsevier") consists of your license details and the terms and conditions provided by Elsevier and Copyright Clearance Center.

License Number	4063931330728
License date	
Licensed Content Publisher	Elsevier
Licensed Content Publication	Progress in Neurobiology
Licensed Content Title	Development of hydrocephalus and classical hypothesis of cerebrospinal fluid hydrodynamics: Facts and illusions
Licensed Content Author	D. Orešković,M. Klarica
Licensed Content Date	August 2011
Licensed Content Volume	94
Licensed Content Issue	3
Licensed Content Pages	21
Start Page	238
End Page	258
Type of Use	reuse in a thesis/dissertation
Intended publisher of new work	other
Portion	figures/tables/illustrations
Number of figures/tables /illustrations	4
Format	both print and electronic
Are you the author of this Elsevier article?	No
Will you be translating?	No
Order reference number	
Original figure numbers	Fig 1,2,3,4
Title of your thesis/dissertation	Cellular obstruction clearance of proximal ventricular catheters using low-voltage Joule heating
Expected completion date	Mar 2017
Estimated size (number of pages)	50
Elsevier VAT number	GB 494 6272 12
Requestor Location	Abhay Sane University of Illinois at Chicago Dept. of Bioengineering 851 S Morgan st. CHICAGO, IL 60607 United States Attn: Abhay Sane
Publisher Tax ID	98-0397604
Total	0.00 USD
Terms and Conditions	

ELSEVIER LICENSE
TERMS AND CONDITIONS

Mar 08, 2017

This Agreement between Abhay Sane ("You") and Elsevier ("Elsevier") consists of your license details and the terms and conditions provided by Elsevier and Copyright Clearance Center.

License Number	4063240276917
License date	
Licensed Content Publisher	Elsevier
Licensed Content Publication	Surgery (Oxford)
Licensed Content Title	Hydrocephalus
Licensed Content Author	Dominic N.P. Thompson
Licensed Content Date	March 2009
Licensed Content Volume	27
Licensed Content Issue	3
Licensed Content Pages	5
Start Page	130
End Page	134
Type of Use	reuse in a thesis/dissertation
Intended publisher of new work	other
Portion	figures/tables/illustrations
Number of figures/tables /illustrations	1
Format	both print and electronic
Are you the author of this Elsevier article?	No
Will you be translating?	No
Order reference number	
Original figure numbers	Fig 1
Title of your thesis/dissertation	Cellular obstruction clearance of proximal ventricular catheters using low-voltage Joule heating
Expected completion date	Mar 2017
Estimated size (number of pages)	50
Elsevier VAT number	GB 494 6272 12
Requestor Location	Abhay Sane University of Illinois at Chicago Dept. of Bioengineering 851 S Morgan st. CHICAGO, IL 60607 United States Attn: Abhay Sane
Publisher Tax ID	98-0397604
Total	0.00 USD
Terms and Conditions	

AMERICAN ASSOCIATION FOR CANCER RESEARCH LICENSE TERMS AND CONDITIONS

Mar 08, 2017

This Agreement between Abhay Sane ("You") and American Association for Cancer Research ("American Association for Cancer Research") consists of your license details and the terms and conditions provided by American Association for Cancer Research and Copyright Clearance Center.

License Number	4063931467904
License date	
Licensed Content Publisher	American Association for Cancer Research
Licensed Content Publication	Cancer Research
Licensed Content Title	A Transient Thermotolerant Survival Response Produced by Single Thermal Doses in HeLa Cells
Licensed Content Author	Eugene W. Gerner,Robert Boone,William G. Connor,John A. Hicks,Max L. M. Boone
Licensed Content Date	1976-03-01
Licensed Content Volume	36
Licensed Content Issue	3
Type of Use	Thesis/Dissertation
Requestor type	academic/educational
Format	print and electronic
Portion	figures/tables/illustrations
Number of figures/tables /illustrations	1
Will you be translating?	no
Circulation	10
Territory of distribution	Worldwide
Title of your thesis / dissertation	Cellular obstruction clearance of proximal ventricular catheters using low-voltage Joule heating
Expected completion date	Mar 2017
Estimated size (number of pages)	50
Requestor Location	Abhay Sane University of Illinois at Chicago Dept. of Bioengineering 851 S Morgan st. CHICAGO, IL 60607 United States Attn: Abhay Sane
Billing Type	Invoice
Billing Address	Abhay Sane University of Illinois at Chicago Dept. of Bioengineering 851 S Morgan st. CHICAGO, IL 60607 United States Attn: Abhay Sane
Total	0.00 USD
Terms and Conditions	

Thesis / Dissertation Reuse

The IEEE does not require individuals working on a thesis to obtain a formal reuse license, however, you may print out this statement to be used as a permission grant:

Requirements to be followed when using any portion (e.g., figure, graph, table, or textual material) of an IEEE copyrighted paper in a thesis:

1) In the case of textual material (e.g., using short quotes or referring to the work within these papers) users must give full credit to the original source (author, paper, publication) followed by the IEEE copyright line © 2011 IEEE.
2) In the case of illustrations or tabular material, we require that the copyright line © [Year of original publication] IEEE appear prominently with each reprinted figure and/or table.
3) If a substantial portion of the original paper is to be used, and if you are not the senior author, also obtain the senior author's approval.

Requirements to be followed when using an entire IEEE copyrighted paper in a thesis:

1) The following IEEE copyright/ credit notice should be placed prominently in the references: © [year of original publication] IEEE. Reprinted, with permission, from [author names, paper title, IEEE publication title, and month/year of publication]
2) Only the accepted version of an IEEE copyrighted paper can be used when posting the paper or your thesis on-line.
3) In placing the thesis on the author's university website, please display the following message in a prominent place on the website: In reference to IEEE copyrighted material which is used with permission in this thesis, the IEEE does not endorse any of [university/educational entity's name goes here]'s products or services. Internal or personal use of this material is permitted. If interested in reprinting/republishing IEEE copyrighted material for advertising or promotional purposes or for creating new collective works for resale or redistribution, please go to http://www.ieee.org/publications_standards/publications/rights/rights_link.html to learn how to obtain a License from RightsLink.

If applicable, University Microfilms and/or ProQuest Library, or the Archives of Canada may supply single copies of the dissertation.